Geology and Petrography of the Igneous Rocks exposed at Hmanpya Taung and Tayoke Taung area in Waingmaw Township, Kachin State

Wai Mar Hlaing[1], Doi Aung[2], Aye Aye Mar[3]
[1] Lecturer, Myitkyina University, Myanmar
[2] Lecturer, Myitkyina University, Myanmar
[3] Lecturer, Myitkyina University, Myanmar

Email: waimarhlaing@umkn.edu.mm

ABSTRACT

The research area is located between 25˚25’N, 97˚ 25’ E and 25˚27’N, 97˚ 27’E, on the eastern bank of Ayeyarwaddy River and situated in Waingmaw Township, Myitkyina District, Kachin State. The study area is mainly composed of acid volcanic rocks. They are mainly dacite and rhyolite and minor amount of pyroclastic rock. Dacite is the oldest, well exposed at Hmanpya Taung, NW part of Tayoke Taung and occurs as domal form of subconical hills. Rhyolite is the youngest, well exposed at Tayoke Taung. After the volcanism, dolerite dykes intruded into these rocks. Then, the alluvial sediments deposit on the remaining parts of the area. According to field and petrographic criteria, the volcanic rocks of the study area are magmatic in origin of calc-alkaline suite. The eruption of volcanic rocks of the study area would be Late Cretaceous to Early Eocene. Igneous activity related to subduction of India plate beneath the Eurasian plate. Age determination for the rocks units of the present area is done on the bases of field observation and lithologic correlation of the surrounding area. There are four faults observed in the present area. The economic aspect is the placer gold deposit. Dacite and Rhyolite are used as the construction materials.

1. INTRODUCTION

1.1 Location and Size

The research area is situated in Maina village, Waingmaw Township, Myitkyina District, Kachin State. It is about five miles northeast of Myitkyina.
It is located between 25˚25’N, 97˚ 25’ E and 25˚27’N, 97˚ 27’E in one-inch topographic map 92 G/7. It covers an area of approximately 63 square miles. The study area is mountainous and rugged Terranes and also covers with fairly dense vegetation. Location map of the study area is shown in fig (1.1).

KEYWORDS: *Dacite, Rhyolite, Volcanic rocks*

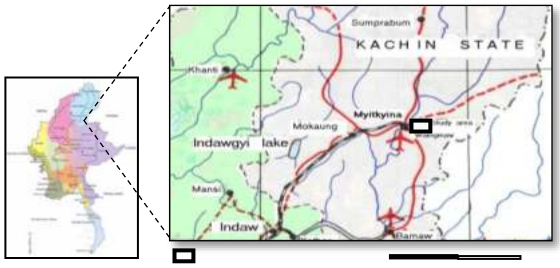

Fig (1.1) Location map of the study area

1.2 Regional Geologic Setting

The present area includes in partly of Central granitoid belt. Igneous rocks along the Shan Boundary Fault system and Tenasserian granitoids in the Sino-Burman Ranges describe by Bender (1983) also lie along this Central granitoid belt. The central granitoid belt of Myanmar extends from Putao and the jade mining areas in Myitkyina in the north. Central granitoid belt is separated from the porphyry Cu (Au) related to the western granitoid belt by the Hnizee-Sagaing fault system (Khin Zaw, 1990). Granite and granitic rocks were found east of Myitkyina, east of Waingmaw and eastern Nayazeik and Hawngpa in Phakant (Maung Maung, 2004). In north-east of the study area, there are mainly of igneous rocks, ultrabasic and basic intrusive, granite and other non-basic intrusive are exposed.

The study area falls in the northern part of Sagaing fault (West Kachin Unit of Bender, 1983) where it branches in various splays terminates in Jade Mine Belt into a compressive horse tail structure, 200km wide from east to west. Tagaung-Myitkyina belt, including present area, is poorly mapped belt characterized by basic and ultrabasic rocks of ophiolite suites mostly forming inliers within late Tertiary sediment and alluvium. The Tagaung –Myitkyina belt narrows northwards between the covering Mogok belt and Kumon range.

2. METHODS OF STUDY

(i) The representative samples of various rock units are collected in the field and plotted the location on the base map to draw the geological map.

(ii) G.P.S and Brunton Compass are used for location and measuring the geological structures.
(iii) 20 thin- sections cut from the representative specimens collected from the research area and studied under the research type polarizing microscope for the petrographic analyses and petrogenetic consideration.
(iv) Detailed geological map of the research area is drawn by field observations and traversed measurements.

3. GENERAL GEOLOGY

3.1 Hmanpya Taung Dacite

The rocks unit is well-exposed at the Hmanpya Taung. This rock unit named as the Hmanpya Taung Dacite. Hmanpya Taung Dacite shows reddish-brown color on weathered surface and whitish pink to chocolate brown colour on fresh surface in fig (3.1). The dacite is fine-grained porphyritic rock and mainly composed of quartz, plagioclase and alkali-feldspar with minor amount of biotite, pyrite and iron ore minerals. This rocks unit found as boulder to massive. It is highly weathered and altered. Kaolinization is formed as a result of hydrothermal alteration. In some places weathered surface is pitted due to the removal of feldspar. The contact boundary between dacite and volcanic tuff is faulted. In some places the possible chilled zone is observed between dacite and rhyolite along the car-road of Kwitu. Therefore, presence of the chilled zone indicates that dacite is older than rhyolite.

Fig.(3.1)

Fig.(3.2)

Fig(3.1) Photograph showing the boulder to massive outcrop nature at Hmanpya Taung Dacite
Fig.(3.2) Photograph showing the well jointed porphyritic rhyolite showing bedding like sheeted joints

3.2 Tayoke Taung Rhyolite

Rhyolite is well exposed only in the Tayoke Taung. So, this rocks unit is named as Tayoke Taung Rhyolite. It is dark grey to brown color on weathered surface and whitish to whitish pink on the fresh surface in fig.(3.2). It is fine-grained porphyritic texture, hard and compact. It is mainly composed of phenocrysts of feldspar and quartz. It is usually found as boulder to massive outcrops. In some places, surfaces of the rhyolite are encrusted by limonite stained due to the weathering of iron bearing minerals, such as pyrite. It is well jointed, voids removed by the weathering of xenoliths grains or escaping of gas are distinct features of this rocks. The boundary between the rhyolite and younger volcanic tuff may also be faulted contact.

Geological map of the Hmanpya Taung and Tayoke Taung area is shown in fig.(3.3).

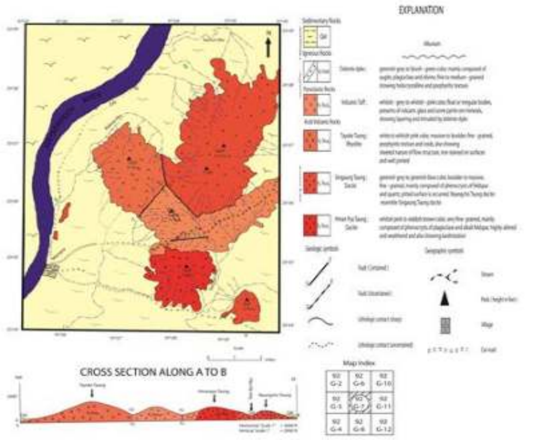

Fig. (3.3) Geological map of the Hmanpya Taung and Tayoke Taung area

4. PETROGRAPHY

4.1 Petrographic description of Hmanpya Taung Dacite

Microscopically, this rock is mainly composed of quartz, plagioclase and alkali-feldspar. The minor accessory minerals are biotite, pyrite and iron ore minerals. This rocks shows hypidiomorphic to allotriomorphic granular texture. The rock is fine-grained, porphyritic in texture. The ground mass shows hypocrystalline texture. Quartz are dominant mineral consisting of about 20% of the thin section. Quartz is anhedral grains and size ranges from 0.1mm to 0.2mm in diameter. Some quartz grains are embayed on corroded nature. Plagioclase occurs as microlite in groundmass and as phenocryst, euhedral to subhedral ranging in size from 1.5mm to 2 mm. Plagioclase feldspar is consisting about 15%. Penetrative twinning of plagioclase feldspar is observed in some thin section fig.(4.1.A). Most of the plagioclase feldspar is altered to epidote due to the hydrothermal alteration after crystallization fig.(4.1.B). Anhedral quartz grain, minute crystals of orthoclase and plagioclase feldspar constituent in groundmass. Biotite rarely occurs in this rock. Its grain sizes are less than 1 mm in diameter. Biotite is seen as small flakes in the groundmass. It is usually altered to chlorite.

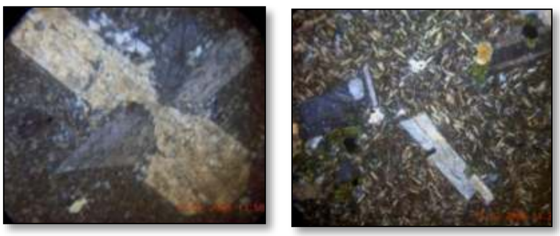

(A) (B)

Fig. (4.1) (A) Photomicrograph showing the penetrative twin of plagioclase
(B) Photomicrograph showing the plagioclase altered to epidote

4.2 Petrographic description of Tayoke Taung Rhyolite

It is composed of quartz, orthoclase and plagioclase. Minor constituent minerals, such as pyrite and zeolite. This rock is fine grained, hypocrystalline and porphyritic texture. Quartz usually forms anhedral grains and occupy the interstitial spaces. The grainsize varies forms 0.1mm to 0.2mm in diameter. Quartz are dominant mineral consisting of about 25%. The groundmass of the rock is mostly glassy. Inclusions are observed in quartz. Quartz grains are not only rounded but deeply embayed. Alkali-feldspar is represented by orthoclase. The grain size range from is euhedral to subhedral grains varying from 0.4mm to 0.7mm in diameter. Othoclase is consisting about of 28%. Cloudily plagioclase is less common than alkali-feldspar. Plagioclase is consisting about 15%. The saturated and oversaturated with silica and alkali is evidenced by the presence of dominant quartz and alkali-feldspar. Biotite and Zeolite are anhedral grain. The grain size ranged from 1mm to 1.5mm. They are consisting of about 15% of in thin section marginal part of feldspar altered to zeolite minerals in Rhyolite as shown in fig. (4.2.A) and corroded and brecciated nature of quartz in rhyolite and showing iron stained in fig. (4.2.B).

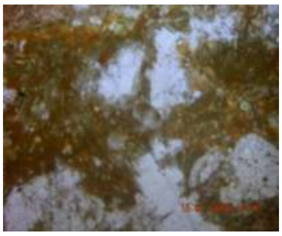

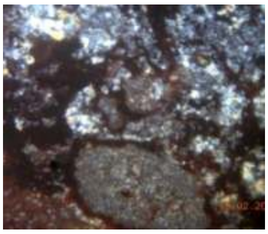

(A) (B)

Fig. (4.2) (A) Photomicrograph showing the marginal part of the feldspar altered to zeolite
(B) Photomicrograph showing the corroded and brecciated nature of quartz

5. CONCLUSIONS

The study area is situated in Waingmaw Township, Myitkyina District, Kachin State. It is situated about five whitish pink to chocolate brown color on fresh surface. miles northeast of Myitkyina. Hmanpya Taung dacite is It composed of quartz, plagioclase and alkalifeldspar with minor amount of biotite, Pyrite and iron ore minerals. It is highly altered and weathered. Tayoke Taung Rhyolite is dark grey to brown color on weathered surface and white to whitish pink on the fresh surface. Sheeted nature of flow structure is common. Some places, the surfaces of rhyolite are encrusted by iron minerals. The rocks in the study area cropped out at the northern part of the central volcanic line which extend from the Jade mine area, through Wuntho Igneous complex, lower Chindwin and Mount Popa areas to the south. They are mainly calc alkaline rocks. The igneous series of the present area may be regarded as basalt-andesite-dacite-rhyolite series. The volcanic rocks of the study are magmatic in origin of calc-alkaline suite. The eruption of volcanic rocks of the study area would be Late Cretaceous to Early Eocene.

ACKNOWLEDGEMENT

I am deeply indebted to Rector Dr. Aung Win, Myitkyina University, for his kind permission, valuable advice, careful reading effective suggestions and encouragements to carry out this research works. I also thank Dr. Myint Oo, Professor and Head, Department of Geology, Myitkyina University, for the reading this manuscript and giving suggestions.

REFERENCES

[1] Bender, F, 1983 Geology of Burma, Geibruder Borntraeger, Berlin, Stutgard.
[2] Best, M.G, 1982 Igneous and Metamorphic Petrology. New York: W.H. Freeman.
[3] Chibber, H.L, 1934 The Geology of Burma, Macmillan, London.
[4] Hyndman, D.W, 1972 Petrology of Igneousand Metamorphic rocks. Mc Graw Hill, Inc, New York.
[5] Khin Zaw, 1990 Geological, Petrological and Geological characteristics of Granitoid rocks in Burma; With Special reference, Journal of Southeast Asia Earth Science, Vol.4, No.4, pp 293-335.
[6] Maung Maung, 2004 Geology around Waingmaw, Waingmaw Township, Kachin State, Geological Research paper. Unpublished, University of Myitkyina.
[7] Raymond L. A, 1995 Igneous Petrology, Inc London, 742 Pp.

Development of Rainfall Intensity-Duration-Frequency (IDF) Curve for Monywa City

Ei Ei Phyu[1], Aye Aye Thant[2]
[1] Mandalay Technological University, Myanmar
[2]Mandalay Technological University, Myanmar

Email: eieiphyu2007@gmail.com

ABSTRACT: The rainfall Intensity-Duration-Frequency (IDF) Curves are crucial for water resources engineering and planning, designing and operating of hydraulic structures against floods. Since Monywa city is one of the largest cities in Myanmar, Intensity-Duration-Frequency (IDF) Curves for given rainfall conditions are necessary for special storm water management due to rapid development in land use. The purpose of the study is to develop the rainfall IDF curves for Monywa city. In this study, IDF curve has been generated from 35-years (1981-2015) recorded maximum daily rainfall data, for different rainfall durations (20, 40, 60, 80, 100 and 120 minutes) with return periods (2, 5, 10, 25, 50 and 100 years) according to Gumbel Distribution Method to predict rainfall intensity for Monywa city. By using empirical formula, the proposed IDF formula is obtained to predict the rainfall intensity for rainfall durations and return periods. Then, the IDF curves for Monywa city derived by the proposed IDF equation are described on log-log scale and natural scale. The IDF curves are developed for the town and recommended for the design of storm drainage.

KEYWORDS: *maximum daily rainfall, rainfall intensity, rainfall duration, Gumbel distribution method, intensity-duration-frequency (IDF) curve*

1. INTRODUCTION

Nowadays, climate change is being faced all over the world including Myanmar due to global warming with the destroying ecosystem. In many parts of the world, climate change leads to the extreme environmental events such as floods, droughts, high winds and long term trends in rainfall (both increase and decrease). The importance of precipitation in the field of Civil Engineering cannot be over-emphasized due to its diverse uses. The quantification and occurrence of extreme precipitation is required by hydraulic engineers and hydrologists in water resources planning, design and operation-Awofadeju (2018). Development of rainfall Intensity-Duration-Frequency (IDF) relationship is a primary basic input for the design of the storm water drainage system for cities. The rainfall depths derived from the intensity duration frequency relationship is being used by water resources managers for planning, designing and operation of water resource related projects. The magnitude of an extreme rainfall event has an inverse relation to its occurrence frequency; therefore, the severe rainfall events have less frequency compared to moderate rainfall events. The IDF relationship is a mathematical relationship between the rainfall intensity (i), the duration (d) and the return period (T) using extreme rainfall data.

Monywa, an agricultural city, is surrounded by Chindwin river and it is also located in tropical zone of Myanmar country. Therefore, proper knowledge of rainfall intensity should be available for the proper and efficient design of the storm water drainage system. Dr. Lamia Abdul Jaleel and Atta Farawn (2013) established rainfall IDF relationships for Basrah city, Iraq using Gumbel method, their results showed that maximum intensities occur at short durations with high variation. P.E.Zope, Eldho T.I and V.Jothiprakash (2016) presented that IDF curves established by using the new modified equation shows better results in the changing hydrologic conditions as observed on 26th July 2005 in Mumbai city, India. While designing the new drainage system, proper information having IDF relationship reflecting recent hydrologic changes has to be used as design-criteria-P.E.Zope (2016). Yaseen (2017) developed rainfall IDF model for Sulaimani city from a period of 23-years (1993-2015) maximum daily rainfalls for rainfall durations of 10, 20, 30, 60, 120, 360, 720 and 1440 minutes to estimate different returning periods of 2, 5, 10, 25, 50 and 100 years. Therefore, in this study, IDF curve for Monywa city is generated by using measured daily rainfall depth data with different return period and rainfall duration.

2. MATERIAL AND METHOD

2.1 Study area and data collection

The study area, Monywa is a city in Sagaing region, Myanmar, located 136 km northwest of Mandalay on the eastern bank of the Chindwin river at Latitude 22 º 06' 30.82" North and Longitude 95 º 08' 8.99" East. The weather of the city is dry and warm in summer with the average temperature of 36°C. In order to propose the empirical formula for intensity-duration-frequency curve of Monywa city, the maximum daily rainfall data are collected from Department of Meteorology and Hydrology, Mandalay, Upper Myanmar. One day maximum annual rainfall data of the study periods of 35-years (1981-2015) for Monywa city are presented in Table 1.

2.2 Precipitation duration reduction formula

From the available 35-years data, the annual extreme values of precipitation were extracted from each year data. The daily (24 hours) data points were reduced to shorter time durations (namely 20, 40, 60, 80, 100 and 120 minutes) using a formula recommended by the Indian Meteorological Department to reduce the rainfall duration to smaller time scale less than 24 hours as shown in equation (1).

$$P_t = P_{24}[\frac{t}{24}]^{(\frac{1}{3})} \qquad (1)$$

Where, P_t is the required precipitation depth for duration less than 24 hours in (mm), P_{24} is the daily precipitation depth in (mm) and t is the required duration time in hours.

Table 1. Maximum daily rainfall for Monywa city during (1981-2015)

No.	Year	Maximum Daily Rainfall (mm)	No	Year	Maximum Daily Rainfall (mm)
1	1981	23.50	19	1999	39.73
2	1982	32.35	20	2000	23.21
3	1983	48.71	21	2001	22.04
4	1984	37.57	22	2002	44.69
5	1985	29.82	23	2003	20.40
6	1986	46.60	24	2004	19.88
7	1987	41.09	25	2005	33.94
8	1988	44.81	26	2006	49.30
9	1989	46.24	27	2007	70.40
10	1990	20.13	28	2008	67.71
11	1991	46.08	29	2009	77.86
12	1992	16.50	30	2010	60.21
13	1993	36.55	31	2011	39.21
14	1994	114.03	32	2012	23.48
15	1995	19.37	33	2013	41.10
16	1996	39.35	34	2014	51.10
17	1997	44.66	35	2015	28.57
18	1998	83.40			

2.3 Frequency distribution and development of IDF curves

In order to establish the IDF relationships, essential information are extracted from the existing rainfall data using statistical tools. To derive the information, probability distribution functions are applied to hydrological data such as normal, lognormal, exponential, Gamma, Pearson, Log-Pearson and extreme values distributions. While the data used in the IDF relationship studies are extreme values of precipitation, for this reason the extreme values distribution which is known as Gumbel distribution found to be effective to model the rainfall intensity. Therefore, in this study, a Gumbel distribution function (which described below) applied to the extreme values of rainfall to explain the change of the parameters of the frequency distribution with time. From the fitted frequency distribution (Gumbel) the rainfall intensity for any duration and returning period can be described according to equation (2)- Hadadin (2005), Al-Hassoun (2011) and El-sebaie (2012).

$$P = P_{av} + KS \qquad (2)$$

Where, P is the frequency of precipitation in (mm) for a specific duration t (minutes) with any returning period of T (years), P_{av} is the average of the maximum precipitation data points (n) as in equation (3).

$$P_{av} = \frac{1}{n}\sum_{i=1}^{n} P_i \qquad (3)$$

K is the Gumbel frequency factor, as in equation (4).

$$K = -\frac{\sqrt{6}}{\pi}[0.5772 + \ln[\ln[\frac{T}{T-1}]]] \qquad (4)$$

S is the standard deviation of precipitation data P as in equation (5).

$$S = [\frac{1}{n-1}\sum_{i=1}^{n}[P_i - P_{av}]^2]^{\frac{1}{2}} \qquad (5)$$

Then the intensity of rainfall I in (mm/hr) for any duration t can be calculated using equation (6) for any return period of T (years).

$$I = \frac{P}{t} \qquad (6)$$

Where, I is the intensity of rainfall (mm/hr), P is the depth of precipitation (mm) and t is the rainfall duration (hours).

2.4 Derivation of IDF empirical formula

A power function can describe generalized IDF relationship between rainfall intensity (I), rainfall duration (t) and return period (T). The following procedure used to derive a formula for intensity of rainfall

(I) from the IDF relationships -Al-Hassoun (2011) and El-sebaie (2012).

The general form of intensity equation can be defined in the form of power-law relation as in equation (7):

$$I = \frac{CT^m}{t^a} \tag{7}$$

Where, I is the intensity of rainfall (mm/hr), t is the duration of rainfall (minutes), T is the returning period (years) and constants (C, m and a) are empirical parameters depend on precipitation data, shape, size and location of the study area which can be obtained from logarithmic transformation of the equation.

After applying logarithmic transformation of equation (7), the following equation (8) can be obtained:

$$\log I = \log(CT^m) - a\log t \tag{8}$$

Assuming ($CT^m = k$), equation (8) can be rewritten as in equation (9).

$$\log I = \log(k) - a\log t \tag{9}$$

For each return period, plot the values of *log I* (log of precipitation intensity values) against *log t* (log of duration time). From the linear relationship, find the slope of the straight line which represent the constant a (the average values of constant a for all returning periods) in equation (8), while the term (*log k*) in equation (9) represents the intercept from the plot for each returning period.

To find the values of C and m, we need to plot the log of that intercept (*log* CT^m) values against the log of returning period (*log T*) in a new graph as in equation (11). Assumed that: $k = CT^m$ (10) Taking log of both sides of equation (10) results in the following equation (11):

$$\log k = \log C + m\log T \tag{11}$$

Plotting *log k* and *log T* in equation (11), a linear equation of the plot can be obtained, then we can find m that represents the slope of the linear relationship. The value of the anti-log of the intercept from the plotted curve represents the C coefficient for equation (7).

3. RESULTS AND DISCUSSION

3.1 Reduction of daily rainfall to shorter duration

Maximum daily rainfall data for the study area were available for a period of 35-years (1981-2015). From this data base, the maximum daily (24 hours) rainfall data (mm) are converted into shorter duration of (20, 40, 60, 80, 100 and 120 minutes) using equation (1). For each rainfall duration, the standard deviation (S) and the corresponding average value of precipitation (P_{av}) are calculated as described in Table 2.

Table 2. Standard deviation and average precipitation values for different durations

Duration (minutes)	Standard Deviation (S)	Average Precipitation (P_{av}) (mm/hr)
20	5.02	10.19
40	6.33	12.84
60	7.24	14.70
80	7.97	16.17
100	8.59	17.42
120	9.12	18.51

3.2 Development on rainfall intensity-duration-frequency (IDF) curves

The frequency of precipitation for each duration of rainfall (20, 40, 60, 80, 100 and 120 minutes) with returning period of (2, 5, 10, 25, 50 and 100 years) are calculated with the average hourly precipitation depth analysis (P_{av}), the Gumbel frequency factor (K) and standard deviation (S) by using Gumbel distribution frequency method. The results of frequency precipitation for different rainfall duration with returning period are expressed in Table 3. It is observed that the frequency precipitation values are increasing for different duration with return periods. After that, the corresponding rainfall intensities (I) are also calculated by using equation (6). To develop rainfall IDF curves, the general form of intensity equation (7) is used. The results of rainfall intensity for Monywa city are shown in Table 4. It is also studied that the rainfall intensity values are decreasing for rainfall duration but increasing for return period. Using equations (8) to (11), the proposed empirical IDF formula is obtained as:

$$I = \frac{192.3T^{0.252}}{t^{0.667}} \tag{12}$$

Then, the IDF curves for Monywa city are constructed between rainfall intensity and rainfall duration of (20, 40, 60, 80, 100 and 120 minutes) for returning period of (2, 5, 10, 25, 50 and 100 years) as illustrated in Fig. 1 on log-log scale and in Fig. 2 on natural scale. Therefore, the values of rainfall intensity are decreasing with increased rainfall duration according to the result of IDF curve for Monywa city.

Table 3. Results of frequency precipitation values for different durations and return periods of 2, 5, 10, 25, 50, and 100 years

Duration (minutes)	Rainfall Frequency Precipitation (P) (mm)					
	2 years	5 years	10 years	25 years	50 years	100 years
20	9.36	13.80	16.74	20.45	23.20	25.94
40	11.80	17.39	21.09	25.77	29.23	32.68
60	13.51	19.90	24.14	29.49	33.47	37.41
80	14.86	21.91	26.57	32.46	36.83	41.17
100	16.01	23.60	28.62	34.97	39.68	44.35
120	17.02	25.08	30.42	37.16	42.16	47.13

Table 4. Results of Rainfall Intensity values for different durations and return periods of 2, 5, 10, 25, 50, and 100 years

Duration (minutes)	Rainfall Intensity (I) (mm/hr)					
	2 years	5 years	10 years	25 years	50 years	100 years
20	31.05	39.12	46.58	58.68	69.88	83.22
40	19.56	24.64	29.34	36.96	44.01	52.41
60	14.92	18.80	22.39	28.20	33.58	39.99
80	12.32	15.52	18.48	23.28	27.72	33.01
100	10.61	13.37	15.92	20.06	23.89	28.44
120	9.40	11.84	14.10	17.76	21.15	25.19

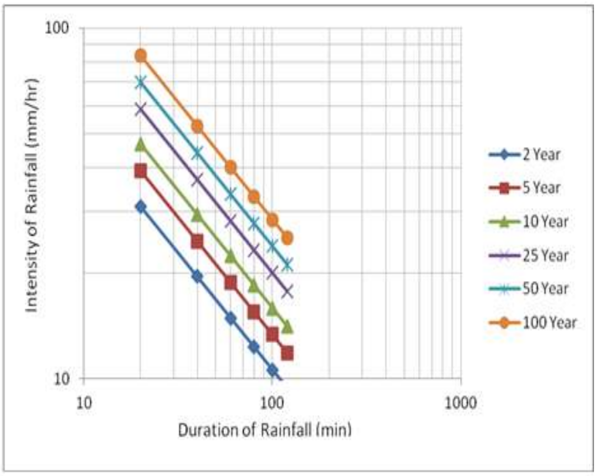

Fig 1. IDF curve derived from empirical formula on log-log scale

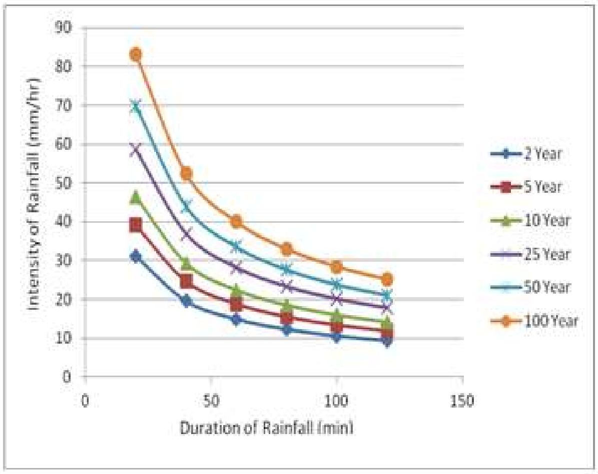

Fig 2. IDF curve derived from empirical formula on natural scale

4. CONCLUSIONS

In this study, the 35-years (1981-2015) annual maximum daily rainfall data are used to generate rainfall intensity duration frequency (IDF) curve. Gumbel Distribution Method is also applied to predict the rainfall intensity. By using the rainfall intensity at rainfall duration of 20, 40, 60, 80, 100 and 120 minutes with returning period of 2, 5, 10, 25, 50 and 100 years, rainfall IDF curve for Monywa city is constructed.

As the result of rainfall IDF curve, the maximum value of rainfall intensity is 83.22 mm/hr for return period of 100 year and the minimum value is 9.40 mm/hr for 2 year. It is detected that the rainfall intensity decreases with increased duration. The proposed empirical IDF formula relates to rainfall intensity as independent variable to rainfall duration and return period as dependent variables. Therefore, this study shows the development of rainfall Intensity-Duration-Frequency (IDF) curve for Monywa city.

ACKNOWLEDGEMENT

Firstly, the author really wishes to record her thanks to Dr. Nilar Aye, Professor and Head, Department of Civil Engineering, Mandalay Technological University, for her guidance. And then, the author is deeply grateful to Daw Aye Aye Thant, Associate Professor, Department of Civil Engineering, Mandalay Technological University, who pays special attention by giving invaluable time in reading this paper and giving suggestions. Finally, the author would also like to express sincere thanks to engineers and staffs from Department of Meteorology and Hydrology, Mandalay, Upper Myanmar.

REFERENCES

[1] Hadadin, N.A., "Rainfall intensity-duration-frquency relationship in the Mujib basin in Jordan" Journal of Applied Sciences, vol.5, No. 10, pp.1777-1784. 2005.

[2] Al-Hassoun, S. A. "Developing an empirical formulae to estimate rainfall intensity in Riyadh region" Journal of King Saud University-Engineering Sciences Vol. 23, No. 2, pp. 81-88. 2011.

[3] El-sebaie, I. H. "Developing rainfall intensity-duration-frequency relationship for two regions inf Saudi Arabia," Journal of King Saud University-Engineering Sciences Vol. 24, No. 2, pp. 131-140. 2012.

[4] Dr. Lamia Abdul Jaleel and Atta Farawn, "Developing Rainfall Intensity-Duration-Frequency Relationship for Basrah City" (K.J.E), ISSN 2207-5528, Vol.5, Issue1, P.P.105-112, Dec., 2013.

[5] P.E.Zope, Eldho T.I and V.Jothiprakash", Development of Rainfall Intensity Duration Frequency Curves for Mumbai City India" Journal of Water Resource and Protection, 756-765, 8, 2016.

[6] Yaseen Ahmed Hamaamin, "Developing of Rainfall Intensity-Duration-Frequency Model for Sulaimani City" Journal of Zankoy Sulaimani JZS 19-3.4 (Part-A), 2017 Awofadeju A. S., Akanni, A. O., Ojeleke T. A., and Oguntayo A. A.,"Development of Rainfall Intensity-Duration-Frequency Curves for South Western," vol. 10, No.4, August, 2018.

Performance Analysis of the Various Calculation Methods for Evapotranspiration

Thinn Thinn Soe [1], Thet Mon Soe[2], Su Myat Wai[3]
[1]Technological University (Mandalay), Myanmar
[2]Mandalay Technological University, Myanmar
[3]Technological University (Mandalay), Myanmar

Email: thinthinsoe@tum-mandalay.edu.mm

ABSTRACT*:* This paper presents the performance analysis of the various calculation methods for evapotranspiration. Reference evapotranspiration (ET_o) is one of the major processes in the hydrologic cycle, and its reliable estimation is essential to water resources planning and management. This study is mainly divided into two portions namely, calculation of reference evapotranspiration and their performance analysis. In this study, ET_o values are determined using temperature-based, radiation-based methods and the results from these methods are compared with the value obtained from FAO 56 Penman-Monteith method for performance analysis. The required data are obtained from Mandalay, Pyin Oo Lwin and Heho meteorology stations in Myanmar. The linear regression and statistical indices of quantitative approaches are used for model performance analysis. The statistical indicators such as correlation coefficient (r), root mean square error (RMSE), mean bias error (MBE) and percentage of error (% Error) are used in performance analysis. As an analysis result, Priestley-Taylor method has been found to have closely related with the FAO 56-PM method for proposed stations.

KEYWORDS: *Evapotranspiration, Penman-Monteith Method, Priestley-Taylor Method, Statistical Analysis*

1. INTRODUCTION

Myanmar is an agricultural country and agriculture sector is the back-bone of its economy. The agricultural sector is related to other social and economic sectors. Agricultural sector represents about thirty-seven percent of the national economy. Besides, Myanmar gets sixty-percent of foreign exchange earnings from agriculture. Irrigation water requirement is based on the computation of evapotranspiration (ET_o) and this computation is very useful for hydrologist, water resources specialists, regional planners, climate modelers, climatologists, ecologists, farmers, regional-scale surface runoff and groundwater, simulate large-scale atmospheric circulation and global climate change and schedule field-scale irrigations and tillage operations over cropland and so on.

The evapotranspiration can be calculated by two methods, namely: direct and indirect method. The direct method is used evaporation pans and lysimeter. However, lysimeter data is rare and available for few years. There are number of methods available for evaluation of evapotranspiration by other indirect method. The indirect method is water-budget, energy-budget and aerodynamic approach or combination process. Available reference evapotranspiration equations range from simple empirical temperature-based equations to complex multi-layer resistance based equations. All of these methods are dependent upon high quality weather parameters collected from well established weather stations. The best method for calculating of the evapotranspiration (ET_o) is FAO 56 Penman-Monteith method under limited data availability conditions. Due to the higher performance of FAO 56 Penman-Monteith (ET_o) model in different parts of the world when compare with other models, it has been accepted as the best method of computing reference evapotranspiration from meteorological data[Drooger, et al. (2002)]. Therefore, this study analyses the performance of the various calculation methods in proposed stations for evapotranspiration with respect to FAO 56 Penman-Monteith method.

2. THEORETICAL BACKGROUND

Temperature based method includes Blaney-Criddle, Thornthwaite and Hargreaves-Samani methods. Radiation based method consists of Priestley-Taylor, Makkink, Turc, Jensen-Haise methods. These methods are described as follows:

2.1. Blaney-Criddle Method

The modified Blaney-Criddle method has been used throughout the world, and is written in the following Equation 1.

$$ET_o = \alpha + \beta f \qquad (1)$$

where,

f $= p\,(0.46T + 8.13)$
ET_o = reference evapotranspiration in (mm/day)
T = monthly mean temperature in (°C)
α = calibration parameter

β = calibration parameter

P = mean daily percentage of total annual day hours for the period

$$\alpha = 0.0043(RH_{min}) - \frac{n}{N} - 1.41$$

$$\beta = 0.82 - 0.0041(RH_{min}) + 1.07\left(\frac{n}{N}\right) + 0.066(u_d) - 0.006(RH_{min})\left(\frac{n}{N}\right) - 0.0006(RH_{min})(u_d)$$

RH_{min} = minimum relative humidity

$\frac{n}{N}$ = the ratio of actual to possible sunshine hours

u_d = daytime wind speed at 2m height in (m/sec)

2.2. Hargreaves-Samani Method

Hargreaves and Samani (1985) developed a simplified equation requiring only temperature, day of year and latitude for calculating ET_0 as shown in Equation 2.

$$ET_o = 0.0135K_T(T_{mean} + 17.78)(T_{max} - T_{min})^{0.5}R_a \quad (2)$$

where,

ET_o = reference evapotranspiration in (mm/day)

$$R_s / R_a = K_T(T_{max} - T_{min})^{0.5}$$

R_s = solar or shortwave radiation in (MJ m^{-2} day^{-1})

R_a = extraterrestrial radiation in (MJ m^{-2} day^{-1})

K_T = empirical coefficient

2.3. Thornthwaite Method

Monthly ET_o can be estimated according to Thornthwaite by the following Equation 3:

$$ET_o = 1.6L_a\left[\frac{10T_{mean}}{I_t}\right]^a \quad (3)$$

where,

ET_o = reference evapotranspiration (cm/month)

L_a = adjustment for the number of hours of daylight and days in the month related to the latitude of the place

T_{mean} = mean monthly temperature (°C)

I_t = the total of 12 monthly values of heat index

$$I_t = \sum_{m=1}^{12}(T_{mean}/5)^{1.514}$$

$$a = 6.75\times10^{-7}I_t^3 - 7.71\times10^{-5}I_t^2 + 1.792\times10^{-2}I_t + 0.49239$$

a = an empirical constant

2.4. The Priestley-Taylor Method

The Priestley-Taylor method is basically the radiation driven part of the Penman Equation, multiplied by a coefficient, and can be expressed as in Equation 4.

$$ET_o = \alpha\frac{\Delta(R_n - G)}{\Delta + \gamma}.\frac{1}{\lambda} \quad (4)$$

where,

ET_o = reference evapotranspiration in (mm/day)

α = calibration factor (α = 1.26)

λ = the latent heat of vaporization (λ = 2.45 MJ kg^{-1} at 20°C)

Δ = the slope of the vapour pressure curve (kPa $°C^{-1}$)

γ = the psychrometric constant (kPa $°C^{-1}$)

G = the soil heat flux

2.5. The Makkink Method

The Makkink method can be seen as a simplified form of the Priestley-Taylor method and was developed for grass lands in Holland. The equation can be expressed as follows;

$$ET_o = \alpha.\frac{\Delta}{\Delta + \gamma}.\frac{R_s}{\lambda} - \beta \quad (5)$$

where,

ET_o = reference evapotranspiration in (mm/day)

α = calibration factor (α = 0.61)

β = calibration factor (β =0.12)

λ = the latent heat of vaporization (λ = 2.45 MJ kg^{-1} at 20°C)

Δ = the slope of the vapour pressure curve (kPa $°C^{-1}$)

γ = the psychrometric constant (kPa $°C^{-1}$)

2.6. The Turc Method

This method only uses two parameters, average daily radiation and temperature and for RH> 50% can be expressed as Equation 6,

$$ET_o = 0.013\frac{T_{mean}}{T_{mean} + 15}\frac{23.8856R_s + 50}{\lambda} \quad (6)$$

And for RH<50% as Equation 7,

$$ET_o = 0.013\frac{T_{mean}}{T_{mean} + 15}\frac{23.8856R_s + 50}{\lambda} \times\left[1 + \left[\frac{50 - RH_{mean}}{70}\right]\right] \quad (7)$$

where,

ET_o = reference evapotranspiration in (mm/day)

T_{mean} = average monthly temperature in (°C)

λ = the latent heat of vaporization (λ = 2.45 MJ kg^{-1} at 20°C)

RH_{mean} = mean monthly relative humidity (%)

2.7. The Jensen-Haise Method

This method is used in computing reference evapotranspiration. The equation can be expressed as:

$$ET_o = C_t(T - T_x)R_s \quad (8)$$

where,

$$C_t = \frac{1}{\left[\left(45 - \frac{h}{1.37}\right) + \left(\frac{365}{e^o(T_{max}) - e^o(T_{min})}\right)\right]}$$

$$T_x = -2.5 - 0.14\left(e^o(T_{max}) - e^o(T_{min})\right) - h/500$$

ET_o = reference evapotranspiration in (mm/day)

C_t = the temperature constant

T_x = the intercept of the temperature axis

h = the altitude of the location in (m)

$e^\circ(T_{max})$ = saturation vapour pressure at mean maximum temperature in (kPa)

$e^\circ(T_{min})$ = saturation vapour pressure at mean minimum temperature in(kPa)

2.8. Penman-Monteith Method

The FAO Penman-Monteith method to estimate evapotranspiration (ET_o) can be expressed as follows[Alexandris, et al. (2008)];

$$ET_o = \frac{0.408\Delta(R_n - G) + \gamma\frac{900}{T+273}u_2(e_s - e_a)}{\Delta + \gamma(1 + 0.34u_2)} \quad (9)$$

where,

ET_o = reference evapotranspiration in (mm/day)

R_n = net radiation at the crop surface (MJm^{-2}day^{-1})

u_2 = wind speed in m/sec at 2 m height

G = soil heat flux density (MJm^{-2}day^{-1})

T = air temperature ($^\circ$C)

e_a = actual vapour pressure (kPa)

e_s = saturation vapour pressure (kPa)

$e_s - e_a$ = saturation vapour pressure deficit (kPa)

Δ = slope vapour pressure curve (kPa °C^{-1})

γ = the psychrometric constant (kPa °C^{-1})

2.9. Coefficient of Correlation

While a relationship exists between the coefficient of correlation and the size of the data set, the following approximations are helpful in interpreting the strength of either positive or negative correlation shown in Table 1 and the correlation coefficient can be calculated using Equation 10 [K. Subramanya (2008)].

Table 1. Interpretation of Correlation Coefficient

Value of r	Interpretation
0.00-0.25	Little or no relationship
0.30-0.45	Fair relationship
0.50-0.75	Moderate to good relationship
0.80-1.00	Strong relationship to perfect correlation

$$r = \frac{\sum P_iO_i - (\sum P_i \sum O_i)/N}{\sqrt{\sum P_i^2 - (\sum P_i)^2/N} \times \sqrt{\sum O_i^2 - (\sum O_i)^2/N}}$$

(10)

where,

O_i = ET_o values of FAO56-PMS

P_i = ET_ovalues of other methods

r = correlation coefficient

3. CALCULATION OF EVAPOTRANSPIRATION BY VARIOUS METHODS

ET_o is calculated by various methods. To know the performance of these methods, the computed ET_o values for three stations are compared with FAO 56 PM method and their comparisons are illustrated in Fig 1 to Fig 3. From these figures, it can be easily seen that Hargreaves-Samani method gives over-estimation of ET_o with respect to FAO56-PM in all three stations but Priestley-Taylor method is very closely related with FAO56-PM in all three stations.

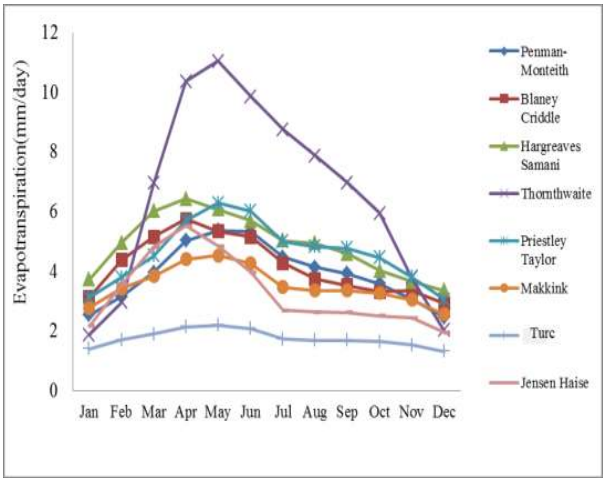

Fig 1. Computed ET_o by Various Methods for Mandalay Station

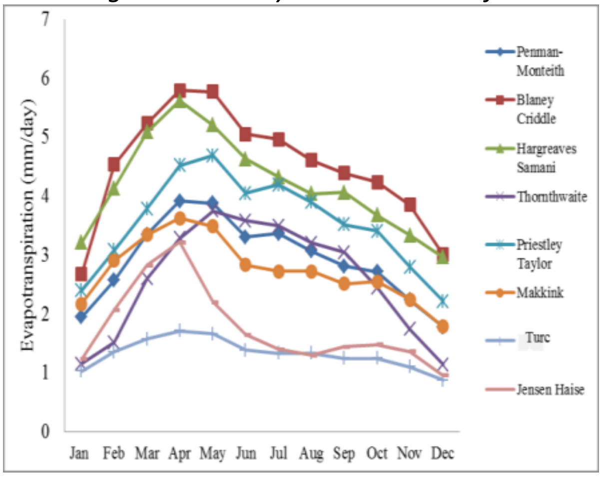

Fig 2. Computed ET_o by Various Methods for Pyin Oo Lwin Station

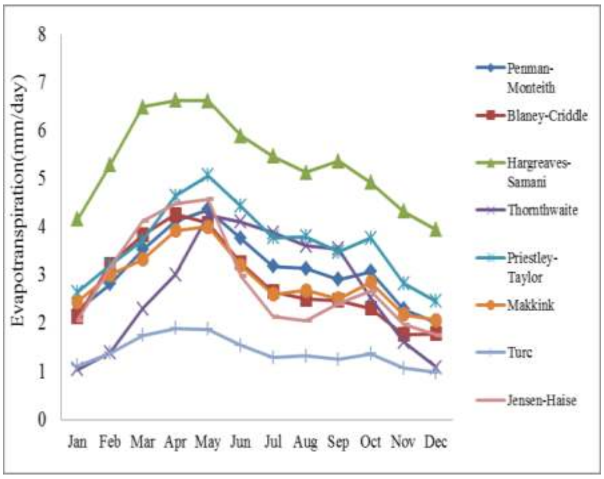

Fig 3. Computed ET_o by Various Methods for Heho Station

4. CALCULATION OF STATISTICAL INDICATORS

The statistical indicators namely correlation coefficient (r), intercept (a) and slope (b) of linear regression, root mean square error (RMSE) and mean bias error (MBE) of various methods with respect to FAO56-PM method are computed to evaluate the performance of various methods in comparison with FAO56-PM.

Regession analysis can be applied to know whether the strength of the evidence of a linear relationship. Thornthwaite method has the highest values of RMSE in Mandalay station. In Pyin Oo Lwin station, there are the lowest values of RMSE for Makkink method. Moreover, the Blaney-Criddle, Jensen-Haise and Makkink methods also gives the lowest RMSE value in Heho station. Priestley-Taylor method give the fairly result of RMSE.The Priestley-Taylor method gives the most fairly result of MBE at all three stations.

The correlation between ET_o computed using FAO56-PM and various methods for each studied station are illustrated in Fig 4 to Fig 15. It can be observed that Priestley Taylor method is strongest relationship for all stations.

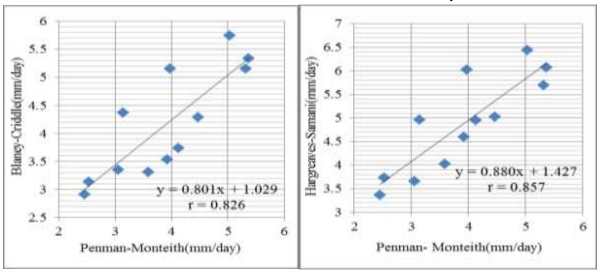

Fig 4. Correlation between ETo Computed Using FAO56-PM and Blaney Criddle & Hargreaves Samani Methods for Mandalay Station

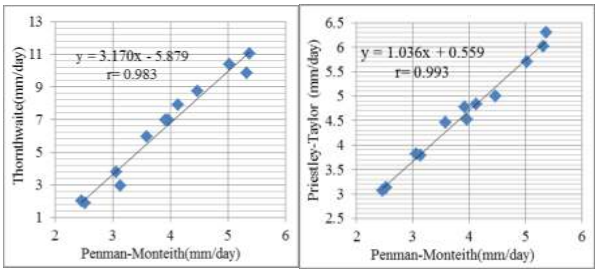

Fig 5. Correlation between ETo Computed Using FAO56-PM and Thornthwaite & Priestley Taylor Methods for Mandalay Station

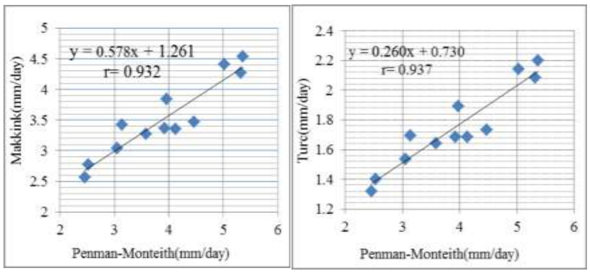

Fig 6. Correlation between ETo Computed Using FAO56-PM and Makkink & Turc Methods for Mandalay Station

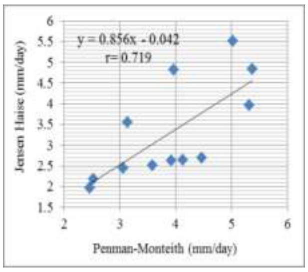

Fig 7. Correlation between ETo Computed Using FAO56-PM and Jensen Haise Method for Mandalay Station

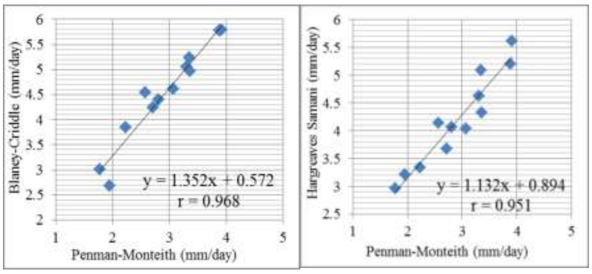

Fig 8. Correlation between ETo Computed Using FAO56-PM and Blaney Criddle & Hargreaves Samani Methods for Pyin Oo Lwin Station

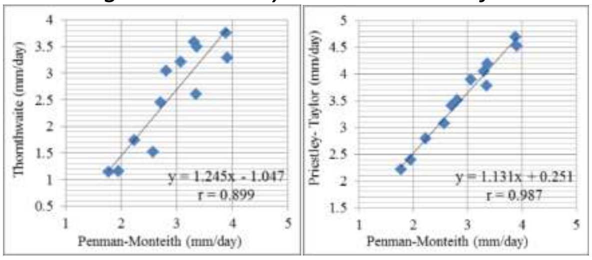

Fig 9. Correlation between ETo Computed Using FAO56-PM and Thornthwaite & Priestley Taylor Methods for Pyin Oo Lwin Station

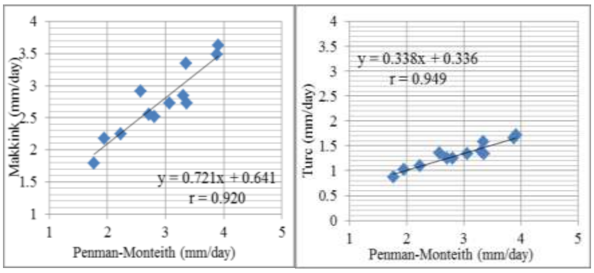

Fig 10. Correlation between ETo Computed Using FAO56-PM and Makkink & Turc Methods for Pyin Oo Lwin Station

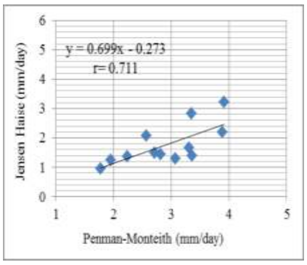

Fig 11. Correlation between ETo Computed Using FAO56-PM and Jensen Haise Method for Pyin Oo Lwin Station

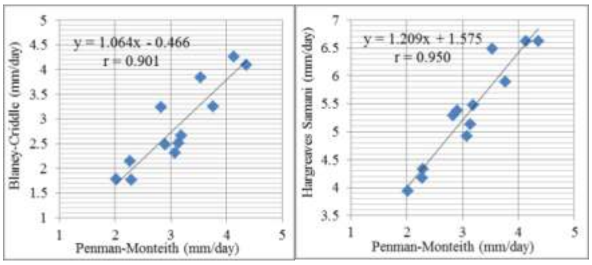

Fig 12. Correlation between ETo Computed Using FAO56-PM and Blaney Criddle & Hargreaves Samani Methods for Heho Station

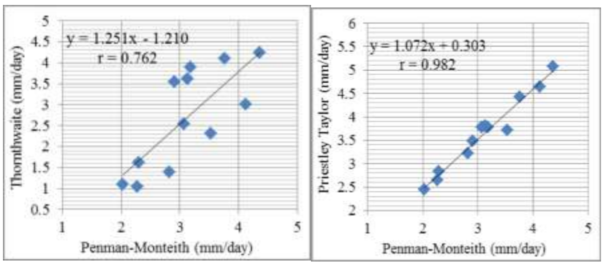

Fig 13. Correlation between ETo Computed Using FAO56-PM and Thornthwaite & Priestley Taylor Methods for Heho Station

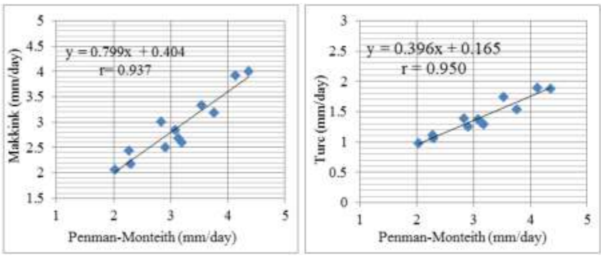

Fig 14. Correlation between ETo Computed Using FAO56-PM and Makkink & Turc Methods for Heho Station

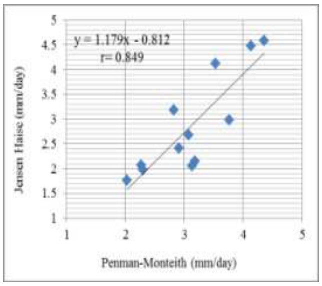

Fig 15. Correlation between ETo Computed Using FAO56-PM and Jensen Haise Method for Heho Station

5. CONCLUSIONS

As a conclusion, the Priestley Taylor method provides the closely related ET_o estimation to FAO 56-PM. It can also be observed that Priestley Taylor method is strongest relationship for all stations. The Priestley Taylor method may be an attractive to the more complicated Penman-Monteith equation although it needs fewer input parameters. This method is suggested as practical method for estimating for proposed stations. Therefore, this study gives general reference tool and some insight application to the adaptive or smart irrigation controllers, water resources specialists, regional planners and so on from these studied areas.

ACKNOWLEDGEMENT

Firstly, the author would like to express her deepest gratitude to Dr. Thiha Zaw, Professor and Head, and Daw San San Myint, Associate Professor, Department of Civil Engineering, Technological University (Mandalay) for their careful guidance, effective suggestions and recommendations. The author also would like to thank all of her teachers for their mentoring, encouragement, and recommending this paper.

REFERENCES

[1] J. Doorenbos and W.O. Pruitt, *"Guidelines for Predicting Crop Water Requirements."* Irrigation and Drainage paper 24, FAO, Rome. 1992.

[2] K. Subramanya, *"Engineering Hydrology"*, Tata Mc Graw-Hill, New Delhi. 2008.

[3] Patra, K.C, "*Hydrology and Water Resources Engineering*", 2nd ed. India: Nerosa Publishing House Pvt.Ltd, 2008.

[4] Peter Droogers and Richard G.Allen, *"Estimating Reference Evapotranspiration Under Inaccurate Data Conditions"*. Irrigation and Drainage Systems 16: 33-45, 2002, Netherlands.

[5] Richard. G.A, L.S. Pereira, D. Raes and M. Smith, "*Guidelines for Computing Crop Water Requirement In Crop Evapotranspiration",* Irrigation and Drainage Paper 56, FAO, Rome. 1998.

[6] S. Alexandris, R. Stricevic and S. Petkovic, "*Comparative Analysis of Reference Evapotranspiration from the Surface of Rainfed Grass in Central Sebria, Calculated by Six Empirical Methods Against the Penman-Monteith Formula*", European Water 21/22: 17-28. 2008.

Groundwater and Aquifer Characteristics of the East Dagon Township,Yangon Region

Khin Thida Lwin[(1)], Toe Toe Win Kyi[(2)], Yin Kay Thwe Tun[(3)]
[(1)]Associate Professor, Loikaw University, Geology Department, Myanmar
[(2)]Professor Geology Department, Loikaw University, Myanmar
[(3)]Professor Geology Department, Loikaw University, Myanmar

Khinthidalwin74@gmail.com

ABSTRACT*:* The study area is located in East Dagon Township. It lies between 16° 46' 00"N to 16° 55' 00"N and 96° 10' 00"E to 96° 12' 00"E. Yangon area is underlain by thick Tertiary deposits and Quaternary deposits. Tertiary deposits of Irrawaddy Formation and Pegu Group are mainly composed of loosely cemented sand and shale. In the area, two main aquifers have been divided into Alluvial Aquifer and Irrawaddian Aquifer. The alluvial aquifer is composed of gravels, fine to coarse sand, silt and clay.The Irrawaddian Aquifer is composed of loosely cemented coarse-grained sandstone and clay.Determining the hydraulic characteristics of aquifer or water bearing layers are tested by pumping out test and recovery test. According to pumping out test, the transmissivity value for the study is $1307m^2/d$.

KEYWORDS: *Tertiary, Irrawaddy Formation, Pegu Group,Aquifer, Transmissivity*

1. INTRODUCTION

Groundwater is the natural resource of the earth.The water resources are useful not only for drinking purpose but also for the agricultural, industrial and animal husbandry use. The study area is located in East Dagon Township. It lies between 16° 46' 00"N to 16° 55' 00"N and 96° 10' 00"E to 96° 12' 00"E. The location map of the study area is shown in Figure 1.

Figure.1 Location of the study area

Objectives; To know surface water system and ground water supply system, nature of the aquifer, quality and quantity of ground water and the geological characteristics of the surface (i.e. stratigraphic and structural features and influence the flow of ground water).

2. METHODS OF STUDY

During the field, the measurements of water level, well depths, well logs, the position of wells by G.P.S and verbal information of the wells from the local people were taken into account and recorded. The water samples to be analysed were collected into bottles and then brought back to the laboratory of Water Resources Utilization Department The study area is to evaluate the chemical characteristics of groundwater and hydraulic characteristics of aquifer by making pumping out test and recovery test. Chemical results are plotted by Surfer Version 8 computer processing programmed.

3. BACKGROUND GEOLOGY

Regional geological and hydro-geological studies of research area underlain by thick Tertiary deposits and Quaternary deposits. were made by Win Naing (1972). The Alluvium Sediment are distributed at the east, west and northwest of the area. The Synclinal valley which is at the west of Yangon Anticlinal ridge is filled with unconsolidated water laid deposits of Quaternary age. Irrawaddian Formation are widely distributed at the southern and middle part of the area. Pegu group are distributed at the northern hilly part of the area. Tertiary deposits of Irrawaddy Formation and Pegu Group are strongly folded and mainly composed of sand and shale.

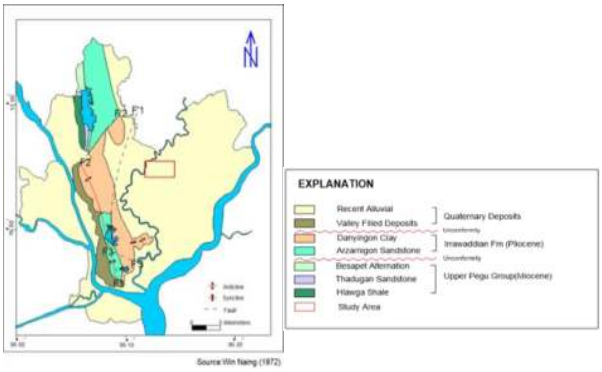

Figure 2. Geological Map of the Yangon Area (Source, Win Naing, 1972)

4. WATER RESOURCES

4.1 Existing Water Supply System

There are two main water supply systems for the study area which are ground water supply by tube wells and surface water from Nga Moe Yeik storage tank at Nyaung Hna Pin.

4.2 Surface Water Supply System

Booster Pumping Station (No.1 and 2)

Booster Pumping Station (No.3 and 4)

There are (4) booster pumping station and (13) tube wells of municipal water system in East Dagon Township. There are (63) ward, (3) villages tract, (6) villages and 32686 households in the study area. Among them the wells and surface water from Nga Moe Yeik storage tank are distributing the water about 6.000,00 gallons of water every day respectively for ward no. 5,7,8,9. Other wards are used groundwater with private tube wells.

4.3 Groundwater Supply System

Tube well No 11, 12, 13 are also distributed by 4 inches and 2 inches pipe line to the ward No.9.It is also being distributed by 24000 gallons of water every day by each tube wells. Tube well No 7,8,9,10,14,15 are also distributed by 4 inches and 2 inches pipe line to the ward No.7.Tube well No 5,6,16,17 are also distributed by 4 inches and 2 inches pipe line to the ward No.8.These are also being distributed by 24000 gallons of water every day by each tube wells.

Quaternary	Alluvium	Recent	Younger Alluvial	Unconsolidated soil	<18 m
		Pleistocene	Valley Fill deposits	Fine to coarse grained Yellowish coloured sand	
Tertiary	Irrawaddy Formation	Pliocene	Danyingone clay shale	Clayey sandstone	<100 m
		Pliocene	Arzarnigon sand rock	Light blue coloured sand rock with grit	320m
	Pegu Group	Miocene	Besapat Alternation	Alternation of shale and argillaceous sandstone	
		Miocene	Thadugan Sandstone	Well consolidated jointed Argillaceous sandstone	600m
		Oligocene	Hlwaga Shale	Generally Indurate shale	?

Table1. Geological Succession of Greater Yangon (After Win Naing, 1972)

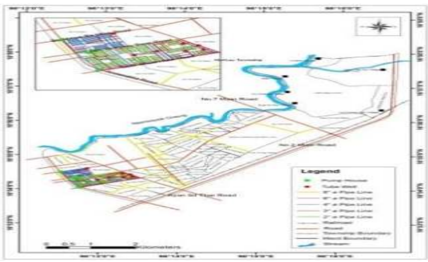

Figure .3 Pipe-lines, Pumping Stations and Supply System to Quarters in East Dagon Township

5. GROUNDWATER AND AQUIFER CHARACTERISTICS

5.1 Groundwater in Alluvial Deposits

Alluvial aquifer is mainly composed of yellow fine sand, yellow medium sand, yellow coarse sand, yellow clay, yellow sandy clay, yellow coarse sand with grave and blue fine sand, blue sandy clay, and blue coarse sand with gravel. According to well log data, the water table is found at 100 to 130ft below the surface varying from one place to another. Aquifer thickness of the alluvial deposit is range from 20 to 50ft. Aquifer depth of alluvial deposit is range from 330 to 505ft.Discharge rate is from 4000gph to 7000gph for 8 inches diameter tube well.

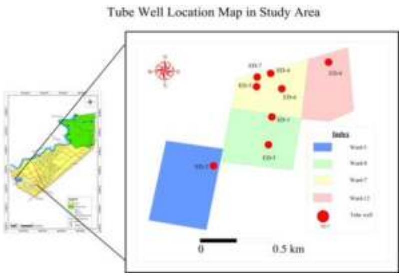

Figure .4 Tube Well Location Map of th East Dagon Township

5.2 Groundwater Movement Fence Diagram

Fence Diagram of the research area shows that sand and clays beddings are towards the south.

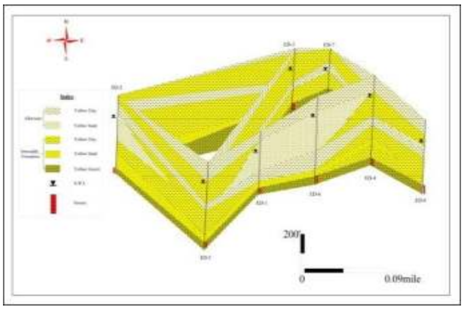

Figure .5. Fence Diagram of the research area

6. HYDRAULIC CHARACTERISTICS OF QUIFER

6.1 Pumping Out Test of the Study Area

Pumping Out test is of measurement of discharge rate and draw down that occur in pumped well and also measuring the drawdown of the piezometer surrounding the pumped well in certain time during pumping of the well.

This measurement indicates how much volume of water that store in the aquifer can be released and cone of depression has increased at a certain time during pumping. By using Jacob's method, it can show hydraulic characteristics of the aquifer i.e.; transmissivity after proper calculation.

In the study area, pumping out test was done at N 16° 12' 35" and E 96° 12' 35", pumping-out test was made at 8" Ø production well of Dagon University, East Dagon Township, Yangon Region. Well water was pumped out by submersible pump. The constant discharge pumping test was performed for three hours with pumping rate of (785) m^3/d. The water level was measured by container method.

(1) In order to determine the hydraulic characteristics of aquifer or water bearing layers. (Aquifer test)

(2) To get the information about yield and drawdown of the well. (well test)

Location: Dagon University, East Dagon Township

Static water level :24.26 m from top of casing

Well casing:8 inches PVC pipe

Discharge Rate: 785 m^3/d

Top of casing: 0.5 m

Water meter: 3.24 meter per day

Time	SWL	Drawdown	s(Residual)
1	24.26	25.94	1.68
2	24.26	26.2	1.94
3	24.26	27.2	2.94
4	24.26	26.98	2.72
5	24.26	27.01	2.75
6	24.26	27.03	2.77
7	24.26	27.03	2.77
8	24.26	27.04	2.78
9	24.26	27.06	2.8
10	24.26	27.03	2.77
12	24.26	27.09	2.83
14	24.26	27.12	2.86
16	24.26	27.1	2.84
18	24.26	27.11	2.85
20	24.26	27.4	3.14
23	24.26	27.4	3.14
26	24.26	27.4	3.14
30	24.26	27.45	3.19
35	24.26	27.48	3.22
40	24.26	27.5	3.24
45	24.26	27.5	3.24
50	24.26	27.5	3.24
60	24.26	27.5	3.24
70	24.26	27.5	3.24
80	24.26	27.5	3.24
90	24.26	27.5	3.24
105	24.26	27.5	3.24
120	24.26	27.5	3.24

Table .2. Pumping out test data of the research area

6.2 Calculation of Pumping Out Test Results

The Jacob's method (Cooper and Jacob's) 1946, drawdown data were plotted on the semi-log paper. On the semi-log plots, most of the points fall on a straight-line semi-log plot. The straight-line drawdown differences per log cycle (Δs) were measured and the hydraulic properties were calculated using the Jacob-straight line method as follows.

Coefficient of Transmissivity, $KD = 2.3Q/4\pi\Delta s$

Where, KD = Transmissivity, m^2/d

Q = Discharge rate, m^3/d

Δs = Drawdown difference per log cycle, m.

In the study area, the pumping test of the Dagon University, East Dagon Township show that hydraulic characteristics at that well are Q = 785 m^3/d, Δs = 0.2m and KD = 718 m^2/d.

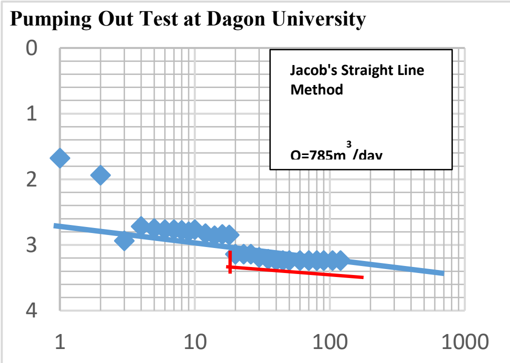

Figure .6. Constant Discharge Pumping Out Test of the well at Dagon University

6.3. Recovery Test

The pumping test is made by Thesis's recovery method. When the pump is shut down after a pumping test, the water levels in the well and the piezometers will start to rise.

This rise in water levels is known as residual drawdown, s'. It is expressed as the difference between the original water level before the start of pumping and the water level measured at a time (t') after the cessation of pumping.

It is always good practice to measure the residual drawdown during the recovery period. Recovery-test measurements allow the transmissivity of the aquifer to be calculated. Residual drawdown data are more reliable than pumping test data because recovery occurs at a constant rate, whereas a constant discharge during pumping is often difficult to achieve in the field.

Procedure

-Plot s' versus t/t' on semi-log paper (t/t' on logarithmic scale)

-Fit a straight line through the plotted points.

-Determine the slope of the straight line, i.e. the residual drawn down difference Δs' per log cycle of t/t'.

-Substitute the known values of Q and Δs' into Equation and calculate KD.

6.4 Calculation of Recovery Test Data Result

Thesis's recovery method is widely used of analysis of recovery test.

Thesis's recovery equation (1935) is described as follow.

$\Delta s' = 2.3Q/4\pi KD$

Where, Q = the constant well discharge, m^3/d

KD = the transmissivity of the aquifer, m^2/d

Δs' = residual drawdown difference, m

The recovery test data performed in the study area; show that hydraulic characteristics of that well are Q = 785 m^3/d, KD = 1307 m^2/d, and Δs' =0.11m.

Table.3. Recovery Test data of the research area

T	T′	T/T′	Drawdown	SWL	s′(Residual)
121	1	121	24.42	24.26	0.16
122	2	61	24.45	24.26	0.19
123	3	41	24.45	24.26	0.19
124	4	31	24.47	24.26	0.21
125	5	25	24.45	24.26	0.19
126	6	21	24.44	24.26	0.18
127	7	18.14286	24.43	24.26	0.17
128	8	16	24.43	24.26	0.17
129	9	14.33333	24.42	24.26	0.16
130	10	13	24.41	24.26	0.15
132	12	11	24.41	24.26	0.15
134	14	9.571429	24.4	24.26	0.14
136	16	8.5	24.39	24.26	0.13
138	18	7.666667	24.39	24.26	0.13
140	20	7	24.35	24.26	0.09
143	23	6.217391	24.38	24.26	0.12
146	26	5.615385	24.37	24.26	0.11
150	30	5	24.37	24.26	0.11
155	35	4.428571	24.36	24.26	0.1
160	40	4	24.36	24.26	0.1
175	45	3.888889	24.35	24.26	0.09
180	50	3.6	24.36	24.26	0.1
190	60	3.166667	24.35	24.26	0.09
200	70	2.857143	24.35	24.26	0.09
210	80	2.625	24.35	24.26	0.09
220	90	2.444444	24.34	24.26	0.08
235	105	2.238095	24.33	24.26	0.07
250	120	2.083333	24.32	24.26	0.06
270	140	1.928571	24.32	24.26	0.06
290	160	1.8125	24.32	24.26	0.06
310	180	1.722222	24.32	24.26	0.06

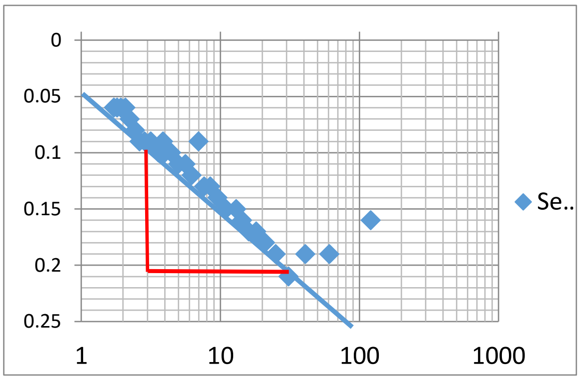

Figure.7 Constant Discharge Recovery Test of Well at Dagon University

CONCLUSIONS

The research area, East Dagon Township is located in northern part of Yangon.The groundwater yield from this unit is about 2000 gph from 8 inches diameter tube well. In our study area pumping test for 3 hours.The pumping out test shows that the transmissivity of the aquiferis 718 m^2/day.In recovery test, the transmissivity of the aquifer is found to be 1307m^2/day.

ACKNOWLEDGEMENT

I would like to thank deeply and firstly, to Dr Htay Aung, Acting-Rector,University of Loikaw, for hisproviding facilities and valuable advice and discussion. Next, I deeply grateful to Dr. Toh Toh Win Kyi, Professor and Head of Geology Department, University of Loikaw, for her close guidance, suggestion and valuable guidances. Then, I wish to express unbounded gratitude to Dr. Yin Kay Thwe Tun, Professor of Geology Department, Loikaw University for her valuable discussion, suggestions, reading the manuscript and preparing for this paper.

REFERENCES

[1] Chibber, H.1., 1934. The Geology of Burma.

[2] Dauis, S. N. & Dewiest (1966). Hydrogeology, 2nd Edition, John Willey & Sons, Inc. Newyork.

[3] David Keith Todd, 1980. Groundwater Hydrology. (2nd Edition) John Wiley and Sons, Inc. NewYork . 463 pp.

[4] Driscoll,F.G.(1986):Groundwater and Wells,2nd edition, Johnson Division, St. Paul Minnesota.

[5] WinNaing,1972, "The Hydrogeology of Greater Rangoon Area".Unpublished M.Sc(Thesiss) Rangoon University.

[6] Win Naing, 1996, "Urban Geology of Eastern Yangon Area". Unpublished M.Sc. (Thesis).

Stress field interpretation by Faulting in the upper part of the Balu Chaung area, Pinlaung Township, Shan State (south)

Sai Yarzar Soe[1], Htay Lwin[2], Toe′ Toe′ Win Kyi[3]
(1) U, Lecturer, Geology Department, Loikaw University, Myanmar
(2) *Dr,* Professor, Department of Geology, University of Yangon, Myanmar
(3) *Dr,* Professor, Geology Department, Loikaw University, Myanmar

Email: yarzarsai7@gmail.com

ABSTRACT: The study area is situated around the upper part of the Balu Chaung, Naungtaya sub-township, Pinlaung Township, Shan State (south), which lies in the western portion of the Eastern Highland. The rock units exposed in the study area are mainly composed of Paleozoic to Mesozoic sedimentary rocks, as well as Tertiary rock unit is cropped out as a minor. In the study area, major strike slip faulting is trending nearly N-S and NNW-SSE direction. Thrusting and normal faulting are also observed in the study area. According to the field evidences of faulting and analysis, right-lateral strike slip motion in NNW-SSE direction, left-lateral strike slip motion in ENE-WSW direction and compressional stress field comes from NE-SW direction. This means σ1 is NE-SW direction which is nearly perpendicular to the general strike position.
Keywords: *Balu Chaung, faulting, stress field, σ1*

1. INTRODUCTION

The processes of rocks cracks, fractures or faults are associated to stress field in the Earth's crust and lithosphere. Properties of the stress field and of the associated fracture processes in the Earth's crust are closely related (Scholz 2002). Type of faulting depends not only on the stress field but also on the orientation of activated fractures or faults with respect to the stress (Vavryčuk 2011a). In addition, the slip vector for shear faulting is close to or coincides with the direction of the maximum shear stress acting on the fault (Wallace 1951; Bott 1959). Therefore, type of faulting, orientation of activated faults and direction of slip along activated faults serve as an important source of information about the stress field and its spatial and lateral variations within the Earth's crust. Methods of determining stress from observed earthquake mechanisms are reported and their robustness is exemplified on numerical tests (Václav Vavryčuk).

2. LOCATION

The study area is situated in the central part of Kalaw-Pinlaung basin, between Aungban and Pinlaung towns, Shan State (south). It is located about 24 km north of Pinlaung and about 25.6 km south of Aungban (Fig.1). The area lies in map No.93D/11 of one inch Topographic map and map No. 2096/11 of UTM map, bounded by latitudes 20º 14' N to 20º 31' N and longitudes 96º 34' E and 96º 45' E.

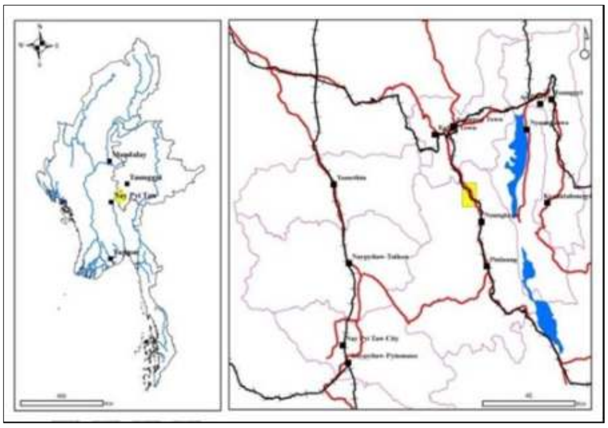

Fig 1: Location map of the study area

3. PURPOSE OF STUDY

The main purpose of the present study is to determine the stress field from major and minor faulting in the study area.

4. METHODOLOGY

To interpret the stress field of the study area, field measurement and analysis take place.

5. GEOLOGICAL SETTING

The study area is situated on the western margin of the tectonic province of Shan-Tanintharyi Block or in the Eastern Highland of Myanmar (Western part of Shan-Thai Block). The Panlaung fault and Shan Scarp fault, trending NNW-SSE is structurally bounded at the western margin of the study area. Kyankkyan fault occurs as structural boundaries in the eastern part. This fault passes through Inlay Lake and west of loikaw and demarcated at the eastern margin of the study area.

The rock units of the entire basin are mainly composed of Paleozoic to Mesozoic sedimentary rocks, as well as Tertiary rock unit is cropped out as a minor. Generally, the trends of the rock units run nearly NNW-SSE in direction. The regional geological map of the study area is shown in Figure 2.

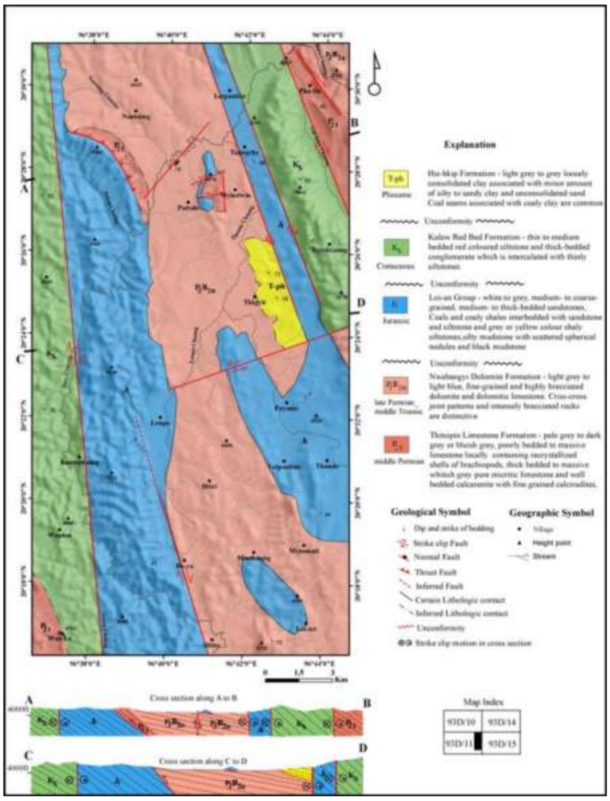

Fig 2: Geological map of the study area

6. RESULTS AND DISCUSSION

Strike-slip Faults

Balu Chaung fault

This fault lies along Balu Chaung. It is a right lateral strike-slip fault, trending in NNW-SSE direction. The length of this fault is about 15 miles. It cut across Kalaw Red Bed Formation and Loi-an Group. Fault evidence is also nearly straight alignment along stream course and fault scarp (Fig 3). Stereo plot analysis and related stress orientation is shown in (Fig 3).

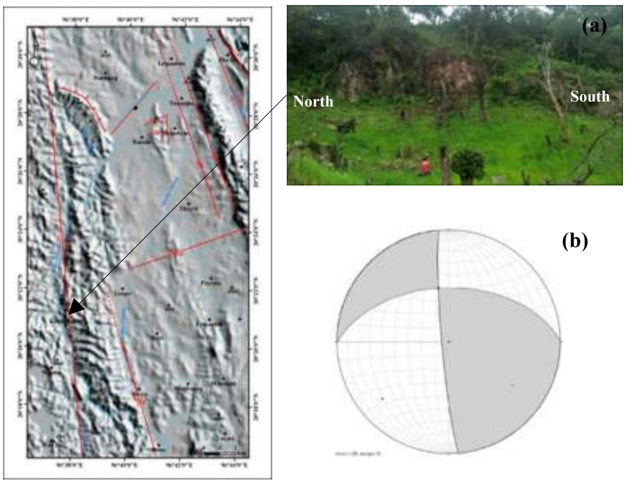

Fig 3: Map showing field data and location of the Balu Chaung right lateral strike-slip fault (a) NNW-SSE trending fault scarp (b) fault plane solution

Pha-Lin fault

This fault is located east of Pha Lin village. It is now a right lateral strike-slip fault, trending in NNW-SSE direction. Normal and strike-slip evidence on the fault plane are found. So, it can be considered that two phases of faulting are formed, firstly fault plane could be slipped with normal and then reactivated as strike-slip fault. The length of this fault is about 2 miles. It cut across Thitsipin Limestone Formation. Fault evidence and stereo plot analysis and related stress orientation are shown in Fig (4).

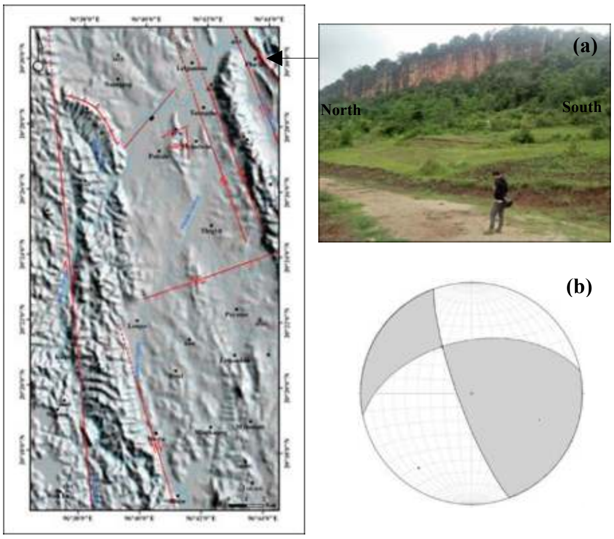

Fig 4: Map showing field data and locality of the Pha-lin right lateral strike-slip fault (a) NNW-SSE trending high angle fault formed in Thitsipin limestone Formation (20°30'22.261"N, 96°43'35.688"E) (b) fault plane solution

Loi-maw Chaung fault

This fault lies along Loi-maw Chaung. It is a right lateral strike-slip fault, trending in NNW-SSE direction. The length of this fault is about 6 miles. Fault evidence of straight stream alignment is shown in Fig (5).

Fig 5: Photograph showing panoramic view of straightstream alignment of Loi-maw Chaung fault

Pinhmigon fault

East Pinhmigon fault and west Pinhnigon fault are trending along the western flank Myatheinthan and Tayoktaung range Fig (6). The length of these faults is about 6 miles. East Pinhmigon fault is faulted contact between Loi-an Group and Kalaw Red Bed Formation. West Pinhmigon fault cut cross Nwabangyi Dolomite Formation, Loi-an Group and Hsi-hsip Formation. Both are now right lateral strike-slip fault, trending in NNW-SSE direction. East Pinhmigon fault are found evidence with two phase of faulting, firstly fault plane could be slipped with normal and then reactivated as strike-slip fault. Fault evidence and stereo plot analysis and related stress orientation are shown in Fig (7).

Fig 6: Photograph showing panoramic view of Pinhmigon fault, faulted contact between Loi-an Group and Kalaw Red Beds

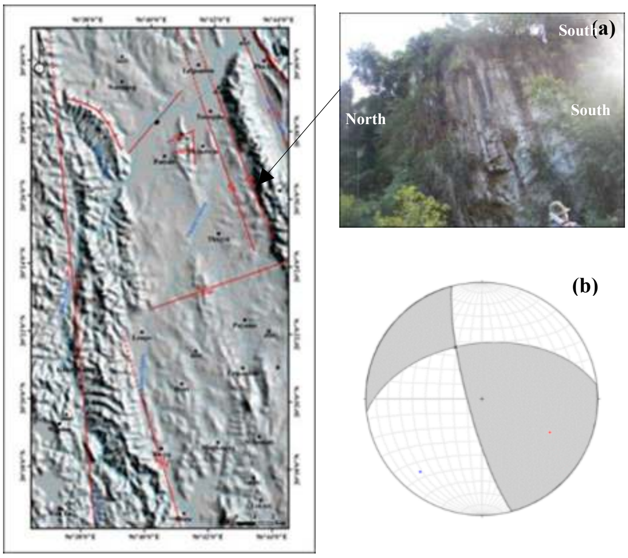

Fig 7: Map showing field data and location of the Pinhmigon right lateral strike-slip fault (a) panoramic view of NNW-SSE trending fault scarp (b) NNW-SSE trending high angle fault formed in Kalaw Red Bed Formation (20°24'41.11"N, 96°43'53.583"E) (c) fault plane solution

Bo-ya fault

This fault is located west of Bo-ya village. It is a right lateral strike-slip fault, trending in NNW-SSE direction. The length of this fault is about 5 miles. It is faulted contact between Nwabangyi Dolomite Formation and Loi-an Group. Fault evidence and stereo plot analysis and related stress orientation are shown in Fig (8).

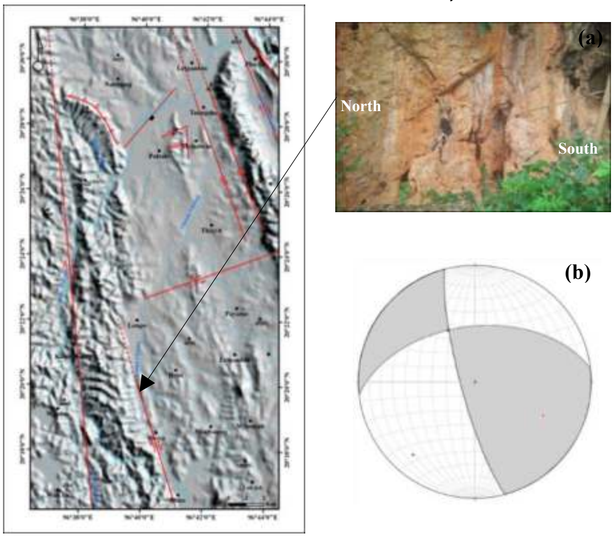

Fig 8: Map showing field data and locality Bo-ya right lateral strike-slip fault (a) NNW-SSE trending fault scarp formed in Nwabangyi Dolomite Formation (20°17'40.333"N, 96°40'54.043"E) (b) fault plane solution

Theingon fault

This fault is located north of Theingon village. It is a left lateral strike-slip fault, trending in ENE-WSW direction. The length of this fault is about 5 miles. It cut across Nwabangyi Dolomite Formation, Loi-an Group, Kalaw Red Bed Formation and Hsi-hkip Formation. Fault evidence and stereo plot analysis and related stress orientation are shown in Fig (9).

One minor E-W trending sinistral lateral strike-slip fault are observed at Dragon Cement Quarry. The length of this fault is about 1 mile. It cut across Thitsipin Limestone Formation and Loi-an Group. Field measurements of slickenplane, stereo plot analysis and related stress orientation are shown in Fig (10).

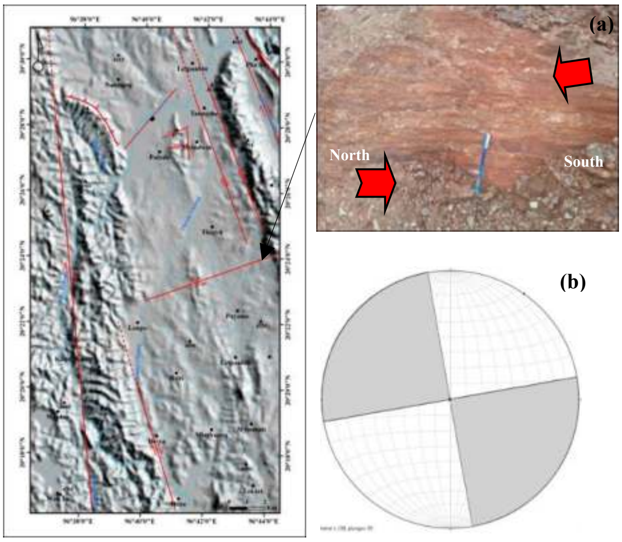

Fig 9: Map showing field data and location of Theingon fault left lateral strike-slip fault (a) left lateral strike slip fault formed in Conglomerate of Kalaw Red Bed Formation (20°26'27.35"N, 96°44'14.208" E) (b) fault plane solution

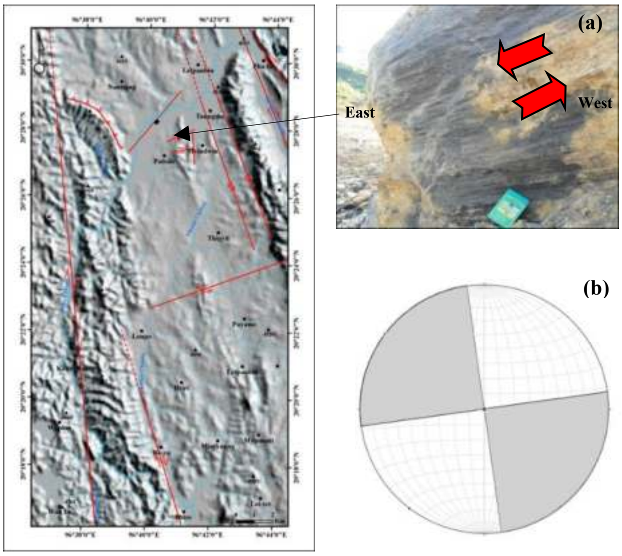

Fig 10: Map showing field data and location of a minor left lateral strike-slip fault (a) slickenside plane formed in carbonaceous mudstone of Loi-an Group (20°27'22.165"N, 96°40'56.459"E) (b) fault plane solution

Thrust fault

One major thrust fault is observed in the study area. The fault plane inclines towards east and thrusting towards the west. Triangular facets are developed along the Thitsipin Limestone range which thrusting on the Loi-an Group Fig (11). Stereo plot analysis of thrust sense shear plane and related stress position are shown in Fig (11).

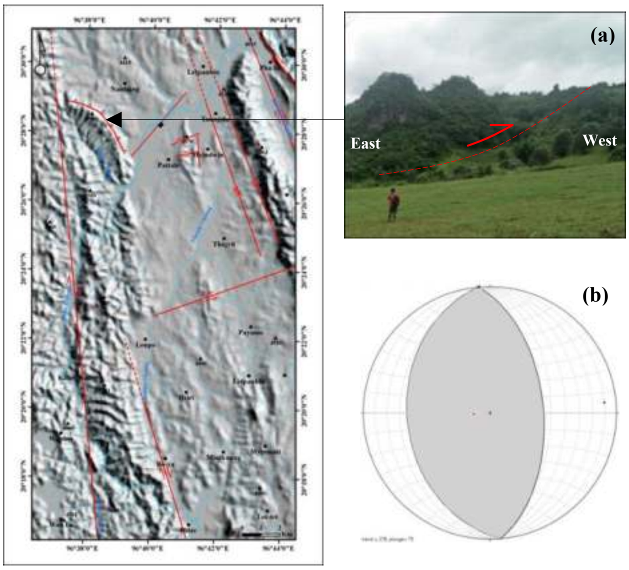

Fig 11: Map showing field data and location of Chaungpwet thrust fault (a) Thitsipin Limestone Formation which are thrusting on the Loi-an Group (20°28'0.58"N, 96°38'50.654"E) (b) fault plane solution

Normal fault

One normal fault, trending in NE-SW direction is observed in the study area. It is located east of Chaungpwet village. The down thrown side is found east of the fault. It is noticed by fault scarp and fault breccias. Triangular facets are developed along the Thitsipin Limestone range (Fig 12). Stereo plot analysis of thrust sense shear plane and related stress position are shown in Fig (12).

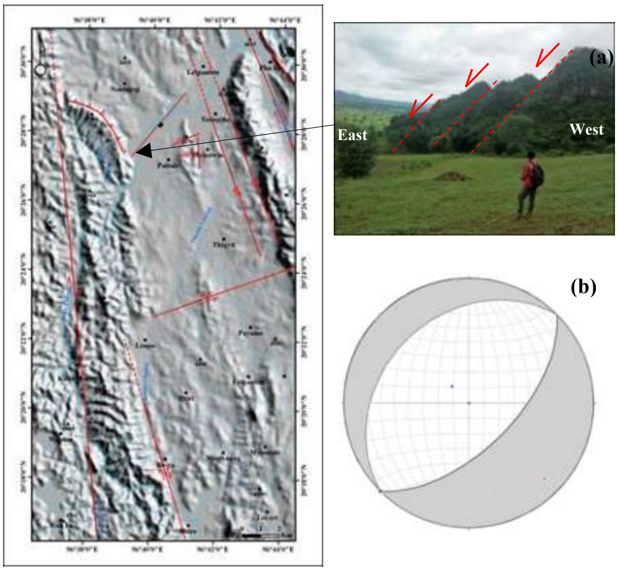

Fig 12: Map showing field data and location of Chaungpwet normal fault (a) a series of triangular facets at the mountain front of the Thitsipin Limestone (20°28'0.58"N, 96°38'50.654"E) (b) fault plane solution

Stress field interpretation of faulting

The orientations of principal stress axes are determined on lower hemisphere, Schmidt projection to get the compressional quadrants (σ1) axis and tensional quadrants (σ3) axis. The distribution pattern of the orientation of principal stress field of faulting is shown in figure (13).

According to stress field distribution, the maximum principal stress axes (σ1) coincide with major force NE-SW trend. However, the directions of the shear fault planes are compatible with the NNW-SSE and ENE-WSW.

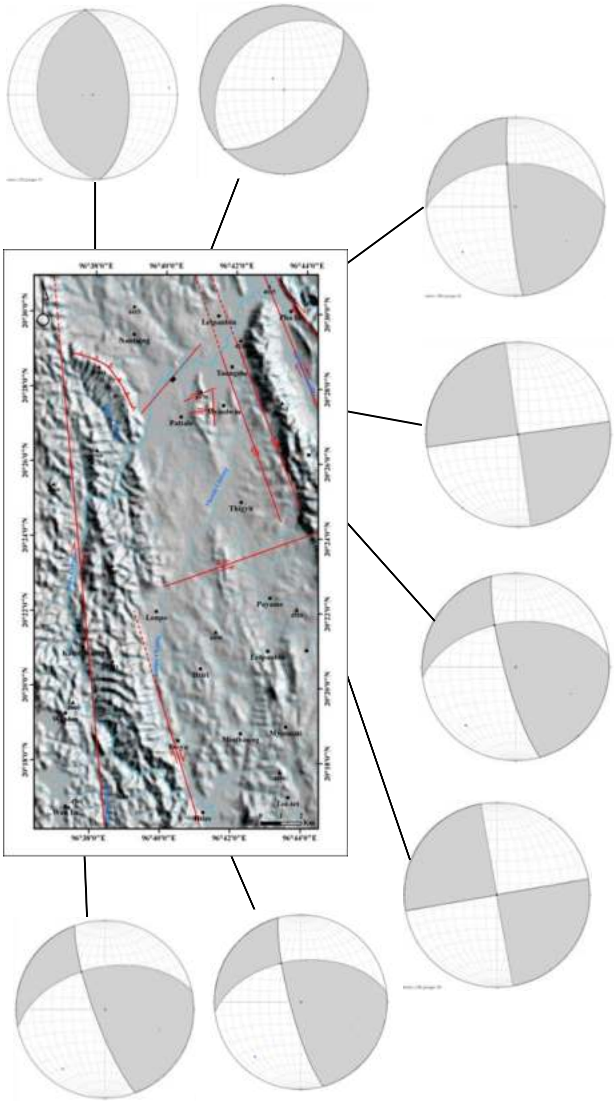

Fig (13) Principle stress distribution pattern based on the stereoplot analysis of the faults in the study area.

7. CONCLUSION

From the overall assessment for the present study concerning with the major faulting, the following inference could be deduced. In the present investigation, major faults of right strike slip faulting are trending nearly N-S and NNW-SSE direction and left lateral strike slip faulting trending NNE-SSW direction. Thrust fault, trending NW-SE direction and normal faulting, trending NE-SW direction are also observed in the study area. According to these studies of faulting, compressional stress field comes from NE-SW direction.

ACKNOWLEDGEMENTS

The authors would like to express my sincere gratitude and thanks to Dr. Htay Aung, Rector (Acting), Loikaw University and Dr. Toe′ Toe′ Win Kyi, Professor and head of geology department, Loikaw University for their kind permission to publish this paper.

REFERENCES

[1] Davis, G.H., & S.J. Reynolds, 1996, *Structural Geology of Rock and Regions*: Second Edition, JohnWiley, New York, 776 p.

[2] Garson, M.S., Amos, B. J., Mitchell, A.H.G., 1976. *The geology of the area around Neyaungga and Ye-ngan, Southern Shan States, Burma*. Overseas Memoir 2, Institute of Geological Sciences, London, pp. 1-70.

[3] Htay Lwin, Thandar Tun, Moh Moh Aye and Shirley Nyein: *The Petrofabric Study of Eastern Part of Pindaya Range, Pindaya Township, Shan state (south)*. (Unpublished)

[4] Myint Lwin Thein. 1973. *The lower Paleozoic startigraphy of the western parrt of the southern shan state*.Geol Soc Malaysia, Bull no. 6, P. 143-163

[5] Ramsay, J.G., & M.I. Huber, 1983, *The Techniques of Modern Structural Geology: Volume1: Strain Analysis*: Academic Press, London.

[6] Ramsay, J.G., & M.I. Huber, 1987, *The Techniques of Modern Structural Geology: Volume2: Folds and Fractures:* Academic Press, London.

[7] Václav Vavryčuk, 2015, *Earthquake Mechanisms and Stress Field*

Design and Layout Plan of Water Distribution System

Swe Swe Tun(1), Nan Yamon Phoo (2)
(1)Technological University (Loikaw), Myanmar
(2) Technological University (Loikaw), Myanmar

Email: sweswetun@tuloikaw.edu.mm

ABSTRACT*:* This study focuses the water distribution design and layout plan for Daw NganYout village. It is rural area and is difficult to dig the wells. Ngwe Taung Dam is chosen as the source of water distribution system and Daw NganYout village is the intended area. The design period is taken as 30 years and present population is about 1030. The design population is calculated by Arithmetical increase method, Geometrical increase method and Incremental increase method. Water consumption for the study area is 15165 lph including domestic use, fire protection and compensates losses and waste. Water from source is transported to the elevated tank by pumping and then distributed to the consumers under gravity flow. Therefore the method of distribution is dual system. The size of elevated tank is 8m length, 4m breadth and 2m depth. The break horse power requirement of pump is 5hp. The main pipe line of future population is 4 in diameter and the sub-main pipe line of present population is 3 in diameter. The values of pressure and velocity are obtained from EPANET software. Dead-end system (Tree system) and Grid-iron system (Reticulation system) are the most suitable systems for the study area.

KEYWORDS: *water distribution system, design period, pipelines, EPANET software and network system.*

1. INTRODUCTION

In this study, the distribution system consists of pump, elevated tank and piping network. Water from source is transported to the elevated tank by pumping flow and then distributed to the consumers under gravity. A water distribution system consists of three major components such as pumps, distribution storage, and distribution piping network.

2. THEORETICAL BACKGROUND

2.1 Population Focusing

Population focusing is one of the most important factors for design of the water distribution system. The increase in population of area depends upon several factors. There are nine methods of population forecasting. They are Arithmetical increase method, Geometrical increase method, Incremental increase method, Decreased rate of growth method, Graphical extension method, Graphical comparison method, Zoning method, Ratio and correlation method and Growth composition analysis method [4]. The following methods are used in this study.

(i) Arithmetical Increase Method

$$P_n = P + nI \tag{1}$$

Where, P_n= future population at the end of n decades
P = present population
I = average increment for a decade

(ii) . Geometrical Increase Method

$$P_n = P\,(1+\frac{I_g}{100})^n \tag{2}$$

Where, P_n = future population at the end of n decades
P = present population
I_g = the average percentage increase per decade

(iii) Incremental Increase Method

$$P_n = P + nI + \frac{n\,(n+1)}{2}r \tag{3}$$

Where, P = present population
I = average increase per decade
r = average incremental increase
n = number of decades

2.2 Consideration on Pipe Sizes and Pumping Power

It is necessary to calculate the diameter of the pipe to meet the required amount of water. Hazen William's formula is used in this study. This is the most widely used formula [1].

$$Q = 0.278\, C\, D^{2.63}\, S^{0.54} \tag{4}$$

$$h_f = 10.70\,(\frac{Q}{C})^{1.852}\,\frac{L}{D^{4.87}} \tag{5}$$

Where, Q = discharge (m^3/sec)
D = diameter of the pipe (m)
S = hydraulic gradient
C = coefficient of roughness of pipe
H = Difference elevation (m)
L = length of the pipe (m)
h_f = head loss due to friction (m)

The pump power is the power required for a pump to lift water to the desired place. It is calculated by the following formulae [1].

$$W.H.P = \frac{QwH}{75} \tag{6}$$

$$B.H.P = \frac{QwH}{75\eta p} \tag{7}$$

Where, W.H. P = water horse power
B.H.P = break horse power
Q = discharge to be pumped
H = total dynamic head
ηp = Efficiency of pump

$$TDH = H = H_{ST} + H_L + H_V \tag{8}$$

Where,

H_{ST} = total static head (or lift), i.e. the elevation difference between the pumping source and point of delivery

H_L = total head loss through the suction and delivery pipe.

H_V = velocity head ($v^2/2g$) at the discharge head.

For diameter of pumping (main)

Lea was the empirical formula for the pipe diameter of pump to be economical and to be the least cost [1].

$$D = a\sqrt{Q} \tag{9}$$

Where, D = diameter of pipe (m)

Q = discharge to be pumped (m)

a = 0.97 to 1.22

2.3 Layout Plan of Water Distribution System

The specific layout of water distribution system is based on type of geography and road networks available on the area. There are four principle methods of laying out distribution system:

(1) Dead End System or Tree System
(2) Grid-iron System or Reticulation System
(3) Circular System or Ring System and
(4) Radial System.

In this study, Dead end system or Tree system is considered according to topography. In this system, one main pipe line runs through the center of the populated area and sub mains takeoff from this to both the sides. The sub mains divide into several branch lines from which service connections are given. Thus the entire distribution area is covered by pipe lines running like a tree. There are no cross-connections between the branches and sub mains. EPANET software is used to analyze the requirement of the pipes. By the use of EPANET that is by filling the data into it about number of nodes, demand, elevation, tanks and pipes.

3. ANALYSIS AND DESIGN OF WATER DISTRIBUTION SYSTEM

3.1 Perdition of Future Population

The first three methods are used in this study because the other methods need many data and it is difficult to get exactly. This study considers two decades (1999 to 2019) for population increment. The following table (1) consists of the computations about increment, % increment and incremental increase per decade for the study area.

Table 1. Increment, % increment and incremental increase per decade

Year	Population	Increment per decade (I)	% increment per decade (I_g)	Incremental Increase (r)	Decrease in % increment
1999	657	-	-	-	-
2009	823	166	25.27	-	-
2019	1030	207	25.15	+ 41	0.12
	Total	373	50.4	41	0.12
	Average	186.5	25.21	41	0.12

(i)Arithmetical Increase Method

P = population in 2019 = 1030

n = number of decades = 3

I = 186.5 (from Table 1)

$P_n = 1030 + 3 \times 186.5$

$= 1590$

(ii) Geometrical Increase Method

$I_g = 25.21\%$ (from Table 1)

$$P_n = 1030\left(1+\frac{25.21}{100}\right)^3$$

$= 2022$

(iii)Incremental Increase Method

I = 186.5

r = average incremental increase = 41 (from Table 1)

$$P_n = 1030 + 3 \times 186.5 + \frac{3(3+1)}{3} \times 41 = 1836$$

The Geometrical Increase Method is suited for the study area because a few decades are collected. Therefore, the future populations for sub main pipe lines are estimated by using Geometrical Increase Method as shown in following table (2).

3.2 Design of Water Distribution System

Water is distributed by dual system. The distribution system designed here is tree system or dead end system and grid-iron or reticulation system.

Fig1. Tentative Layout of the Study Area

EPANET software is used to analyze the requirement of pipes. By the use of EPANET that is by filling the data into it about number of nodes, demand, elevation, tanks and pipes. Pipe diameters are calculated by using Hazen William's formula. The above fig (1) shows the tentative layout of the study area. Table (2) presents the required data for pipeline network.

Table 2. Required Data for Pipeline Network

No	Pipe line	Design Population	Length (ft)	Elevation (ft)		Difference elevation (ft)
				H	L	
1.	AB	2022	293.12	2956	2953	3
	BC	2022	857.71	2953	2951	2
	CD	2022	857.71	2951	2948	3
	DE	2022	1350.7	2948	2934	14
2.	FG	351	1236.4	2958	2930	28
3	HI	373	1162.1	2944	2941	3
4.	JK	310	1182.2	2947	2937	10
5.	LM	236	1413.1	2938	2934	4
6.	NO	752	1920.4	2953	2946	7

The pipe sizes are calculated the demand of the study area. There are one main pipe line (ABCDE) and five sub-main pipe lines (FG, HI, JK, LM and NO). Water consumption for the study area is computed by multiplying the population forecast and the total quantity of water. Table (3) shows the total quantity of water per capita per day.

Table 3. Total Quantity of Water

No.	Types of Water use	Quantity of Water
1.	Domestic use	135 lpcd
2.	Public use including fire protection	30 lpcd
3.	Compensate losses and waste	15 lpcd
	Total	180 lpcd

For main pipe line (ABCDE),

For segment AB,

Total population = 2022

Demand, Q = 2022 × 180

= 363960 lpd

= 4.213×10^{-3} m^3/sec

By using Hazen William's formula,

$$Q = 0.278\, C\, D^{2.63}\, S^{0.54}$$

H = 3 ft (Table 2)

L = 293.12 (Table 2)

$$\text{Hydraulic gradient, } S = \frac{H}{L} = 0.01$$

D = 0.08 m= 0.263 ft (4 in)

For sub main pipe line (FG),

Total Population =351nos

Demand, Q = 351 × 180

= 63180 lpd

= 7.313×10^{-4} m^3/sec

H = 28 ft (Table 2)

L = 1224.51 (Table 2)

S =0.02

D =0.118 ft (1 in)

The following table (4) and table (5) consist of the diameters of the main and sub-main pipe lines for the study area. It is calculated based on the Hazen William's equation.

Table 4. Diameters of Main Pipe Lines

Segment	Demand, $Q \times 10^{-3}$ (m^3/sec)		S = H/L	Current Diameter (in)	Future Diameter (in)
	Current	Future			
AB	2.15	4.213	0.01	3	4
BC	2.15	4.213	0.002	3	4
CD	2.15	4.213	0.002	3	4
DE	2.15	4.213	0.01	3	4

Table 5. Diameters of Sub-main Pipe Lines

Segment	Demand, $Q \times 10^{-4}$ (m^3/sec)		S = H/L	Current Diameter (in)	Future Diameter(in)
	Current	future			
FG	3.73	7.313	0.02	1	2
HI	3.958	7.77	0.003	2	2.5
JK	3.292	6.458	0.008	1	2
LM	2.5	4.917	0.003	1	2
NO	7.98	0.1567	0.004	2	3

For design population, 4 in diameter for main pipe line (ABCDE) and 3 in diameter for sub-main pipe line (FG, HI, JK, LM and NO) are estimated.

3.3 Calculation of Pumping Power Requirement

Pumps are used to provide water flow between water source and water distribution network. In this study, water is to be lifted from the source to the elevated tank. So, the required horse power of pump is computed [5].

According to surveying data,

Elevation of tank = 2956 ft

Elevation of source = 2934 ft

Tank height = 30 ft

Tank depth = 7 ft

Suction head = 8 ft

Length of pipe = 2218.68 ft (676.25 m)

TDH $= H = H_{ST} + H_L + H_V$

Total static head, $H_{ST} = (2956 - 2934) + 30 + 7 + 8$

$= 67$ ft

By using Lea's formula, $D = a\sqrt{Q}$

$$Q = 30330\text{lph} = \frac{30330}{1000 \times 3600} = 8.425 \times 10^{-3}\ \text{m}^3/\text{sec}$$

$$a = 1.22,\ D = 1.22\sqrt{8.425 \times 10^{-3}} = 0.1\ \text{m (4 in)}$$

Total head loss, $H_L = H_f$

$$= 10.70\left(\frac{Q}{C}\right)^{1.852}\frac{L}{D^{4.87}}$$

$= 8.185$ m (27ft)

$$\text{Velocity head, } H_v = \frac{v^2}{2g} = \frac{Q^2}{A^2 \times 2g} = 0.06\ \text{m (0.2ft)}$$

TDH , H $= 67 + 27 + 0.2$

$= 94.2$ ft (29 m)

$$\text{W.H.P} = \frac{QwH}{75} = \frac{8.425 \times 10^{-3} \times 1000 \times 29}{75}$$

$= 4$h.p

$$\text{B.H.P} = \frac{QwH}{75\eta_p} = \frac{8.425 \times 10^{-3} \times 1000 \times 29}{75 \times 0.7} = 5\text{h.p}$$

Therefore, the horse power requirement of pump is 5 h.p. The pump efficiency for pumping system (half load) is 70 % [1].

3.4 Results from EPANET Software

The distribution network of the study area for design population is obtained and analyzed. The entire distribution network consists of 16 pipes of same materials, 15 junctions, 1 tank and 1 source reservoir from which water is pumped to the elevated service reservoir. The following table (6) shows network table for nodes and table (7) describes the network table for pipes.

Table 6. Network Table for Nodes

Node ID	Elevation (ft)	Base Demand (CFS)	Pressure (psi)
N-3	2941	0.028	0.3
N-4	2953	0.028	2.09
N-5	2953	0.014	3.4
N-6	2953	0.014	3.26
N-7	2958	0.014	1.07
N-8	2944	0.014	7.08
N-9	2947	0.014	5.76
N-10	2938	0.014	9.64
N-11	2934	0.014	11.37
N-12	2930	0.0024	13.2
N-13	2941	0.0025	8.38
N-14	2937	0.0021	10.09
N-15	2934	0.0016	11.38
N-16	2954	0.0051	2.96
N-17	2946	0.0051	6.42

Table 7. Network Table for Pipes

Pipe ID	Start Node	End Node	Length (ft)	Diameter (in)	Roughness	Velocity (fps)
P-1	1	3	221.38	4	140	6.29
P-2	3	4	1701.24	4	140	3.12
P-3	4	2	305.51	4	140	3.28
P-5	2	5	293.12	4	140	0.67
P-6	5	6	857.71	4	140	0.53
P-7	6	7	265.74	4	140	0.45
P-8	7	8	684.08	4	140	0.36
P-9	8	9	664.68	4	140	0.26
P-10	9	10	564.12	4	140	0.17
P-11	10	11	610.82	4	140	0.08
P-12	7	12	1236.44	3	140	0.02
P-13	8	13	1162.06	3	140	0.03
P-14	9	14	1182.2	3	140	0.02
P-15	10	15	1413.08	3	140	0.02
P-16	5	16	385.86	3	140	0.1
P-17	16	17	1534.5	3	140	0.05

The following figure (2) shows the pressure-velocity distribution of the study area, which shows the variation of velocity in different pipes with respect to the pressure provided to the particular pipe line. Then, the following figure (3) describes the base demand-flow distribution of the study area; figure (4) illustrates demand-unit head loss distribution of the study area which describes between demand rate and amount of head loss at each node. The following figure (5) consists of the head-friction factor distribution of the study area that is between demand rate and amount of head loss at each node.

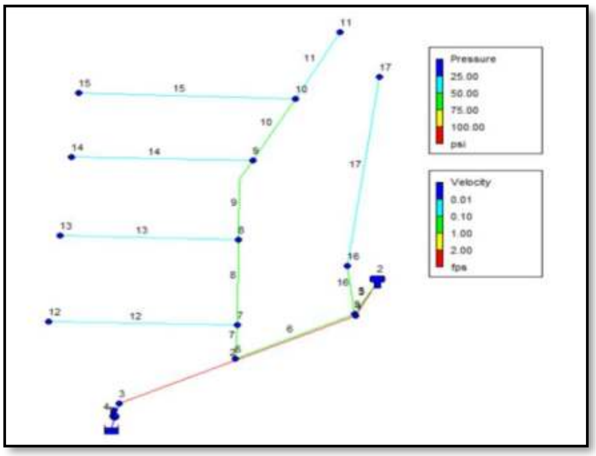

Fig 2. Pressure-Velocity Distribution of the Study Area

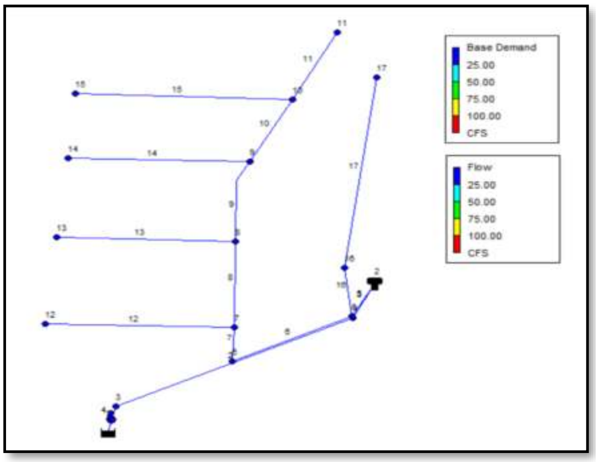

Fig 3. Base Demand-Flow Distribution of the Study Area

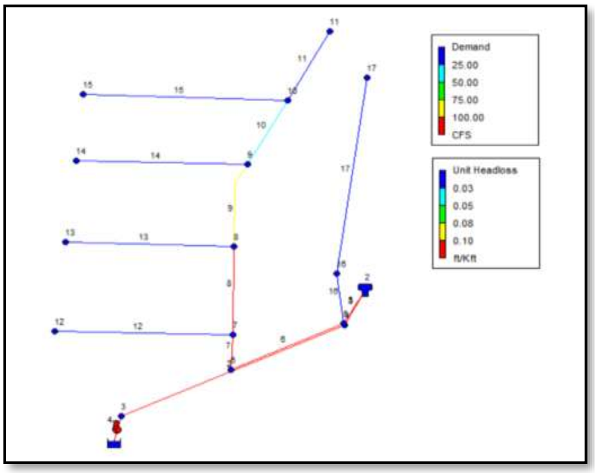

Fig 4. Demand-Unit Head Loss Distribution of the Study Area

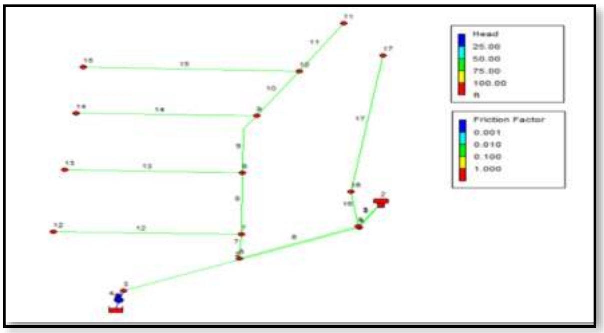

Fig 5. Head-Friction Factor Distribution of the Study Area

4. CONCLUSIONS

In this study, the network contains one main pipe line, five sub-main pipe lines, a supply pipe line, a pump and an elevated reservoir. For current population, the main pipe line is 3 in diameter, the sub-main pipe lines are 2 in and 1 in diameter respectively.

For 30 years, design flow is based on estimated future requirements. Geometrical increase method is the most suitable method of population forecast and so it is used to calculate the design population of Daw Ngan Yout village. For future population, the main pipe is 4 in diameter and the sub-main pipe diameter is 3 in diameter respectively. The material of supply and distribution pipes is PVC pipes. Dead-end or Tree system and Grid-iron or Reticulation system are used as a method of layout of distribution system in the study.

ACKNOWLEDGEMENT

The author would like to express her deepest gratitude to Dr. Zaw Win Aung, Pro rector of Technological University (Loikaw), for his invaluable permission and encouragement to carry out this study. The author would like to express her thanks to sincere gratitude and indebtedness to her colleagues, Daw Nan Yamon Phoo, Assistant Lecturer of Civil Engineering Department, Technological University (Loikaw), for her precious advices, invaluable encouragement, and her help throughout the study.

REFERENCES

[1] Dr.B.C Punmia,Er.Ashok K.Jain and Dr.Arun K.Jain,1995, 'Environmental Engineering',Second edition.

[2] AviOstfeld (2001). "Reliability Analysis of Regional Water Distribution Systems, Urban Water", 3, 253-260.

[3] B S N Raju, 1995, ' Water Supply and Wastewater Engineering,' Tata McGraw Hill Publishing Company Limited, New Delhi.

[4] Howard S. Peavy, 1985, 'Environmental Engineering', Mc Graw-Hill Book Company; International Edition, Singapore.

[4] V. M. CHERKASSKY, 1980, "Pumps Fans Compressors" Mir Publishers, Moscow.

[6] Alperovits, U. (1977). "Design of Optimal Water Distribution Systems." Water Resources Research, Vol. 13[6], pp. 885-900.

Engineering Geology of Nancho Multipurpose Dam Project

Hline Wint Wint Hmue [1], Thin Thin Hlaing [2]
[1] Technological University (Lashio), Myanmar
[2] Technological University (Mawlamyaing), Myanmar

Email: hlaingwintwinthmue@tulashio.edu.mm, soeh41526@gmail.com

ABSTRACT: Nancho Hydropower Project is located at about 16 miles far from the eastern part of Pyinmana Township, Mandalay Region. Engineering Geological study, geological study and data analysis are used for investigation of Nancho dam Project. The type of dam is Conventional Vibrating Concrete dam (CVC). This Project was selected as a run-off river type, narrow valley, good strength in bed rock and easily get the construction materials near the project site. The Nancho area is in the strongly deformed zone and emplacement of granite and related rock types occurred probable during late Mesozoic. Most of the pegmatite veins occur parallel to the foliation in the gneissose granite. The engineering geological study is carried out GSI, RMR, slope stability analysis. The study area is situated in the two major fault zones: Paunglaung fault in the east and Sagaing fault in the west. The generally trend of the fault line is nearly NNW-SSE direction. Construction materials are mainly composed of cement, river sand, pozzolith and rock aggregated.

KEYWORDS: *good strength, GSI, RMR, major fault.*

1. INTRODUCTION

Nancho hydropower project is constructed by Department of Hydropower Implementation, Ministry of Electric Power No (1) in cooperation with Colenco Geotechnical Engineering Co., Ltd. This is designed to have an installed capacity of 40 NW (2 × 20 MW) and is planned to produce average annual energy of 152 million kilo watt hour. Maximum dam height is 167 ft, and length is 443 ft. The catchment area is 317 sq miles.The type of the dam is Conventional Vibrating Concrete Dam. It is the first kind of concrete dam design in Myanmar.

Engineering geological investigation of Nancho Hydropower Project was carried out from 1 to 4 May in 2012 by Post Graduated Diploma in Engineering Geology Students, Yangon Technological University. The primary objectives of study are: to classify the lithologic unit of the study area, to study the influence of engineering geological factors on this project, to analyze the RMR and Q-system classification for tunnel and to identify the reinforcement base on RMR and Q-system result.

According to Yin Min Htun(2012),among several methods of tunneling Full Face method was applied in the Nancho Hydropower Project.

1.1 Location, Physiography and Drainage

Nancho Hydropower Project is located at about 16 miles east of Pyinmana, Mandalay Region. The study area is bounded by North latitude 19˙42' to 19˙47' and East Longitude 96˙25' to 96˙30'. Map index number of the study area is 94A/6 (Figure 1). The study area is approximately 4 square miles.

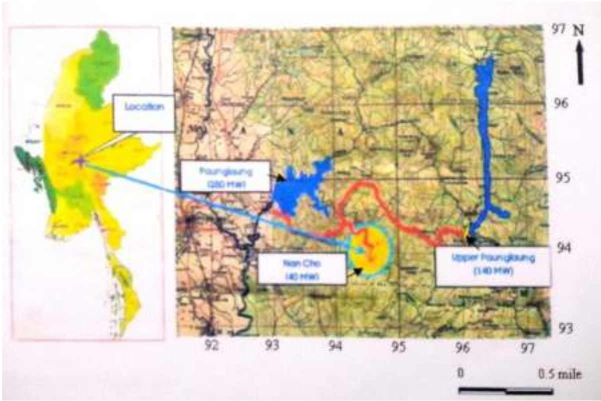

Fig 1 The Location Map of the Nancho Area

The Nancho area is a mountainous region generally with hills and valleys. In this area, the highest point is about 3785 ft and the lowest point is about 385 ft above sea level. Overburden soil is mostly thin to medium and gradually thick to the flanks of the mountains.

The Nancho Chaung is the major stream and Salu Chaung, Sadaw Chaung and Saungdaung Chaung are the tributaries of Nancho Chaung. The drainage pattern of the study area is medium to coarse dendritic pattern with few angular band (Figure 2).

1.2 Climate and Vegetation

As the study area has the tropical monsoon climate with the average annual rainfall of about 65″, the tropical forest yields a large number of valuable hardwood trees. Paunglaung Reserved forest is in the southern part of the study area.

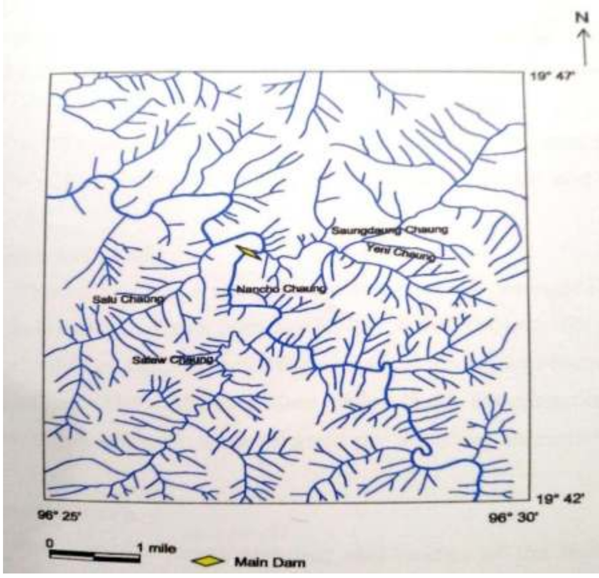

Fig 2 Drainage Pattern of Nancho Area

1.3 Purpose of the Study

To study the geological setting of the study area and influence of engineering geological factors on Nancho Hydropower Project.

1.4 Method of Study

Engineering geological data are obtained from field observation and local geological frame work, and geotechnical investigation. The collected data from field investigation used to establish the comprehensive engineering geological profile along tunnel alignment.

2.REGIONAL GEOLOGY OF THE STUDY AREA

The study area occupies the western edge of the Shan Plateau, which is bounded by the Paunglaung fault zone running about 13km in the East with NNW-SSE direction. In the area, granite intrusion took place in the Mesozoic to Cenozoic Era. The main rock type is granite, which is very hard and uniaxial compressive strength is about 115.8 MPa. Moreover quartzite, gneiss, schist and sandstone are found the minor rock type. Granite in this area is whitish to pale grey, boundinage structure in (Fig; 3) and pure granite, which is fine-grained to coarse-grained. Pegmatite veins intruded in granitic gneiss. Overburden soils are red and buff to yellowish brown colour, silty and clayey soils. The geological condition in the site is good condition.

Fig 3 Boundinage Structure in Right Abutment

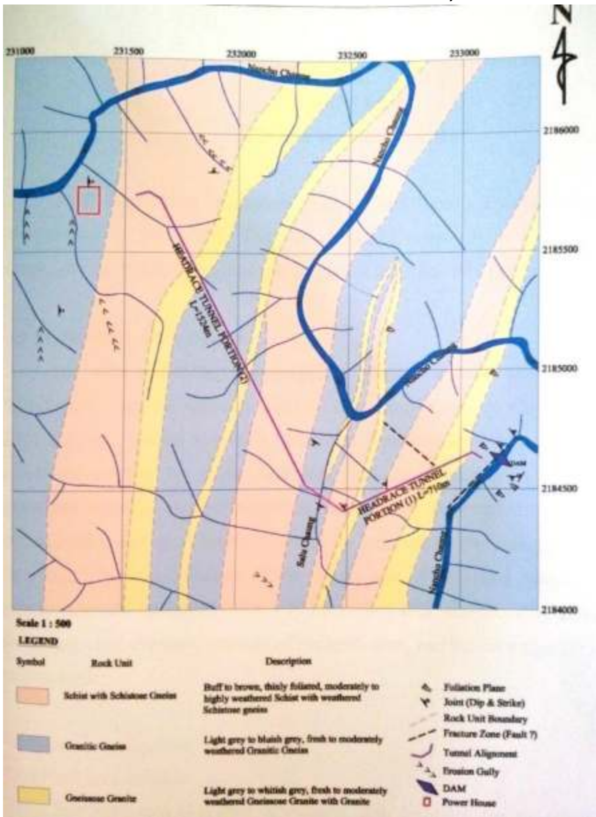

Fig 4 Geological Map of the Nancho Area
Source: Adapted from DHP-1

2.1 Detailed Geology of Nancho Area

In this region, buff to brown, moderately to highly weathered schist, thinly foliated schist occurs as a thin layer between the gneissose granite rock. Granitic gneiss is well exposed on both sides of the Nancho Chaung and in western part of the main dam. The rocks are exposed light grey to bluish grey, fresh to moderately weathered granitic gneiss (Figure 5). Lenses and banding are noteworthy.

Gneissose granite is well exposed on both abutments of main dam. Pegmatite vein is intruded into the gneiss with NW-SE trend. The rocks are strong and medium to thick bedded, light grey to whitish grey, fresh to moderately weathered gneissose granite. Around the dam axis, the exposed rock is good for dam construction.

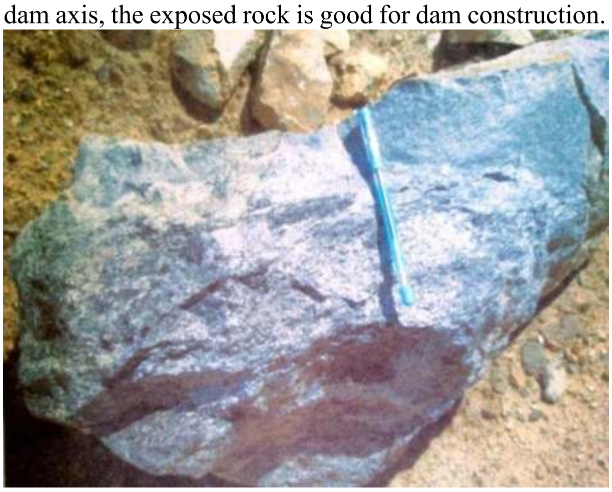

Fig 5 Granitic Gneiss in Quarry Site

2.2 Structural Geology of the Project Area

Structural geology of the site area is complex. The strike of the rock formation generally trends the direction of NNW-SSE. However, strike variations can be occurred from its general condition to the direction of E-W dipping.

The project site is located between Panlaung fault and Sagaing fault. In study area, the prominent fault line is located near the Headtank and trending nearly NNW-SSE direction. Some small faults are found crossing the major fault. Two fault lines are cutting across the direction of the tunnel alignment. Along the fault line, many joints and slickenside are observed.

The rock outcrops are moderately to highly jointed. There are having mainly two joint sets and random joint. Major joints are commonly long and generally vertical direction. The orientation of joints is measured. Joints are opened and other were filled with clay.

Fig 6 Fault at Right Abutment (EL 300 m)

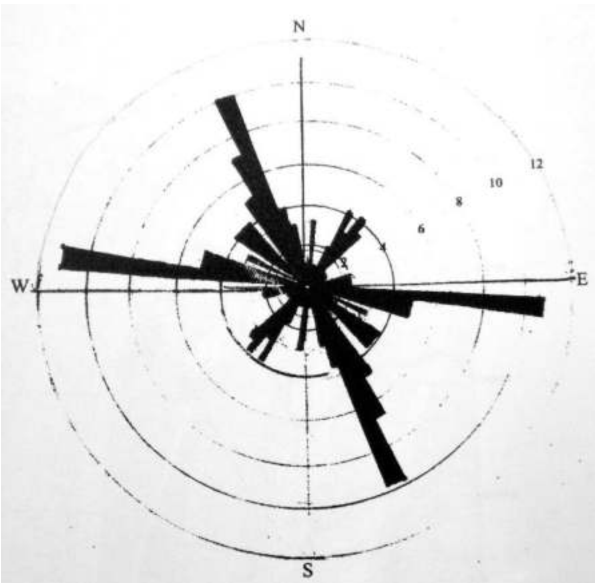

Fig 7 Strike Rose Diagram

2.3 Seismicity of the Study Area

The study area falls on the active earthquake zone. Some of great earthquakes have taken place along the Sagaing fault, which runs in N-S direction.

The seismic data suggest that the earthquake intensity ranges from low to moderate but some might be strong with Modified Mercalli scale 7.5 to 8.5. The value of g of the project area is within 0.05 to 0.1 ranges. (Source from DHP-1)

3. RESEARCH PROCEDURES

3.1 Preliminary Investigation

For the preliminary investigation stage, regional geological map and topographic maps are observed to get the information about the study area. Before the field trip, the ground condition, lithologic characteristics, structure geology are carefully studied by using structural geological map of Myanmar, regional geological map and aerial photographs. By studying topographic map to identify the estimate lithology by estimate; lithology by interpreting the drainage pattern and to estimate the possible structure of the project area. By studying Aerial photographic map to study the structural features of the project area, and literature survey to study the geology and structural geology of the study area, and the investigation stage of the project area.

3.2 Detail Investigation (Field Investigation)

For RMR and Q-system calculation, four locations are classified along the Headrace tunnel alignments. For RMR and Q-system parameters the dip and strike of bedding plane or foliation plane, joint plane, fault plane, slope angle, joint amount and direction, joint spacing and joint aperture were measured. Besides, joint filling and joint water condition were studied. The weak zone along the tunnel alignment was explored. By studying drill core logs can study the lithology and structure of the tunnel, the drill core quality for RQD, and can estimate calculation of rock quality designation (RQD).

3.3 Field Geological Data

In this section were measured geological characteristics and taken engineering geological works. They are discontinuity characteristics, bedding nature and slope gradient, distribution of rock units, drilling record or borehole data, mapping of all the excavations, foundation improvement works and grouting works. Strength of rocks can be estimated on the base of field geological data by using GSI (Geological Strength Index) method and RMR (Rock Mass Rating).

3.4 Laboratory Analysis

Laboratory tests are used for the purposes of determining the properties of the materials such as strength, mineral composition and for future reference. Representative samples are taken from the field.

3.5 Result Interpretation

The results from RMR and Q-System calculations were interpreted to know the rock mass class in tunnel and to estimate the stand-up time for tunnel support system.

3.6 Report Writing

Report writing is carried out by combining writing of the results from laboratory analysis, RMR and Q-system calculation, and tunnel sequence, conclusion and recommendations.

4. EVALUATION OF ROCK MASS QUALITY

The rock mass quality is identified by using Geological Strength Index (GSI) and Rock Mass Rating (RMR) system for dam site foundation. GSI values are attempted based on the intervals of volumetric joint count (J_v) and corresponding descriptions for the blocking rating, structure rating (SR) and surface condition rating (SCR).

4.1 Evaluation by Rock Mass Rating (RMR)

Evaluation of RMR is based on the compressive strength of the rock, drill core quality, spacing of joints, joint condition, ground water condition, joint orientations and geomechanics classification of rock masses. For example, evaluation by RMR of the right side of the intake tunnel is shown in Table 1.

Table 1 (a) Evaluation by RMR System (Location-200 ft from portal)

No	Classification Parameter	Description	Rating
1.	Strength of Rock (MPa)	115.8	12
2.	(RQD) Rock Quality Designation	82.5%	17
3.	Spacing of discontinuities	0.35 m	15
4.	Condition of discontinuities	rough, unweathered	19
5.	Groundwater condition	Dry	15
Rating			78

Description of rock type	Class No.	Adjustment for orientation of joint	Total Rating
Good rock	II	-0	78

Table 1 (b) Evaluation by RMR System (Location-315 ft from portal)

No	Classification Parameter	Description	Rating
1.	Strength of Rock (MPa)	115.8	12
2.	Rock Quality Designation	82.5%	17
3.	Spacing of discontinuities	0.7 m	15
4.	Condition of discontinuities	rough, moderately	13
5.	Groundwater condition	wet	7
Rating			64

Description of rock type	Class No.	Adjustment for orientation of joint	Total Rating
Good rock	II	-2	62

Table 2 (a) Evaluation by Q-system (Location-200 ft from portal)

No	Description	Accessment	Value
1	Rock Quality Designation (RQD)		82.5%
2	Excavation Support Ratio (ESR)	Portal intersections	1
3	Span (B)		5.32m
4	Number of Joint Sets (J_n)	Two joint sets + Random	6
5	Joint alteration (J_a)	Slightly alter	2
6	Roughness of joint (J_r)	Rough and irregular undulating	3
7	Joint water reduction factor(J_w)	Minor inflow	1
8	Stress Reduction Factor (SRF)	σ_c/σ_1 =115.8/5.2 =22.27	1
$Q = \frac{RQD}{Jn} \times \frac{Jr}{Ja} \times \frac{Jw}{SRF} = \frac{82.5}{6} \times \frac{3}{2} \times \frac{1}{1} = 20.625$			13(support category)
Parameter support= Systematic bolting, untensioned, grouted, tempory support=none			
Rock mass quality for tunneling	Good rock		

$$\text{Support estimate} = \frac{B}{ESR} = \frac{5.32}{1} = 5.32$$

$$\text{Length} = 2 + \frac{0.15B}{ESR} = 2 + \frac{0.15 \times 5.32}{1} = 2.798\text{m}$$

Table 2 (b) Evaluation by Q-system (Location-portal)

No	Description	Accessment	Value
1	Rock Quality Designation (RQD)		82.5%
2	Excavation Support Ratio (ESR)	Portal intersections	1
3	Span (B)		5.32m
4	Number of Joint Sets (J_n)	Three joint sets	9
5	Joint alteration (J_a)	Slightly alter	2
6	Roughness of joint (J_r)	Rough and irregular undulating	3
7	Joint water reduction factor (J_w)	Medium inflow, occasional outwash of joint fillings	0.66
8	Stress Reduction Factor (SRF)	σ_c/σ_1 =115.8/5.2 = 22.27	1(medium stress)
$Q = \frac{RQD}{Jn} \times \frac{Jr}{Ja} \times \frac{Jw}{SRF} = \frac{82.5}{9} \times \frac{3}{2} \times \frac{0.66}{1} = 9.08$			17(support category)
Parameter support= Shotcrete 2-3 cm			
Rock mass quality for tunneling	Fair rock		

$$\text{Support estimate} = \frac{B}{ESR} = \frac{5.32}{1} = 5.32$$

$$\text{Length} = 2 + \frac{0.15B}{ESR} = 2 + \frac{0.15 \times 5.32}{1} = 2.798\text{m}$$

4.2 Geological Strength Index (GSI)

GSI is based on visual inspection of geological conditions. Hoek and Brown (1997) devised simple charts for estimating GSI based on the following two correlations.

GSI = RMR – 5 for GSI ≥ 18 or RMR ≥ 23

= 9 log Q + 44 for GSI < 1

$$Q = \frac{RQD}{Jn} \times \frac{Jr}{Ja} \times \frac{Jw}{SRF}$$

Where,

Q = modified tunneling quality index

RQD = Rock Quality Designation

J_n = Number of Joint Sets

J_r = Roughness of the most important joints

J_a = the wall rock condition and/or filling material

J_w = the water flow characteristics of the rock

SRF = Stress Reduction Factor

RMR = Rock mass rating

4.3 Calculation of GSI Value

Volumetric joint count (J_v)

$$Jv = \left[\frac{1}{J1} + \frac{1}{J2} + \frac{1}{J3} + \cdots + \frac{Nr}{5}\right]$$

For example: J_1= 0.5 m, J_2= 0.4 m, J_3 = 0.2m,
No of random joint (Nr) = 10

$$Jv = \left[\frac{1}{0.5} + \frac{1}{0.4} + \frac{1}{0.2} + \frac{10}{5}\right] = 11.5\text{m}$$

(i) Structure Rating (SR)

Sr = 79.8 – 17.5 ln (J_v)

= 79.8 – 17.5 × 2.44 = 37

(ii) Surface Condition Rating (SCR)

SCR = $R_r + R_w + R_f$

Table 3 (a) Surface Condition Rating (SCR)

Roughness	Very Rough	Rough	Slightly Rough	Smooth	Slickensided
Rating (R_r)	6	5	3	1	0
Weathering	None	Slightly Weathered	Moderately Weathered	Highly Weathered	Decomposed
Rating (R_w)	6	5	3	1	0
Infilling	None	Hard <5 mm	Hard >5 mm	Soft <5 mm	Soft >5 mm
Rating (R_f)	6	4	2	2	0

GSI value can be known by placing SR and SCR values on the GSI chart. Table 3(b) is picked up according to actual rock mass classification in discontinuity surface condition.

Table 3 (b) Modified Quantitative GSI System (Harun Sonmez, Resat Ulusay, 2002)

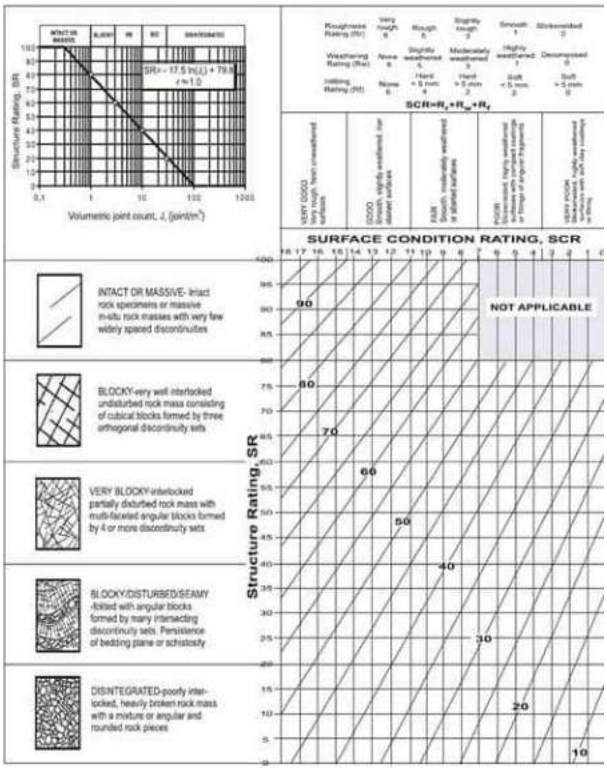

4.4 GSI Value in Left Abutment

The value of volumetric Joint (J_v) is at least from 7.2 to 13.6. The value of SR is changing from 34.1 to the point 45. The value of SCR is among 11 to 12.5. The smallest value of GSI is 47 to 60.

4.5 GSI Value in Right Abutment

The value of volumetric Joint (J_v) is at least from 9.3 to 13.6. The value of SR is changing from 34.1 to the point 41. The value of SCR is among 7.5 to 15. The value of GSI is 35 to 53.

4.6 GSI Value in Dam Foundation

The value of volumetric Joint (J_v) is at least from 6.3 to 9.3. The value of SR is changing from 41 to the point 47.6. The value of SCR is among 8 to 17. The value of GSI is 43 to 64.

5. SUPPORTING SYSTEM FOR TUNNEL CONSTRUCTION

5.1 Steel Rib Installation

Along the tunnel alignment, gneiss, granite and gneiss-granite rocks are exposed. So only in the portal portion of the tunnel, steel ribs are systematically installed in 1.5 to 2 m interval. Steel ribs are connected by 5.5 m diameter connection bar steel rib installation. In tunnel phase, 4 steel ribs are used in canopy and 17 steel ribs in entrance part of the tunnel. In tunnel phase 2, only 8 steel ribs were placed in canopy as shown in Figure 8.

Fig 8 Steel Rib Installation in Nancho Tunnel

5.2 Rock Bolting

The rock bolt pattern or the number of rock bolt depends on the weight of the block and the nature of joint in the block. The length of the rock bolt is 3m and the diameter of rock bolt is 25 mm. The rock bolts are performed in conjunction with unstable rocks for the purpose to provide resistance to sliding and collapse. Rock bolts are provided for the unstable rocks in the tunnel crown and tunnel face to improve strength, deformation and stability as shown in Figure 9.

Fig 9 The Rock Bolting in the Tunnel Crown

5.3 Shotcreting

In Nancho Hydropower Project, shotcreting was mostly carried out on the excavated surface of tunnel portal area and on the left side of the head tank slope. The shotcreting is performed for the purpose to reduce weathering in weak rocks, to provide the slope surface protection and to reinforce fracture rock masses in slopes and tunnels. The materials consist of a dry-mix mortar (sand and cement) with aggregates, which are projected by air jet directly onto the rock face covered with wire meshes. Rocks bolts are often used in conjunction with the shotcrete to increase the reinforcement effectiveness.

5.4 Lining

Concrete lining is performed in tunneling after the other support had been constructed. The lining is most often cast-in-place at the tunnel face by the use of a steel frame work. Concrete lining covers the roof and the wall of the tunnel. After 5m supporting have done, concrete lining is made one by one. Concrete lining is required to prevent friction loss, to keep water velocity and to maintain the tunnel stabilization. Concrete lining thickness in Nancho Hydropower Tunnel is 0.5m.

5.5 Grouting

Grouting is defined as the injection of fluidized materials into voids of the ground or spaces between the lining and the wall rock. Types of grouting used in Nancho Hydropower tunnel are consolidation grouting, joint grouting and backfilled grouting.

5.6 Concrete Replacement

The concrete replacement is generally performed for weak zone existing locally, such as faults, partial weathered zone, weak layer, etc. in the tunnel as a dental treatment. The depth of replacement is generally determined by the following equation.

$$D = 1.5\text{-}3.0 \times W$$

Where, D = replacement depth

W = width of weak zone

After planning the dental concrete, consolidation grouting is generally performed.

6. CONSTRUCTION MATERIAL

Structural concrete for project is composed of cement, sand and coarse aggregate and water.

6.1 Quarry Site

Quarry site is situated at the eastern part of the dam site. Granitic gneiss rocks are exposed in quarry site. It can produce for dam construction. Typical product sizes are 5 mm, 20 mm, 40 mm and 80 mm. The quarry site area of the Nancho Hydropower project is shown in Figure 10.

Fig 10 Quarry Site Area

6.2 Pozzolan

Pozzolan is a kind of volcanic tuff. Pozzolan is used to reduce high cost and to get good strength. Pozzolan is not only strengthen and seal the concrete, they have many other beneficial features will realize.

The pozzolan is defined as a siliceous and aluminous material, which in itself possesses little or no cementing property but to a finely divided form and in the presence of moisture-chemical react with calcium hydroxide at ordinary temperatures to form compound possessing cementations properties.

7. CONCLUSIONS

Nancho Hydropower Project is located approximately 25.7 km away from the eastern part of Pyinmana Township, Mandalay Region. The type of dam is Conventional Vibrating Concrete Dam (CVC). The project is constructed by Ministry of Electric-Power No (1) Nancho Hydropower project is designed to have an installed capacity of 40 MW (2 × 20 MW). Maximum dam height is 167 ft and the length of dam is 443 ft. Average annual inflow of Nancho area is 767110 Acre ft and catchment area is 821 km^2. Nancho CVC dam type is selected depending upon the factors such as bed rock is strong, steam valley is narrow, run-off river type and required construction materials can be obtained easily near the project area. Nancho area consists of hard granite, gneiss and granitic gneiss are found along the tunnel alignment. Mainly granite intrusions took place in the Mesozoic to Cenozoic Era. All rocks are slightly to moderately weathered, strong and thick to medium bedded with light to dark grey in color. Average compressive strength of the study area is between 115.8 MPa and 135 MPa respectively. The strike of the rock formation generally trends the direction of NNW-SSE. The major structure found in the study area is parallel to the generally strike of the rock formation. The two major faults which are found in the study area Panung Laung fault in east and Sagaing fault in west of study area. The quarry site is located in the south-east of main dam. Nancho CVC concrete aggregates for the project construction are composed of Portland cement, pozzolan, pozzolith, fine and coarse aggregate.

ACKNOWLEDGEMENT

We have to our gratitude firstly to Professor Dr. Kyaw Htun (Retire) Head of Engineering Geology Department (YTU) for his kind of permission to carried out this research and his closely supervision, critically reading the manuscript, valuable suggestions and editing. We would like express our thanks to Professor Dr. Khin Soe Moe, Head of Engineering Geology Department (YTU) for her advice, suggestion and encouragement throughout the duration of this research.

Especially, this project is supported by the authorities of the Ministry of Electric Power No (1), Department of Hydropower Implementation and special thanks are due to U Kyaw Nyein (SE), U Nyein Chan (SE) (Director of Construction (1) and U Aye Lwin (Executive Engineer), U Aung Myint (AE) Civil, U Kyaw Kyaw Lwin (AE), U Soe Moe Naing (SAE) for their providing field facilities and sharing experiences during field observation. We wish to express our thanks to all people who helped in our research during May, 2012.

REFERENCES

[1] Aye Lwin. “Geology Report on Nancho Hydropower Project,” Department of Geology, Ministry of Electric Power No (1), unplished.

[2] Yin Min Htun, “Engineering Geological studies and Assessment of Headrace Tunnel in Nancho Hydropower Project.” MSc; Thesis, University of Yangon. 2012.

[3] Yu Maung. “Lecture Notes on Geomechanics for Mining Engineers.” Ministry of Sciences and Technology.

[4] Student’s Dissertation. “Geotechnical Investigation of Headrace Tunnel in Nancho Hydropower Project.” Diploma in Applied Geology Department D.A.G. Engineering Geology. 2010.

[5] Student’s Dissertation. “Comparison of RCC Dam Type and CVC Dam Type of Upper Paunglaung and Nancho Hydropower Project.” Post Graduate D.A.G. Engineering Geology. 2012.

[6] Bieniawski. Rock Mass Rating, Cited in “Engineering Geology for Civil Engineering,” Ministry of Higher Education. 1989.

[7] Deer. Rock Quality Designation Index, Cited in “Engineering Geology for Civil Engineering,” Ministry of Higher Education. 1964.

[8] Hoke and Brown. Rock Mass Rating, Cited in “Engineering Geology for Civil Engineering,” Ministry of Higher Education. 1997.

[9] Hoke, E et al.. “Variability of Engineering Properties of Rock Masses Quantified by the Geological Strength Index” The Case of Ophiolites with Special Emphasis on Tunneling, Volume: 65, Issue: 2, Publisher: Springer, 2005, pp.129-142

DESIGNING, PLANNING AND SCHEDULING OF RIGID PAVEMENT OF THA HTAY KWIN–MAUNGE MA ROAD

Lei Lei Win [(1)], Nyan Phone [(2)]
[(1)] Department of Civil Engineering, Technological University (Thanlyin), Myanmar
[(2)] Department of Civil Engineering, Technological University (Thanlyin), Myanmar
leileiwin8888@gmail.com
nyanphone.civil@gmail.com

ABSTRACT: This study deals with the design of rigid pavement for Tha Htay Kwin-Maunge Ma road. The length of the road is 18 miles and 4 furlongs. The design life is considered as 20 years. The estimate Average Daily Traffic (ADT) and the design Equivalent Single-Axle Loads (ESAL) are calculated using truck factors according to collected traffic data between two weeks. Starting with the general features of rigid pavement and design concepts are considered. The required CBR test results are taken from Ministry of Construction Department of Highways (Road and Airfield Design and Drawing Section). The structural design of rigid pavement studies with three methods including American Association of State Highway and Transportation Officials (AASHTO) method, Road Note 29 design method and Joint method. AASHTO method and Road Note 29 design method are used for design thickness comparison. Joint method is used for calculation of dowel bars and tie bars. And then, Critical Path method is used for planning and scheduling for road construction.

KEYWORDS: *rigid pavement, axle load survey, design thickness, planning and scheduling*

1. INTRODUCTION

Road plays an important role in both urban and rural areas for supporting cargoes and products from one region and another. In Myanmar, the total numbers of vehicles are increasing day by day. This study deals with studying the structural design of rigid pavement. The purpose of the thesis is to study the design of Tha Htay Kwin-Bagan Taung-Phar Kuu-Maunge Ma Road in Thanlyin Township, Yangon Region. This road is constructed with rigid pavement and it is the road network of Tha Htay Kwin village, Bagan Taung village, Phar Kuu village and Maunge Ma village. The length of the road is 18 miles and 4 furlongs. The design life of it is considered as 20 years. Average daily traffic and the design equivalent single-axle loads are calculate using truck factor according to collected traffic data between two weeks. The underlying soil is tested to evaluate its quality. In this pavement design, the require California Bearing Ratio (CBR) values are tested.

Fig 1.Tha Htay Kwin-Maunge Ma road

Fig.1 shows that Tha Htay Kwin-Maunge Ma road. The red line represents the route of Tha Htay Kwin-Maunge Ma road. The structural components of rigid pavement are designed by using Group Index Method and American Association of State Highway and Transportation Officials (AASHTO) method.

2. STRUCTURAL DESIGN OF RIGID PAVEMENT

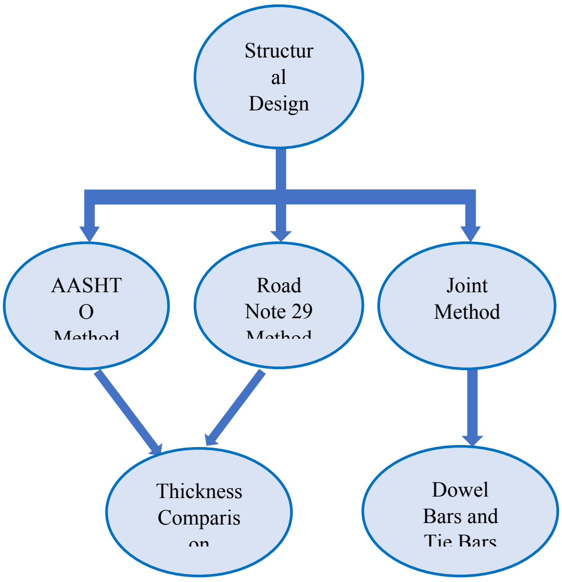

Fig 2. Calculation procedure of structural design of rigid pavement

Fig.2 describes the rigid pavement has been designed by calculating equivalent single axle load (ESAL), two kind of pavement design methods and design of dowel bars and tie bars for joint. The pavement design methods of the American Association of State Highway and Transportation Officials (AASHTO) Design Method, Road Note 29 Design Method are chosen for the road. Considering durability of concrete pavements, Tha Htay Kwin-Maunge Ma road have been built with jointed cement concrete pavement.

3. DATA COLLECTION

Both primary and secondary data were collected and analyzed for this research.

3.1 Primary data collection

The primary data are collected the start point and end point. This point are include Tha Htay Kwin, Pa Gan

Taung, Phar Kuu, Maunge Ma road. This study are start point and end point to collect the number of traffic passes through on this road. And then, vehicles types are classified depending on axle. The required CBR results are taken from ministry of construction of highways. The primary factors considered under pavement performance are the structural and functional performance of the pavement.

Table 1. Data Collection from Start and End Point

Date	Start Point	End Point
26.6.2019	Tha Htay Kwin	Pa Gan Taung
27.6.2019	Pa Gan Taung	Phar Kuu
28.6.2019	Phar Kuu	Maunge Ma
29.6.2019	Maunge Ma	Tha Htay Kwin
30.6.2019	Tha Htay Kwin	Pa Gan Taung
1.7.2019	Pa Gan Taung	Phar Kuu
2.7.2019	Phar Kuu	Maunge Ma
18.7.2019	Maunge Ma	Tha Htay Kwin
19.7.2019	Tha Htay Kwin	Pa Gan Taung
20.7.2019	Pa Gan Taung	Phar Kuu
21.7.2019	Phar Kuu	Maunge Ma
22.7.2019	Maunge Ma	Tha Htay Kwin
23.7.2019	Tha Htay Kwin	Pa Gan Taung
24.7.2019	Pa Gan Taung	Phar Kuu

Table 1 shows that the different portions of the road along the Tha Htay Kwin - Maunge Ma road.

3.2 Secondary data collection

The secondary data were collected from different equivalent axle load passing through the survey road. The traffic data collection survey within two weeks.

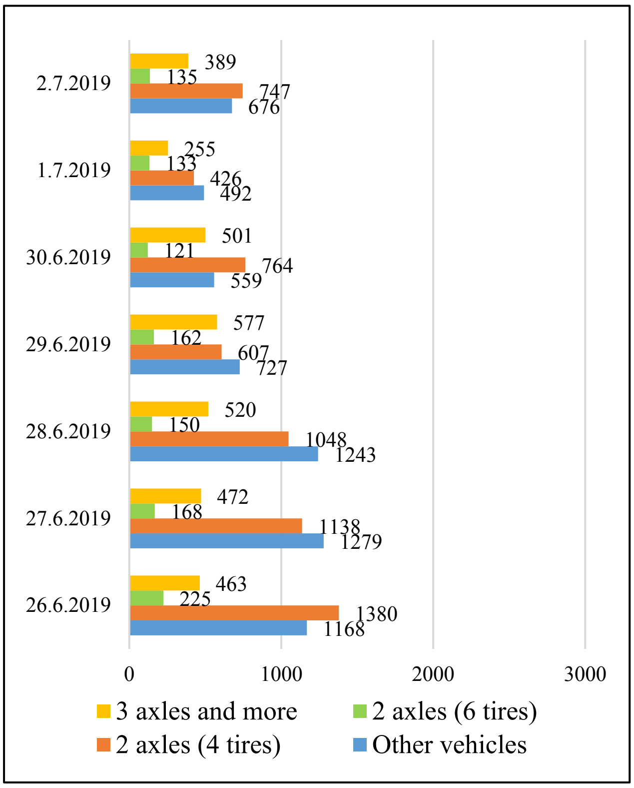

Fig 3. Traffic data collection survey (1st week)

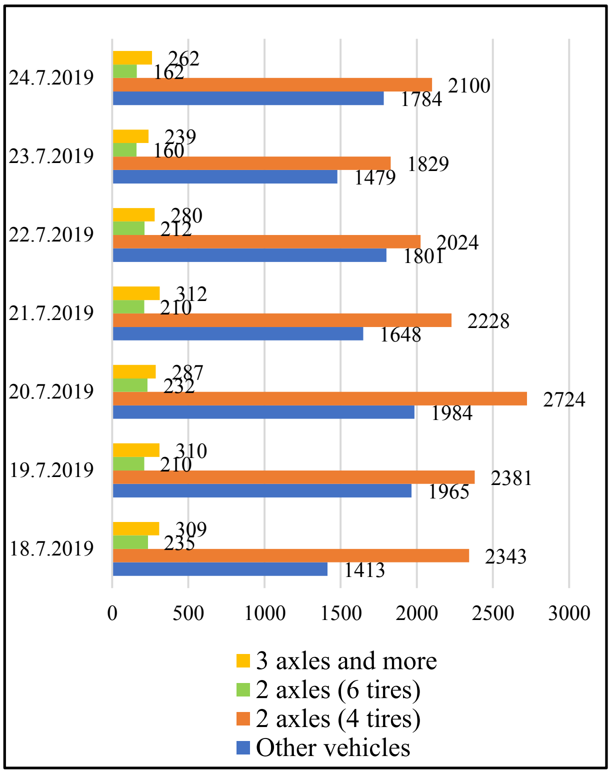

Fig 4. Traffic data collection survey (2nd week)

Average annual daily traffic (AADT) is considered as average daily traffic (ADT). 3% of traffic growth is estimated for design life. The collected traffic data during two weeks are shown in fig.3 and fig.4.

Table 2. Data Collection for Value of ESAL

Vehicle Type	Number of Vehicle During First Year	Track Factor, f_i	Growth Factor, G_{jt}	ESAL
Other vehicles	237067.5	0.39	24.3	2246688.7
2 axles, 4 tires	285065	0.015		103906.2
2 axles, 6 tires	31937.5	0.24		186259.5
3 axles and more	68072.5	1.02		1687244.9
Total				4783543.1

ESAL value = 4.8x 10^6= 0.005x10^6kips

The distributions of different types of vehicles expected to use the proposed roadway can be obtained from results of classification counts that are taken by on-board survey at regular intervals. The value of growth factor (G_{jt}), truck factor (f_i) and design lane factor (f_d), the equivalent single load values are shown in table 2.

4. ANALYZING DATA

The data that were gathered were analyzed through the use of the two methods of AASHTO design method and Road Note 29 design guide method.

AASHTO Design Method

Calculation of Rigid Pavement Thickness Design

W_{18} = 0.005×10^6 (maximum value of ESAL)

R = 95% (rural, arterials)

Z_R = -1.645 (in reliability 95%)

S_o = 0.5 (0.4~0.6)

Initial PSI = 4.5 (approximately 4.2~4.5)

TSI = 2.5 (principal arterial)

S_c' = 800 lb/in^2 (500~1200 lb/in^2)

For good drainage characteristics,

k = 137.5 lb/in^2

$$\log_{10}W_{18} = Z_R\times S_o+7.35\log_{10}(D+1)-0.06+\frac{\log_{10}\left(\frac{\Delta PSI}{3}\right)}{1+\frac{1.624\times10^7}{(D+1)^{8.46}}}+(4.22-0.3TSI)\log_{10}\left[\frac{S_c'\times C_d\,(D^{0.75}-1.132)}{215.63\times J\left(D^{0.75}-\frac{18.42}{\left(\frac{E_c}{k}\right)^{0.25}}\right)}\right] \quad (1)$$

Substitute in equation 1, D= 5.83 = 6 in

Road Note 29 Design Guide

According to the above ESAL calculation,

W_{18} = $0.005\text{x}10^6$ 18-kip ESAL for 20 years

CBR = 5% (cross-section from department of highway)

From Fig. 5, Thickness of subbase = 140 mm or 5.46in

From Fig. 6, Slab thickness, D = 127 mm or 4.95in

Use 6 in thickness for sub-base and 5 in thickness for slab of rigid pavement.

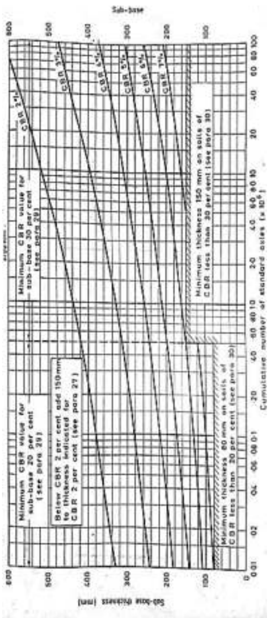

Fig 5. Thickness of Sub-base

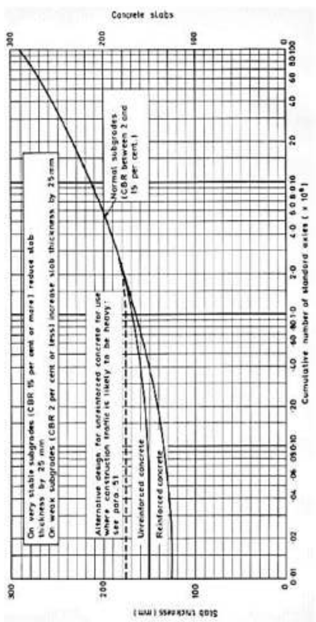

Fig 6. Concrete Minimum Thickness of Slabs

Table 3. Comparison of AASHTO and Road Note 29 Design Guide Method

Design Guides	CBR value	ESAL	Slab Thickness
AASHTO Design Guide	5%	$0.005\text{x}10^6$	6 in
Road Note 29 Design Guide	5%	$0.01\text{x}10^6$	5 in

Comparison of rigid pavement thickness by AASHTO design guide and Road Note 29 design guide based on same CBR value and ESAL value is shown in table 3. According to calculation, slab thickness of pavement by AASHTO design guide is 6 inches and by Road Note 29 design guide is 5 inches. From economic point of view, 6 inches is suitable because 1 inch is not much of a difference. Therefore, 6 inches is selected to be carried out for safety and for more accurate calculation of AASHTO design guide.

Dower bar and tie bar are calculated by joint method.

Calculation Procedure of Dowel Bar

Assume thickness of pavement = 20 cm(design guide)

Radius of relative stiffness = 50 cm

Wheel load design = 2000 kg

Joint width = 2 cm

Permissible stress in shear of the dowel bar=1000 kg/cm^2

Permissible stress in bending (dowel bar) =1400 kg/cm^2

Permissible stress in bearing (dowel bar) = 100 kg/cm^2

Assume d =2 cm

Length of the dowel,

$$L_d = 5d\sqrt{\frac{F_f\,(L_d+1.5\delta)}{F_b\,(L_d+8.8\delta)}}$$

$$= 5\times2\sqrt{\frac{1400\,(L_d+1.5\times2)}{1000\,(L_d+8.8\times2)}}$$

$$= 10\sqrt{\frac{14\,(L_d+3)}{(L_d+17.6)}}$$

L_d = 31.34 cm

Minimum length = $L_d+\delta$ = 31.34+2 = 33.34 cm

So 35cm long, 2cm diameter.

L_d = 35-2 = 33 cm

P_s = $0.785d^2F_s = 0.785\times2^2\times1000 = 3140$ kg

$$P_f = \frac{2d^2F_f}{L_d+8.8\delta} = \frac{2\times2^2\times1400}{33+(8.8\times2)} = 303 \text{ kg}$$

$$P_b = \frac{F_b L_d^2 d}{12.5\,(L_d+1.5\delta)} = \frac{100\times33^2\times2}{12.5\,(33+1.5\times2)} = 484 \text{ kg}$$

$$\text{Max}\left[\frac{0.4\times2000}{3140}, \frac{0.4\times2000}{303}, \frac{0.4\times2000}{484}\right]$$

Max [0.254, 2.64, 1.65] = 2.64

Effective distance load transfer = 1.8L = 1.8×50

= 90 cm

Assume 25 cm spacing,

Actual capacity,

$$1 + \frac{90-25}{90} + \frac{90-50}{90} + \frac{90-75}{90}$$

= 2.33 < 2.64 (required capacity)

Not ok.

If 20 cm spacing,

$$1 + \frac{90-20}{90} + \frac{90-40}{90} + \frac{90-60}{90} + \frac{90-80}{90}$$

= 2.778 > 2.64 (required capacity)

It is ok.

Calculation Procedure for Tie Bar

Assume thickness of concrete = 20 cm

Width of road = 164 cm (two-lane)

h = 20 cm

b = 164/2 = 82 cm

S_s = 1750 kg/cm^2

S_b = 24.6 kg/cm^2

W = 2400 kg/cm^2

F = 1.5

$$A_s = \frac{bhWf}{100S_s} = \frac{82\times2\times2400\times1.5}{100\times1750} = 3.37 \text{ cm}^2$$

d = 1.6 cm

$$A = \frac{\pi d^2}{4} = \frac{\pi\times1.6^2}{4} = 2.01 \text{ cm}^2$$

$$\text{Spacing} = \frac{100\times2.01}{3.37} = 59.6 = 60 \text{ cm}$$

$$\text{Length of tie bar, } L = \frac{1.6\times1750}{2\times24.6} = 60 \text{ cm}$$

It is ok!

5. PLANNING AND SCHEDULING

CPM Scheduling Methods

Industry uses various scheduling methods today. The scheduling method shows how the activities and relationships relate to one another. Among these types are:

- Bar chart
- Fenced bar chart (time-scaled)
- Arrow diagram method
- Precedence diagram method

In this study, arrow diagram method is used.

Arrow Diagram Method

Arrow diagramming method combines the representation of sequence and duration. The two elements of arrow diagramming are arrows and nodes. One arrow is created for each activity to be accomplished. If not required, the length of the arrow is often scaled to be proportional to the activity. Nodes are used to graphically show where activities end and begin in sequence.

The procedure of CPM methods are include forward pass, backward pass and total float.

Forward Pass;

- Calculate an activity's early dates.
- Early dates are the earliest times an activity can start and finish once its predecessors have been completed.
- The calculation begins with the activities without predecessors.

Early Start + Duration – 1 = Early Finish

Backward Pass;

- Calculate an activity's late dates.
- Late dates are the latest times an activity can start and finish without delaying the end date of the project. The late dates are the New York State Department of Transportation (NYSDOT) contractual dates.
- The calculation begins with the activities without successors.

Late Finish – Duration + 1 = Late Start

Total Float;

- The amount of time an activity can slip from its early start without delaying the project.
- The difference between an activity's late dates and early dates.
- Activity with zero total floats are critical.

Late Date – Early Date = Total Float

Construction Procedures of Rigid Pavement

- Preparation of subgrade and sub-base
- Placing of formwork
- Batching of materials
- Proportioning of the mix
- Preparation of the mix
- Transportation and laying the mix
- Compaction
- Joints
- Screeding and finishing the surface
- Curing
- Opening of traffic

Table 4. Activity Description of Tha Htay Kwin-Maunge Ma road

No.	Activity Code	Activity	Duration (day)
1.	A_1	Cutting and collection soil for earthwork	6 days
2.	A_2	Dump truck and worker the soil for subgrade	9 days
3.	A_3	Water spraying and consolidation the soil (4 miles)	13 days
4.	A_4	Dressing or shaping the subgrade	3 days
5.	A_5	Mixing the soil with crushed rock by mixer	24 days
6.	A_6	Hauling and spreading the gravelly soil for sub-base course	18 days
7.	A_7	Consolidation the gravelly soil	9 days
8.	A_8	Mixing the material by using batching plant	20 days
9.	A_9	Hauling and spreading the base course	9 days
10.	A_{10}	Compacting the mixture	2 days
11.	A_{11}	Cleaning the base course surface with roller	5 days
12.	A_{12}	Consolidation the base course surface with roller	7 days
13.	A_{13}	Laying the concrete with concrete mixing transport trucks	30 days
14.	A_{14}	Excavating and dumping the soil for each shoulder	10 days
15.	A_{15}	Hauling the soil for hard shoulder	22 days
16.	A_{16}	Spreading, water spraying and consolidation for hard shoulder	12 days
17.	A_{17}	Dressing of shoulder by grader	2 days

In table 4 and table 5 are describe the activity description and activity dependence schedule for Tha Htay Kwin-Maunge Ma road.

Projection Duration =149 days

Table 5. Activity Dependence Schedule Maunge Ma

No.	Activity	Proceeding Activity	Following Activity
1.	A_1	-	A_2, A_3
2.	A_2	A_1	A_3
3.	A_3	A_1	A_4
4.	A_4	A_2, A_3	A_5, A_6, A_7
5.	A_5	A_4	A_8, A_9, A_{10}
6.	A_6	A_4	A_8, A_9, A_{10}
7.	A_7	A_4	A_8, A_9, A_{10}
8.	A_8	A_5	A_{11}
9.	A_9	A_6	A_{11}
10.	A_{10}	A_7	A_{11}
11.	A_{11}	A_8, A_9, A_{10}	A_{12}
12.	A_{12}	A_{11}	A_{13}
13.	A_{13}	A_{12}	A_{14}
14.	A_{14}	A_{13}	A_{15}, A_{16}
15.	A_{15}	A_{13}	A_{17}
16.	A_{16}	A_{14}, A_{15}	A_{17}
17.	A_{17}	A_{16}	-

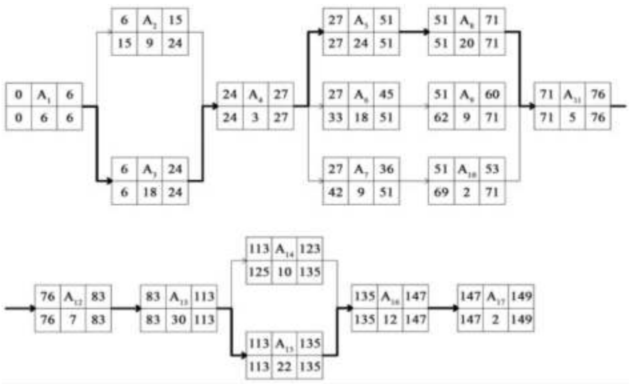

Fig. 7 describes the projection duration is 149 days. This study delay project duration.

Table 6. Activity Schedule

Activity	Activity Duration	Early Start	Early Finish	Late Start	Late Finish	Total Float	Remarks
A_1	6	6	0	6	0	0	CA
A_2	9	6	15	15	24	9	-
A_3	18	6	24	6	24	0	CA
A_4	3	24	27	24	27	0	CA
A_5	24	27	51	27	51	0	CA
A_6	18	27	45	33	51	6	-
A_7	9	27	36	24	51	15	-
A_8	20	51	71	51	71	0	CA
A_9	9	51	60	62	71	11	-
A_{10}	2	51	53	69	71	18	-
A_{11}	5	71	76	71	76	0	CA
A_{12}	7	76	83	76	83	0	CA
A_{13}	30	83	113	83	113	0	CA
A_{14}	10	113	123	125	135	12	-
A_{15}	22	113	135	113	135	0	CA
A_{16}	12	135	147	135	147	0	CA
A_{17}	2	147	149	147	149	0	CA

Critical path is $A_1 – A_3 – A_4 – A_5 – A_8 – A_{11} – A_{12} – A_{13} – A_{15} – A_{16} – A_{17}$.

In this table 6, activities: A_1, A_3, A_4, A_5, A_8, A_{11}, A_{12}, A_{13}, A_{15}, A_{16}, A_{17} comprise the critical path while activities: A_2, A_6, A_7, A_9, A_{10}, A_{14} are not the critical path with float of 6 days, 9 days, 10 days, 11 days, 12 days, 15 days, and 18 days respectively. Where activities that are not the critical path have float and are therefore not delaying completion of the project, those on the critical path have critical path drag.

6. CONCLUSION

In this study, thickness of rigid pavement is calculated with AASHTO method and Road Note 29 design method to compare these two methods. And then, to prevent random cracking, design of joint is calculated and the length and spacing of dowel bar and tie bar is calculated. For this task, Tha Htay Kwin-Maunge Ma road, Yangon Region was selected as the case of study. In this study, the ESAL value is needed to be calculated first. In order to figure out ESAL value, the number of vehicles that passes through are required to know. Vehicles are counted according to the number of axle (single, tandem, triple) in this ESAL calculation. And AASHTO method and Road Note 29 design method are calculated with input data. CBR is obtained 5% from thanlyin -kha yan department of highway. For the same input design traffic data, surface thickness is 6 inches for AASHTO method and 5 inches for Road Note 29 design method. After that, the length and spacing of dowel bar and tie bar is calculated by using Bradury's analysis according to design result are obtained 20 cm spacing in dowel bar and 60 cm spacing in tie bar. The critical path is $A_1 – A_3 – A_4 – A_5 – A_8 – A_{11} – A_{12} – A_{13} – A_{15} – A_{16} – A_{17}$ and project duration is 149 days.

ACKNOWLEDGEMENT

The author is sincerely thankful to Dr. Nyan Phone, Professor and Head of Department of Civil Engineering of Technological University (Thanlyin), for his skillful guidance, helpful suggestions and editing of thesis paper.

REFERENCES

[1] Google Maps Satellites, Tha Htay Kwin-Maunge Ma Road, Thanlyin Township, Yangon
[2] "Traffic and Highway Engineering (Fourth Edition)," by Nicholas J. Garber and Lester A. Hoel (University of Virginia)
[3] AASHTO. 1993. "Guide for Design of Pavement Structures,". American Association of State Highway and Transportation Officials. Washington D.C
[4] "The Civil Engineering Handbook Second Edition," (W.F.Chen J.Y.Richard Liew)
[5] "Road Research Laboratory," Ministry of Environment by Mr.P.D.Thompson
[6] MCGraw-Hill "Handbooks [Handbook of Transportation Engineering]"
[7] Rigid Pavement Design [Lecture notes in Transportation Systems Engineering, 3 August 2009]
[8] Concrete Roads: PQC, "Methods of Construction and How it is Made," by Mugda P
[9] "Preplanning and Scheduling of Road Construction," by using Preplanning Project Management (PPM) by T.Subramani and M.Sekar

The Relationship Between Geology and Engineering Geology of Upper Paunglaung Hydropower Dam

Thin Thin Hlaing [(1)], Hline Wint Wint Hmue[(2)]
[(1)] Technological University (Mawlamyaing), Myanmar
[(2)] Technological University (Lashio), Myanmar

Email: soeh41526@gmail.com, hlaingwintwinthmue@tulashio.edu.mm

ABSTRACT*:* Upper Paunglaung Hydropower Project is located at about 26 miles far from the eastern part of Pyinmana Township, Mandalay Region. The one inch to one mile scale topographic map index for dam is 94 A/9, N 19˙ 45' 24.7" and E 96˙ 35' 40". The type of dam is Roller Compacted Concrete dam. The height of the dam is 322 feet and its length is 1690 feet. The objective of construction of Upper Paunglaung Hydropower Dam is to generate 140 megawatt by the use of two generators with 70 megawatt respectively and average annual energy of 454 million kilowatt. Geomorphologically the entire area consists of steeply sloping hills. The Paundlaung Chaung and Paunglaung Nge Chaung are tributaries of Paunglaung River.

Engineering geological study, geological study, data analysis is used for investigation of Upper Paunglaung dam project. The project site is situated at the western edge of the Shan Plateau. The Sagaing Fault and Shan Scarp Fault are two major faults in the study area. Granite and meta-sandstone are found in the area and well exposed in the left and right abutments of the dam. Limestone occurs at the quarry site. Major joints are mostly long and vertical direction. The engineering geological study is carried out by the field pressure testing. Seismicity of the project area is observed within the past earthquake records and previous geophysical data. The RCC aggregates for the project construction are composed of pozzolan cement, natural pozzolan, river sand, free water and coarse aggregate.

KEYWORDS: *RCC Dam, engineering geological study, pozzolan*

1. INTRODUCTION

The study area is situated about 26 miles east of Pyinmana Township, Mandalay Region, Central Myanmar. This project is constructed by Ministry of Electric Power No. (1), Department of Hydropower Implement and CO- operate with Colenco Geotechnical Engineering Co., Ltd. The dam is constructed on the Paunglaung Chaung which is a tributary of Sittaung River and covers 993 square miles of catchment area. The Paunglaung Hydropower Project is to generate 140 megawatts by the use of two generators with 70 megawatts respectively and average annual energy of 454 million kilo watt hour. The type of dam is Roller Compacted Concrete (RCC).

2. LOCATION, SIZE AND ACCESSIBILITY

Upper Paunglaung Hydropower Project is located at about 26 miles east of Pyinmana Township, Mandalay Region. The one inch to one mile scale topographic map index for dam site is 94 A/9, N 19˙45' 24.7" and E 96˙35' 40". The location map of the study area is shown in figure 1. The study area is easily accessed by motor cars and motor cycles all the year round.

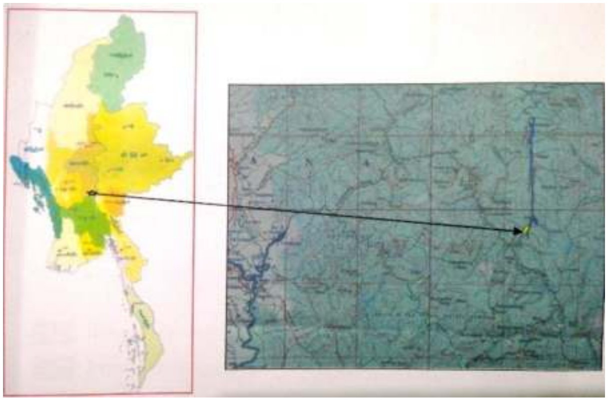

Fig 1 Location Map of the Study Area

2.1 Regional Geology

The study area is located on the mountainous region of the western margin of Shan Plateau, 26 miles east of Pyinmana. It lies between two major faults, Paunglaung Fault and Sagaing Fault. Sagaing Fault is situated western part of the study area and Paunglaung Fault is situated eastern part of the study area. The area occupies the western marginal zone of the Shan Plateau, had been a stable block since the close of the Mesozoic. It is a strongly deformed zone in which large scale emplacement of granites and related rock types occurred probably during late Mesozoic. Granite and related igneous rocks of the present area are actually the northern continuation of large igneous body of batholithic dimension that continues southwards to the east of Taungoo. On the basis of regional trend (NNW-SSE), the meta- sedimentary sequence of the area appears to be laterally continuous with the similar sequence of the Yamethin area in the north.

Along the western border of the Shan Plateau, a narrow belt of sediments with the high-grade metamorphic and granite intrusions have been named the

Mogok belt. Regional geological map of the study area is shown in figure 2.

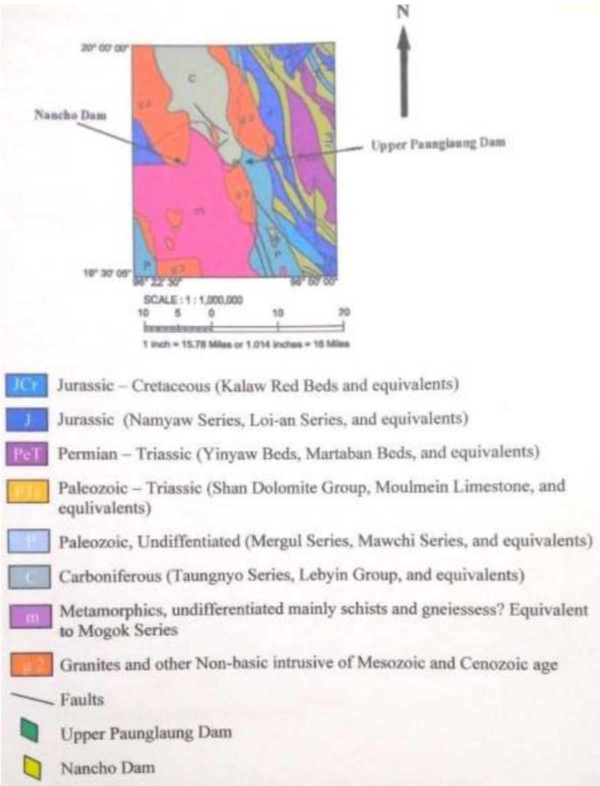

Fig 2 Regional Geological Map of the Study Area.

Source: Geological Map of the Socialist Republic of the Union of Burma.

3. GEOLOGY OF THE STUDY AREA

The study area is located on the western margin of the Shan Plateau. Generally, it is topographically rugged with deeply eroded valleys. Physiographically, the entire area consists of the steeply sloping hills. In this area, the highest point of mountain is about 3050 ft and the lowest point of the mountain is about 2300ft above the sea level. The trends of mountain ranges are roughly NNW-SSE. Overburden soil is mostly thin to medium bedded and gradually thickness to the flanks of the mountains. In the study area, there are three rock units which are granite, meta-sandstone and limestone.

3.1 Lithology

Granite is well exposed in the left abutment of dam. It is occurred as massive, whitish grey, fine to coarse grained, moderately strong and slightly weathered with vertical joints. In the right abutment, granite intrusion is occurred as circular shape. Quartz veins are occurred in the granite body as shown in Figure 3. Limestone is occurred at the quarry site which is in south-east of the dam site. They are medium bedded, bluish grey to dark grey colour and fine-grained rock with calcite veins. Bedded limestone is shown in figure 4. Meta-sandstones are widely distributed in the study area. They are buff to dark brown colour, fine to coarse grained, moderately weathered and moderately strong. In some places, these rocks are highly weathered and intruded by quartz veins. Three sets of joints are dominantly occurred. Meta-sandstone outcrop is shown in figure 5.

Fig 3 Granite Intrusion occurred as Circular Shape in the Right Abutment.

Fig 4 Bedded Limestone at the Quarry Site

Fig 5 Meta-sandstone Intruded by Quartz Veins at the Right Abutment

3.2 Structural Geology

Structural geology of the site area is complex. Most of the area is covered by residual soil deposit expect gullies and stream sections. Thick bedded meta-sandstone unit is exposed along the dam axis. In the right abutment of the dam, meta-sandstone and granite contact is found by nearly NNW-SSE trending.

3.3 Fault

The study area is located between two major faults. They are Paunglaung fault in the eastern part of the study area and Sagaing Fault in the western part of the study area. In the study area, another fault line is located near the right abutment and trends 225˚ as shown in figure 6. Along the fault line, meta-sandstone and granite are exposed and many joints and fault gauge are observed. The faults can be caused by local tectonic activities and might be associated with Sagaing Fault and Paunglaung Fault.

Fig 6 Major Fault at the Right Abutment

3.4 Joint

In this area, the rock outcrops are moderately to highly jointed and having mostly three sets and random nature. In this joint system, bedding joints are more dominantly observed than any other joints. Major joints are commonly long and generally vertical. In the right abutment, granite is highly brecciated and formed as daylight condition as depicted in figure 7.

Fig 7 Highly Brecciated Granite as Daylight Condition at the Right Abutment

3.5 Seismicity of the Study Area

The region of the study area falls in the earthquake zone. Some of the great earthquakes have taken place along the Sagaing Fault which runs in NS direction. The fault is located 30 km west of the study area. The Paunglaung fault runs NS direction and is located 13km east of the study area. The seismic data suggests that the earthquake intensity ranges from low to moderate but some might be strong with Modified Mercalli scale of 7.5 to 8. (Source from DHP)

4. ENGINEERING GEOLOGY OF THE STUDY AREA

The Upper Paunglaung dam is a Roller Compacted Concrete dam (RCC-type). The height of dam is 322 ft and its length is 1690 ft. It is constructed on the Paunglaung River which mainly flows from nearly NS. Average annual inflow is 2,106,500 acre feet and catchment area is 933 square miles. The type of spillway is Ogee type (Ungated). This type of dam is selected based on the factors because bedrock is strong, stream valley is narrow, and required construction materials can be obtained easily near the project area.

4.1 Left Abutment of Dam Site

Granite intrusion is observed at the left abutment. It is massive, whitish grey, fine to coarse grained, moderately strong and slightly weathered with vertical joints. Meta sandstones exposed on this slope are light grey to light yellowish brown, moderately weathered, highly jointed and weathered.

Meta sandstone is fresh to moderately weathered, strong and light grey. The granite intrusion is occurred between the discontinuity planes. Power house, separation wall penstocks, bottom outlet and power intakes are situated at the left abutment of the dam.

4.2 Stream Section

The dam foundation is sound rock foundation which is composed of met- sandstone and granite. The decomposed and partly weathered rocks below the original surface must be excavated to provide a proper bounding of the concrete gravity dam with foundation. In the upstream coffer dam, the rocks are found on moderately to highly weathered granite.

4.3 Right Abutment of Dam Site Area

In right abutment, meta-sandstone is well exposed as reddish yellow to buff, moderately to highly jointed, decomposed rocks in which consisting of clayey silt and small rock pieces. The dam alignment is kink at the right abutment because the foundation rock is highly jointed by structural control. Diversion tunnel is located at the right abutment below the dam footprint area EL-355 m. The diameter of the diversion tunnel is 10 m and 295 m length. Beside the inlet of diversion tunnel, slightly to moderately meta- sandstone with sub-vertical joints were observed.

4.4 Coffer Dam

Coffer dam is a temporary dam constructed for facilitating construction. Coffer dam is constructed on the upstream of the main dam to divert water into a diversion tunnel during the construction of the dam. In the study area, the height of coffer dam is 304 m.

5. ROCK MASS CHARACTERIZATION

Rock mass is assemblage of intact rock blocks separated by different types of geological discontinuity. Intact strength of rock is the dominant control on the resistance of rock to failure along the natural partings. The properties of the intact rock may strongly influence the gross behaviour of the rock mass. Deformability, strength and permeability are greater importance than the properties of the intact rock material. In the study area, the geometrical, mechanical and hydrological properties of discontinuities are investigated.

5.1 Rock Quality Designation (RQD)

Strength of rocks can be estimated on the base of field geological data by using RQD. The core drilling is shown in Figure 8.

Fig 8 Core Drilling

RQD=100 x length of core pieces ≥ 100 mm/length of borehole

RQD = 115- 3.3 J_v

The values of RQD as shown in table 1.

Table 1. Relationship between the Numerical Value of RQD and the Engineering Quality of the Roc

RQD %	Rock Quality
<25	Very Poor
25-50	Poor
50-75	Fair
75-90	Good
90-100	Very Good

Source: Deere (1964)

5.2 Evaluation of GSI Value in Dam

In the dam site, GSI value is calculated by defining 11m block interval on the bedrock. The results of GSI values are shown in Table 2.

Table 2. GSI Value in Dam Foundation

J_v	SR	SCR	GSI
8.2	42.9	17	63
7.3	45.0	14	56
13.6	34.1	16	55
9.3	40.8	12	48
10.3	38.9	10	42.5
6.3	47.6	16	62.5

5.3 Rock Mass Rating (RMR)

The Rock Mass Rating (RMR) is the commonly used system for classifying rock mass, proposed by Bieniawski (1989) of South African Council for Scientific and Industrial Research (CSIK). The Rock Mass Rating System is shown in Table 3.

Table 3(a) Evaluation by RMR System
Location N 19 45 432, E 96 35 677 (Right Abutment)

No	Classification Parameter	Description	Rating
1.	Strength of Rock UCS(MPa)	93.1	7
2.	(RQD) Rock Quality Designation	75%	17
3.	Spacing of discontinuities	0.5 mm	10
4.	Condition of discontinuities	Hard filled, slightly weathered	19
5.	Groundwater condition	Completely dry	15
Rating			68

Description of rock type	Class No.	Adjustment for orientation of joint	Total Rating
Good rock	II	-0	68

Table 3(b) Evaluation by RMR System
Location N 19 45 288, E 96 35 582 (Left Abutment)

No	Classification Parameter	Description	Rating
1.	Strength of Rock UCS(MPa)	70.6	7
2.	(RQD) Rock Quality Designation	73.7%	13
3.	Spacing of discontinuities	300 mm	10
4.	Condition of discontinuities	No filled, slightly weathered	27
5.	Groundwater condition	Completely dry	15
Rating			72

Description of rock type	Class No.	Adjustment for orientation of joint	Total Rating
Good rock	II	-0	68

6. PARTS OF DAM CONSTRUCTION

They are metal forms, green cut, acess galleries and thermocouples, waterstops, pendulum shaft, power intakes, penstocks, power house, switchyard, separation wall, tailrace channel, bottom outlet and spillway. Parts of the dam construction are shown in Figure 9.

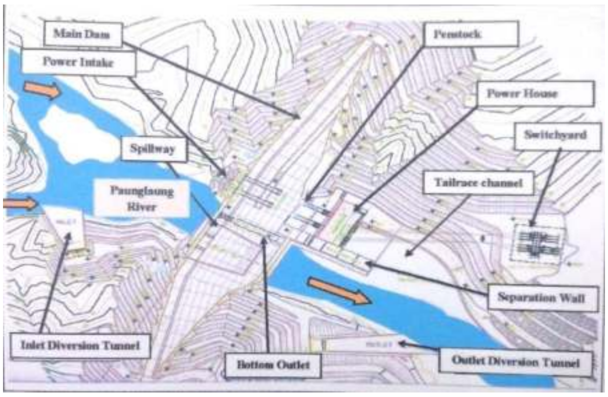

Fig 9 Parts of the Dam Construction

Source: Aye Lwin (No Date)

6.1 Metal Form

The upstream RCC face is vertical face formed with metal form panels of 2.1 m height and 4.0 m length tied back with anchors into the RCC. Moreover the downstream RCC face is stepped face formed with metal form panels of 0.6 m height and 0.48 m length tied back with anchors into the RCC. The metal form surfaces were cleaned before placing RCC and faces were scraped to remove the grout film. Then the form oil was applied and providing a 50 x 50 mm V-notch crack inducer on the formed face.

6.2 Access Gallery and Thermocouple

Access gallery is placed in the interior of the dam body. It is 2.4 m wide and 3 m height along the dam axis. Two types of gallery are horizontal and inclined galleries. This dam includes four horizontal and inclined galleries. The main purpose is to maintain dam body after construction and to check seepage. Thermocouple is sunk at the center of the dam body to measure concrete temperature.

6.3 Waterstops

All surfaces of waterstops must be free from dried mortar from previous placement and other foreign substance, before the adjacent or surrounding concrete placement is begun. Two waterstops are installed at every contraction joint such as one is 1000 mm far from the upstream surface of the dam body and the other is at the interval of 750 mm. Waterstops must be placed and secured in position so that they will not be displaced during the concrete placement. Waterstop is used to prevent leakage of water from upstream face of dam.

6.4 Spillways, Power Intake and Penstocks

The spillway is Ogee type and used to divert the water more than full tank level of the dam. Intake structure consists of trash racks and penstock gate. Penstocks are usually steel pipes used to carry water from the storage reservoir for the turbine.

6.5 Bottom Outlet, Diversion tunnel and Separation Wall

It is used to reduce the sedimentation in the reservoir on the upstream of a dam. Sometimes, it is applied to discharge water if not possible by spillway.

Diversion tunnel is constructed for the purpose of diverting water of the river during construction. It is usually of low height and has a small storage reservoir on its upstream. In this dam, diversion tunnel must be closed after the construction works. Inlet and outlet diversion tunnels are shown in Figure 10.

Separation wall is located between bottom outlet and power house. It is mainly used to prevent water from entering the power house.

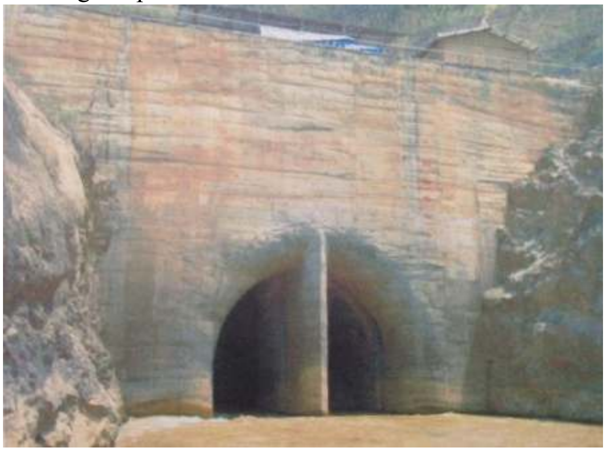

Fig 10 Diversion Tunnel

7. CONSTRUCTION MATERIALS

7.1 Quarry Site

Quarry site is located in the east and about 8 km far away from dam site. There are two quarry sites which are Myan Shwe Pyi MSP and High Tech HTCT. Bedded limestones are exposed at quarry site. They can produce for dam construction. Overburden thickness of the quarry site is about site is about 2m thick or more in some places. Sinkhole is found at the quarry site. Blasting produces rock sizes with a high maximum size typically 300-800 mm. The required rock aggregate sizes for construction material are 40 mm, 20 mm, 10 mm and 5 mm.

7.2 Crushing Plant and Batching Plant

Crushing plant is situated at the northwest corner of dam site. It is breaking out the boulders obtaining from quarry site and produces suitable rocks for batching plant. Crushing plant has a greater effect on intact rock properties. Batching plant is located on the left abutment of thedam site. It is controlling the proportion of RCC mixing design by using computer system. It is a place where rocks of various sizes have been divided. There are three pozzolan silos and two cement silos in batching plant.

7.3 Pozzolan

Pozzolan is a siliceous or aluminous material which possesses little or no cementitious value. It can take from Popa volcanic region of Myanmar. When the pozzolan is mixed with siliceous limestone in pneumatic machine, it gives the best properties of concrete and reduces the use of cement by 70 percent.

Pozzolan is commonly used as an addition to Portland cement concrete mixture to increase the long-term strength. Pozzolan is used in different construction of Conventional Vibrated Concrete (CVC) and Roller Compacted Concrete (RCC) gravity dam.

7.4 Water Supply for RCC Concrete

In the study area, water is important not only for the production of the GEVR grout but also for the forging machines, high pressure tests for damping the RCC surface and RCC concrete mixing. Water must be clean and potable free of all deleterious materials. Purified water machine was constructed at the upstream face left abutment of the dam site. It is composed of composed of sedimentation tanks, small tank, big tank and sand filter tank. Each filter tank includes sand and gravel one feet respectively and sedimentation tank to small tank, primary and secondary pressure sand filter tank, and big tank. Finally, purified water is taken to use for water chilling plant by machine pump with the capacity of 15 hp engine.

8. CONCLUSIONS

The Upper Paunglaung dam is situated about 62 km east of Pyinmana Township, Mandalay Region in Central Myanmar. The study area is bounded by North Latitude 19˙44' 147" to 19˙ 46' 228" and East Longitude 96˙35' 674" to 96 ˙ 37' 259". Types of dam are varying according to topography of the project site. Gravity dams can be classified into two categories. They are Roller Compacted Concrete Dam and Conversional Vibrating Concrete Dam. Dam type is Roller Compacted Concrete type which is the second type of the concrete dam design in Myanmar. The study area lies between two major faults; they are Sagaing Fault and Shan Scarp Fault. Sagaing Fault is situated the western part of the study area and Shan Scarp Fault is eastern part of the study area. The regional geology of the upper Paunglaung area trends NNW-SSE. In the area, there are three rock units which are granite, metamorphosed sandstone and limestone. Major joints are commonly long and generally vertical. Parts of dam construction are metal forms, green cut, access galleries and thermocouples, waterstops, pendulum shaft, power house, switchyard, separation wall, tailrace channel, bottom outlet and spillway. Construction materials are produced from quarry site, crushing plant and batching plant. Pozzolan is used as an addition to pozzolan cement concrete mixture to increase the long-term strength.

ACKNOWLEDGEMENT

We have to our gratitude firstly to Professor Dr. Kyaw Htun (Retire) Head of Engineering Geology Department (YTU) for his kind of permission to carry out this research and his closely supervision, critically reading the manuscript, valuable suggestions and editing. We would like express our thanks to Professor Dr. Khin Soe Moe, Head of Engineering Geology Department (YTU) for her advice, suggestion and encouragement throughout the duration of this research.

Especially, this project is supported by the authorities of the Ministry of Electric Power No (1), Department of Hydropower Implementation and special thanks are due to U Kyaw Nyein (SE), U Nyein Chan (SE) (Director of Construction (1) and U Aye Lwin (Executive Engineer), U Aung Myint (AE) Civil, U Myo Khaing (AE), U Nyan Soe (SAE) for their providing field facilities and sharing experiences during field observation.

We wish to express our thanks to all people who helped in our research during April, 2012.

REFERENCES

[1] Aye Lwin. No Date. Geology Report on Upper Paunglaung Hydropower Project, Department of Geology, Ministry of Electric Power No (1).

[2] Bieniawski. 1989. Rock Mass Rating, Cited in Engineering Geology for Civil Engineering, Ministry of Science and Technology.

[3] Deer. 1964. Rock Quality Designation Index, Cited in Engineering Geology for Civil Engineering, Ministry of Science and Technology.

[4] Hoke and Brown. 1997. Rock Mass Rating, Cited in Engineering Geology for Civil Engineering, Ministry of Science and Technology.

[5] Hoke, E et al.2005. Variability of Engineering Properties of Rock Masses Quantified by the Geological Strength Index: The Case of Ophiolites with Special Emphasis on Tunneling, Volume: 65, Issue: 2, Publisher: Springer, Pages 129-142.

[6] Min Soe et al. 2012. Geotechnical Investigation of the Main Dam at Upper Paunglaung Hydropower project, Applied Geology Department, Yangon.

PETROCHEMICAL ANALYSIS OF IGNEOUS ROCKS AT SHWEZALI AREA, MANDALAY REGION

Win Win Maw[1], Naing Lin[2]
[1]Pakkokku University, Myanmar
[2]Kyaukse University, Myanmar
Email:winwinmaw95456@gmail.com

ABSTRCT: The study area is situated as a boundary zone between the Shan Scarp and Central Cenozoic Belt. The area is mainly composed of igneous rocks. Metamorphic rocks are exposed only as roof pendent. The present study, however, focused on the igneous rocks on the basis of geochemical analysis. In terms of major elements, all the granitic samples in the present study area are characterized by subalkaline and peraluminous nature. Based on the petrochemical analyzed data the granitoid rocks of the area are in accordance with the S-type nature and derived from the supracrustal origin. According to the ternary plot of normative Q-Ab-Or, the igneous rocks of the study area were consolidated under the low-pressure condition. The granite unit of the area corresponds to syn-collision rocks and tend towards the post orogenic zone in terms of R_1-R_2 diagram. Based on the analyzed data, the granitoid magmatism of the region formed in relation to the pre-dated and post-dated collision of India with Eurasia.

KEYWORDS: *S-type, supracrustal origin, collision*

I. INTRODUCTION

The study area is located about 16 km southeast of Kume, Myittha Township. It is bounded by latitude 21° 14´40´´ N to 21° 17´N and longitude 96° 10´ E to 96° 11´ 30´´E in one-inch topographic map of 93 C/4. It covers about 40 km^2 of mountainous and rugged terrain (Figure 1). Generally, the area forms the northeastern part of Pyetkaywe batholith within the Central Granitoid Belt, and Mogok Metamorphic Belt of Myanmar.

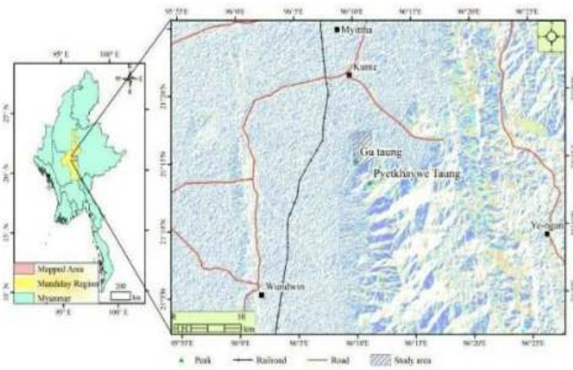

Figure 1. Location map of the Shwezali area

The area is occupied mostly by igneous rocks and roof pendent of metamorphic rocks. Igneous rocks of the area include from older to younger; diorite, hornblendite, biotite granite and porphyritic biotite granite[7]. Metamorphic rocks include from older to younger; marbles, quartzite and calc-silicate rock, banded biotite gneiss and hornblende biotite gneiss (Fig. 2). In this research work, igneous rocks of the area are emphasized to know the chemical characteristic, genetic type and condition of crystallization based on the geochemical properties.

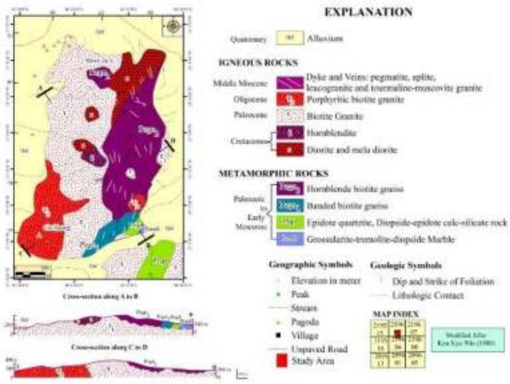

Figure 2. Geological map of the Shwezali area

2. GEOLOGICAL BACKGROUND

Generally, the proposed area forms northeastern part of the Pyetkaywe batholith. It lies within the well-known Mogok Metamotphic Belt (Searle and Haq ,1964). The granitic rocks of the study area form part of Central Granitic Belt, characterized by mesozonal, mostly Late Cretaceous to Early Eocene granitoid plutons associated with abundant pegmatites and aplites, numerous vein-type W-Sn deposits, and almost lack of comagmatic volcanics (Khin Zaw, 1990). The generation of Late Cretaceous to Early Eocene I- and S- type granites in the Mogok belt was related either to crustal shortening or to subsequent extension in the Mogok belt according to Mitchell (1993).

The study area, which is located between the Shan scarp and the Central Lowland, lies in the dry zone. It is a N-S trending isolated range measuring 3.2 km in length and 1.5 km in width. It is a fairly rugged terrain, and the highest peak is marked by the Shan Pagoda hill, 396 meters above mean sea level. At the study area, the eastern part is covered by gneiss unit and lacks thick soil cover with moderate vegetation. The western part is covered by porphyritic biotite granite and biotite granite units with fairly extensive rock exposures. Diorite unit locally crop out in the middle part of the area. Gradational changes from diorite to meladiorite and hornblendite are locally observable (Figure 2).

3.EXPERIMENT

3.1 Experiment apparatus

A total of 11 representative samples from the study area have been selected and analyzed. Major elements whole rock analyses and trace element concentrations for the various samples were determined by X-ray fluorescence spectrometry (XRF) at the Defense Services Science and Technology Department, Pyin Oo Lwin.

3.2 Data

Four granite samples, four diorite samples, two hornblendite samples and pegmatite sample from the study area were analyzed for major and trace elements. The results are shown in Tables (1 - 3).

Table 1. Major- and minor-element analysis (in wt%) of the igneous rocks in the study area

Sample No.	Biotite Granite				Pegmatite	Diorite				Hornblendite	
	SP1	SP2	SP6	SP9	SP8	SP3	SP24	SP25	SP26	SP5	SP27
SiO_2	71.6900	71.2200	72.9000	72.7300	77.9300	55.0500	68.6800	68.4700	50.8000	45	44.96
TiO_2	.0800	0.2080	0.0656	0.1160	0.0200	1.1700	0.3400	0.5700	0.5300	0.699	1.23
Al_2O_3	15	15.6000	14.8000	15.4000	13.8200	16.1000	14.6200	15.0600	17.8000	17.8	17.14
Fe_2O_3	2.4100	2.0620	0.7176	1.4740	0.7400	8.3260	3.5600	3.1000	6.3200	9.289	9.56
MnO	.0170	0.0468	0.0140	0.0345	0.0300	0.1340	0.0700	0.0700	0.1200	0.13	0.15
gO	0.5200	0.4150	0.5500	0.2850	0.1300	5.0100	1.6000	1.6700	8.6400	9.093	8.9
CaO	0.5400	1.5700	1.6000	1.8800	0.5500	7.6370	3.3000	4.0300	12.1000	12.72	12.88
Na_2O	3.1200	3.1700	4.3800	4.4800	4.7600	3.2600	2.5000	3.1400	2.0300	2.62	2.9
K_2O	6.5100	5.0600	2.8400	2.9900	3.4000	1.5700	4.5100	2.9800	0.7700	0.369	0.4
P_2O_5	.0100	0.0630	0.0100	0.0560	0.0200	0.2000	0.0900	0.1700	0.1300	0.1	0.16
Sum	99.8970	99.6580	97.8772	99.4455	101.400	98.4570	99.2700	99.2600	99.2400	97.8200	98.28

Table 2. CIPW norm of the igneous rocks

Quartz	24.3780	25.4780	23.6250	28.8840	27.8000	8.9010	26.3200	26.7100	2.1810	0.0000	1.9770
Corundum	1.8020	1.702	0.763	1.661	1.989	0	0	0	0	0	0
Orthoclase	31.1410	30.141	19.187	17.809	40.13	9.499	27.268	17.958	4.552	2.208	2.416
Plagioclase	39.659	39.759	54.052	49.59	31.85	55.234	38.682	47.32	55.446	57.256	57.133
Albite	33.3190	32.3190	44.9730	40.5540	30.2070	29.9760	22.9720	24.7580	18.2370	23.8310	26.6210
Anorthite	7.4390	7.4390	9.0790	9.0360	7.3770	25.2580	15.7110	18.5630	17.2090	33.4250	30.5120
Diopside	0.0000	0.0000	0.0000	0.0000	0.0000	6.8600	0.0000	0.0000	16.5100	18.2990	15.8660
Hypersthene	1.1650	1.1550	1.7370	0.7930	0.0200	10.7390	4.5220	4.7040	15.6180	13.1400	14.3710
Olivine	0.0000	0.0000	0.0000	0.0000	0.0000	0.0000	0.0000	0.0000	0.0000	2.3610	0.0000
Ilmenite	0.0640	0.0740	0.0250	0.0550	0.1000	0.2150	0.1120	0.1120	0.1880	0.2070	0.2410
Hematite	1.4488	1.4490	0.5720	1.0360	2.0620	5.9430	2.5390	2.2040	4.4070	5.1460	5.3870
Apatite	0.1332	0.1330	0.0000	0.1180	0.1550	0.4280	0.1930	0.3630	0.2720	0.2120	0.3420
Titanite	0.0000	0.0000	0.0000	0.0000	0.0000	2.1820	0.2670	0.4200	0.8260	1.1700	2.2680
Rutile	0.1090	0.109	0.04	0.054	0.038	0	0.097	0.209	0	0	0
Sum	100	100	100	100	100	100	100	100	100	100	100
DI	87.9380	87.9380	87.7850	87.2470	91.2000	48.3760	76.5800	73.4280	24.9700	46.0390	31.0140
CI	7.4390	7.4390	9.0790	9.0360	89.8100	32.1180	15.7110	18.5630	53.7190	151.7240	46.3780

Table 3. Trace element analyses (in ppm) of igneous rocks from the study area

Rock Types	Sample No.	Rb	Ba	Th	U	Nb	La	Ce	Sr	Nd	Hf	Zr	Sn	Tb	Y	Cr	Cu	Zn
Biotite Granite	Sp.1	357	294	78	22	24	38	118	72	58	4.4	89	12.4	<2	18	2	<2	60
	Sp.2	297	190	56	20	38	69	98	146	62	4.2	62	13.8	<2	16	2	<2	40
	Sp.6	158	192	40	11	14	26	80	55	38	3.8	43	4.8	0.28	22	<2	<2	<2
	Sp.9	254	194	90	12	10	32	68	126	40	4.2	82	3.4	0.42	23	1	<2	30
Pegmatite	Sp.8	493	139	9	3	14	12	28	42	16	<2	28	<2	<2	<2	1	<2	72
Diorite	Sp.3	138	70	18	3	10	26		353	18	<2	121	<2	<2	16	90	77	80
	Sp.24	189	415	39	4	11	29	56	196	28	<2	94	<2	<2	22	15	<2	39
	Sp.25	129	498	23	5	12	24	49	300	16	<2	162	<2	<2	13	28	<2	45
	Sp.26	49	142	7	<2	6	11	25	404	11	<2	48	<2	<2	12	588	<2	52
Hornblen-dite	Sp.5	20	138	2	<2	4	12	22	730	<2	<2	144	<2	<2	15	516	40	50
	Sp.27	45	143	2	<2	3	11	24	368	14	<2	114	<2	<2	22	387	<2	77

4. ANALYSIS

4.1 Geochemical Characteristics of Igneous Rocks:

The study area is composed of felsic to ultramafic rocks. Chemically SiO_2 content is ranging from 40.80% to 72.69%; granite sample - 71.69% to 72.69%, diorite - 50.80% to 60.68%; meladiorite and hornblendite - 40.80% to 50.14%.

In Harker variation diagrams, major oxides of TiO_2, Al_2O_3, Fe_2O_3, CaO, MgO and P_2O_5 are negatively correlated with SiO_2. K_2O and Na_2O are positively correlated with SiO_2 (Figure 3) suggesting that this granitic pluton was derived from the evolved magma (Winter, 2010). Selected trace elements versus SiO2 variation diagrams show that the compatible trace elements such (Nb, Ba, Rb and Zr) show positive trends against silica increase whereas incompatible element (Sr) shows negative correlation with increasing silica.

In the Normative Ab-Or-An diagram (O Conner, 1965), granite rock units of the area fall in the granite field, diorite rocks fall in the granodiorite field, meladiorite and hornblendite fall in the tonalite field (Figure 4). In TAS diagram (Middlemost, 1985), granitic rock units of the area fall in the granite field, diorite unit fall in the diorite and granodiorite field, hornblendite and meladiorite units fall in the gabbro field (Figure 5). The total alkali versus silica (TAS) diagram (after Cox-Bell-Pank, 1979) is also shown in (Figure 6).

According to alkali wt % versus SiO_2 diagram (Irvine & Baragar, 1971) the igneous rocks of the study area fall in the subalkaline field (Figure 7). The subalkaline field was subdivided in the SiO_2 versus FeO/MgO diagram (Miyashiro, 1974) in which most granitic rocks of the study area fall in the calc-alkaline series (Figure 8). In the Na_2O-Al_2O-K_2O diagram (Shand, 1927), the granitoid rocks of the area fall in the peraluminous field (Figure 9).

Consequently, the calc-alkaline nature of granitic rocks of the study area is generally restricted to the subduction related plate tectonic process.

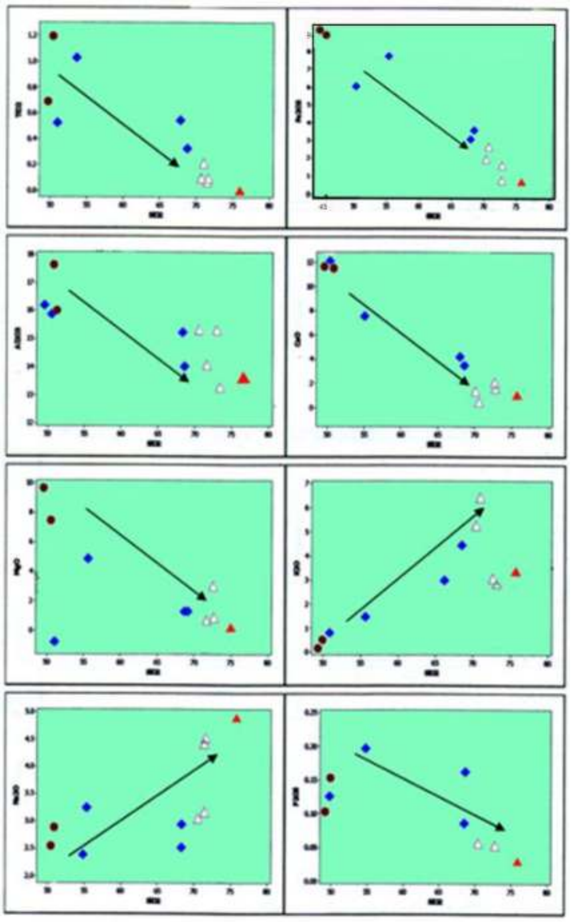

Fig. 3(a). SiO_2 versus major oxide (wt.%) Harker variation diagram of the igneous rocks

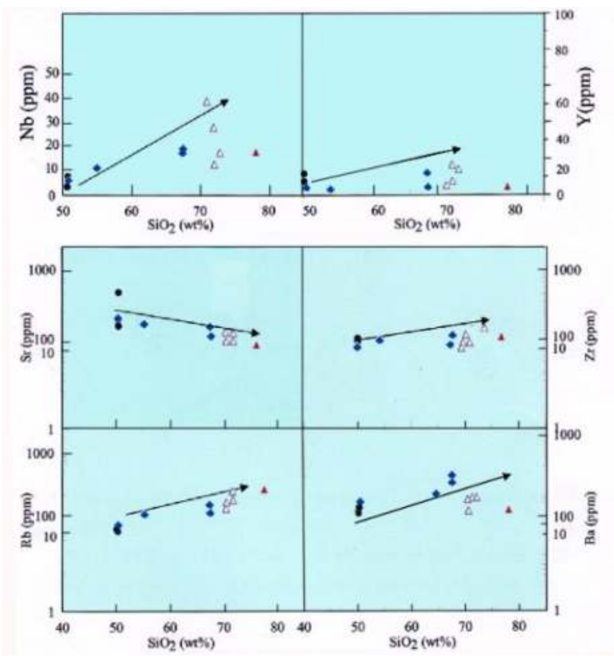

Figure 3(b). SiO_2 versus trace elements (ppm) Harker variation diagram of the igneous rocks

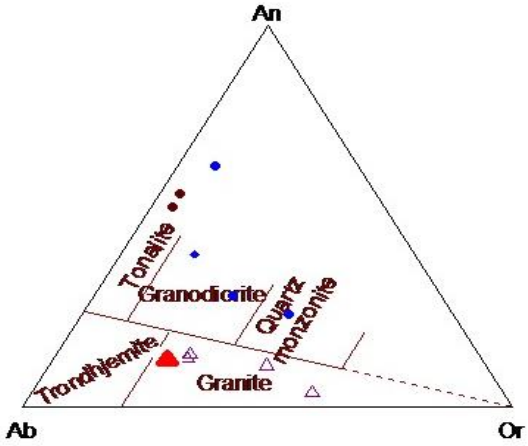

Figure 4. Normative Ab-Or-An diagram for the igneous rocks of the study area, with dividing lines

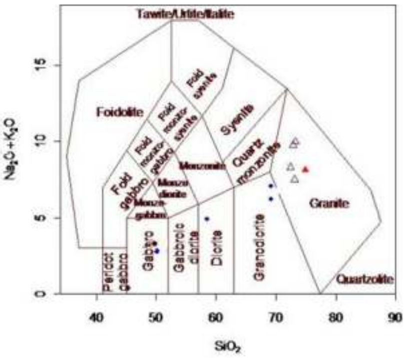

Figure 5. TAS diagram showing the granite field of study area

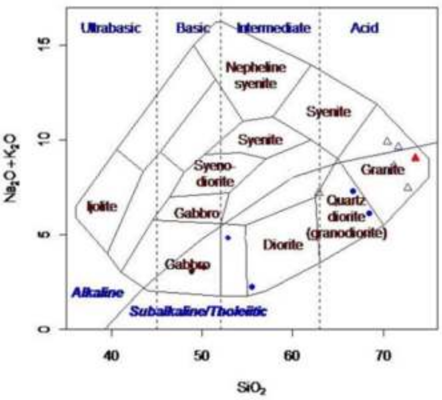

Figure 6. Total alkali versus silica diagram

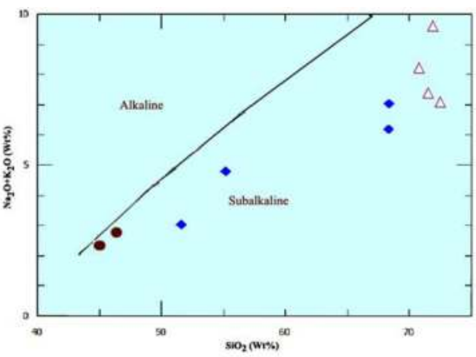

Figure 7. Alkali wt % versus SiO_2 diagram

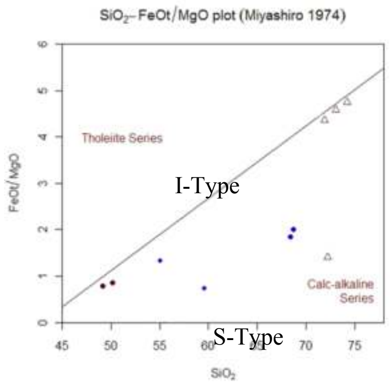

Figure 8. SiO_2 vs FeO_t/MgO diagram for the igneous rocks of the area

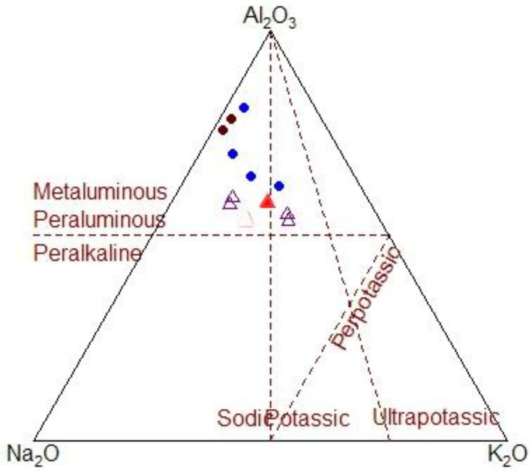

Figure 9. Na_2O-Al_2O-K_2O diagram, for the igneous rocks of the area

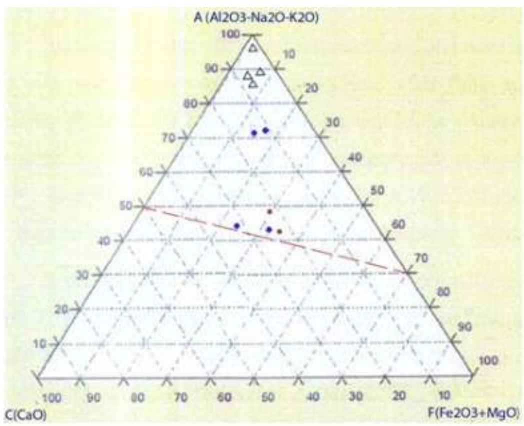

Figure 10. ACF diagram for granitoid rocks of the study area

4.2 Type of Granitoid Rocks

Based on the petrochemical analyses data, the weight percent of silica is high in granitic rocks, reaching up to 72.73%. The Alumina Saturation Index (ASI) of granitic rocks in the area is A/CNK >1.1 with average wt% ratio of 1.42, indicating high degree of peraluminous. Normative corundum ranges from 0.8111 to 1.546 (>1%) in igneous rocks of the area and lack of normative magnetite is characteristics.

In this respect, the granitoid rocks of the study area are in accordance with the S-type nature according to

Chappell and White (1974). In addition, ACF diagram pointed out that granitoid rocks of the study area belongs to the S-type field (Hyndman, 1985) (Figure 10). The relative high quartz content up to 31.93 wt% of this S-type granite can be considered that these granites were derived from partial melting of quartz rich sedimentary rocks or from the supracrustal origin (Chappell and White, 1974).

4.3 Condition of the Crystallization of Granitoid Rocks

According to Tuttle and Bowen's (1958) in the ternary plot of normative Q-Ab-Or, it can be supposed that granitic rocks of the study area was consolidated under the low-pressure condition, between 0.5 Kb to 5Kb (Figure 11).

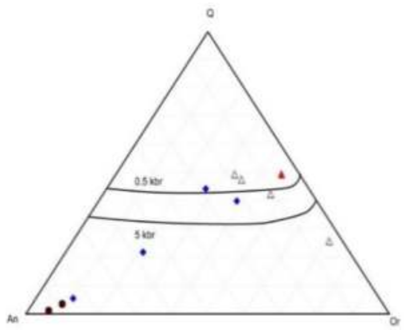

Figure 11. Ternary plot showing normative Q-Ab-An (wt%) composition of the granitoid rock of the area

If the granitoid racks were assumed as crystallization of minimum pressure of 2Kb, their liquidous temperature can be estimated from the differentiation index and temperature at 2 Kb water pressure diagram (Piwinskii and Wyllie, 1970). From this diagram, liquidus temperatures are 630°, 680°, 720°and 920° for pegmatite, granite, diorite and hornblendite respectively (Figure 12). Depth of the crystallization of the igneous rocks can be deduced from the schematic depth-temperature diagram (Marmo, 1969). From this diagram, pegmatitic magma probably differentiated at depth of 21km, biotite granite probably crystallized at 22.5 km, diorite segregated at 24 km, and meladiorite and hornblendite fractionated at 31.5 km (Figure 13). According to the R_1-R_2 binary (in millications) diagram of Batchelor and Bowden (1985), granite units correspond to syn collision rocks and tend towards the post orogenic zone, diorite unit corresponds to pre-plate collisional rock and pegmatite to post-collisional zone (Figure 14).

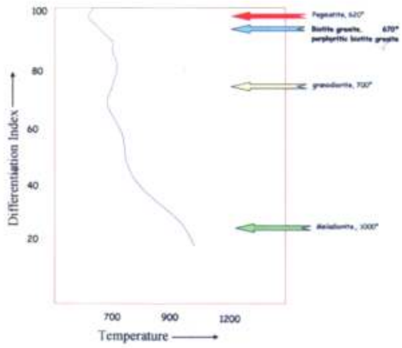

Figure 12. Temperature-differentiation index diagram for the igneous rocks of the study area, at 2kb water pressure

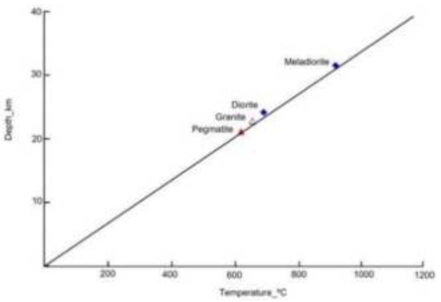

Figure 13. Schematic depth-temperature relation diagram

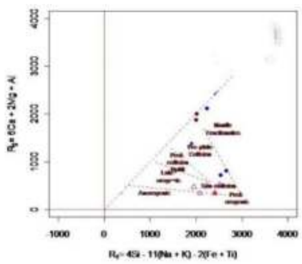

Figure 14. R_1-R_2 binary (in millications) diagram for the discrimination of tectonic environment in the study area

5. CONCLUSION

The igneous rocks in the study area ranges from granite through granodiorite to tonalite. According to SiO_2 versus FeO/MgO diagram, most granitic rocks of the study area fall in the calc-alkaline series, generally restricted to the subduction related plate tectonic process. The granitoid rocks of the study area are in accordance with the S-type nature, according to their weight percent of silica and the Alumina Saturation Index (ASI), and derived from the supracrustal origin. Based on the analyzed data, the granitoid magmatism of the region formed in relation to the pre-dated and post-dated collision of India with Eurasia.

ACKNOWLEDGEMENT

We would like to express our gratitude to Rector (Acting) Dr. Thet Lwin and Pro-Rector Dr. Yaw Han Tun, Pakokku University, for their permission to carry out this research. We also thank to Dr. Than Than Nu, Professor and Head of Geology Department, University of Mandalay, for her comments for this work. We are indebted to Dr. Tin San, Pro-Rector, Technological University Lashio, for her permission and invitation of paper.

REFERENCES

[1] Batchelor, R.A., Bowden, P, Petrographic interpretation of granitic rocks series using multicationic parameters. *Chem, Geol*., 48, p 43-55, 1985.

[2] Chapple, L.B. & A.J.R. White, The contracting granite types: *Pacific Geology*, v. 8, p. 173-174, 1974.

[3] Cox, K.J., Bell, J.D., PanKhurst, R.J., *The interpretation of igneous rocks*. George Allen and Unwin (Publisher), Ltd. P 450, 1979.

[4] Hyndman, D. W., *Petrology of Igneous and Metamorphic Rocks*. New York, McGraw-Hill, Inc., 786p, 1985.

[5] Irvine, T. N., Baragar, W. R. A., A guide to the geochemical classification of the common volcanic rocks. *Can. J. Earth Sci*. 8, p523-548, 1971.

[6] Khin Zaw, Geological, petrological and geochemical characteristics of granitoid rocks in Burma: with special reference to the associated W-Sn mineralization and their tectonic setting. *Journal of Southeast Asian Earth Sciences*. Vol.4, No.4, pp. 293-335, 1990.

[7] Kyu Kyu Win, Petrology and structures of the rocks of the Gu-Taung Hill area, Myitha Township, M.Sc. Thesis (Unpublished), University of Yangon, 1980.

[8] Marmo, V., On the emplacement of Granites. *Amer.Jour*., Sci. vol.254., p 479-492, 1956.

[9] Middlemost E.A.K., *Magmas and magtic rocks*.Longman London, 1985.

[10] Mitchell, A.H.G., Cretaceous-Cenozoic tectonic events in the western Myanmar (Burma)-Assam Region. *Journal of the Geological Society of London*. vol. 150, p.1090-1102, 1993.

[11] O' Corner, J.T., Classification of quartz rich igneous rocks based on feldspar .ratios. *U.S.Geol.Surv Prof* .Paper.525B,P 79-84, 1965.

[12] Pececrillo, A., & Taylor, S,R., Geochemistry of Eocene calc alkaline rocks from the Kastamonu area, Northern Turkey. *Contribution to Mineralogy* and *Petrology*. 58, p.68-81, 1976.

[13] Philpotts, A.R., *Principles of Igneous and Metamorphic Petrology*, Prentice Hall Inc, Eaglewood Cliff, New Jersey, U.S.A, 1990.

[14] Piwinskii,A.J., and Willie P.J., Experimental studies of igneous rocks series : felsic body suit from the Needle point pluton,Wallowa Batholith,Orogon. *Jour, Geol.*V.78, No2,p. 52-76, 1970.

[15] Searle, D.L and Haq, B.T., *The Mogok Belt of Burma and its relationship to the Himalayan Orogeny.* Paper read at 22nd. International Geol., Congr., India 11, 133-161, 1964.

[16] Shand, S.J., Eruptiverocks. Their Genesis, Composition, Classification and their relation to Ore-deposit. 3rd ed. John Wiley & Sons, New York, 488P, 1947.

[17] Tuttle .O.F., and Bowen, N.L., Origin of granite in the light of experimental studies in the system $NaAlSi_3O_8$-SiO_2-H_2O. *Geol.Soc. America Mem*. 74, P.153, 1958.

[18] Winter, J. D., *An introduction to Igneous and Metamorphic Petrology.* 2nd ed. Prentice Hall, New Jersey. 702p, 2010.

Experimental Study on Physical Properties of Materials in Ready-Mixed Concrete

Khaing Su Tin[1], Ba Nyar Oo[2], Kyaw Zeyar Win[3]
[1]Department of Civil Engineering, Technological University (Thanlyin), Myanmar
[2] Department of Civil Engineering, Technological University (Thanlyin), Myanmar
[3] Department of Civil Engineering, Technological University (Thanlyin), Myanmar
Email:khaingsutin2018@gmail.com,banyaroo@ttu.edu.mm,kyawzeyarwin@ttu.edu.mm

ABSTRACT: This study presents experimental study on physical properties of materials in ready mix concrete. In this study, three kinds of cement (Alpha, Double Rhino, Elephant) and aggregates which are taken from different regions (Thaketa, Mawlamyaing, Mandalay) are used to test the physical properties of materials. In this research, physical properties of cement and aggregates are carried out. The specific gravity of Apache, Double Rhino and Elephant are 3.18, 3.15, and 3.13 respectively. For Portland cement, specific gravity of value has around 3.15. The fineness of elephant cement exists in the standard range (3500-3800 cm^2/g) according to ASTM standards. The compressive strength of at the age of 3 days and 28 days. The specific gravity and absorption of fine and coarse aggregates were taken from (Thaketa, Mawlamyaing, Mandalay) test results are as nearly 2.6. For In this study, test of cement and aggregates are based on standard specification of American Society for Testing and Materials (ASTM).

KEYWORDS: *Ready-Mixed Concrete,Sieve Analysis, Fine and Coarse Aggregate,Cement, Laboratory Tests, ASTM*

1. INTRODUCTION

The Union of Myanmar is a developing country that many construction projects are carried out to improve the infrastructure of the country at present. Most of the heavy projects are especially carried out by the reinforced concrete structures. Yangon, being a commercial city of Myanmar, there are crowded population and have upcoming projects such as urban redevelopment projects, low cost housing projects, and industrial zone development. Therefore, it is needed to get the high qualities concrete to save the public's lives and their properties. To get the high qualities concrete, it is therefore necessary to test the materials in ready-mixed concrete before delivering and placing to the site. In its simplest form, ready-mixed concrete is a mixture of paste, sand, and aggregates. This paste, composed of sand water, coats the surface of fine and coarse aggregates and binds them together into a rock like material known as concrete. All aggregates should be of a washed type material with limited amounts of fines or dirt and clay. Ready-mixed concrete is bought and sold by volume- usually expressed in cubic meters. Ready mixed concrete is batched or manufactured under controlled conditions.

2. PHYSICAL PROPERTIES OF MATERIALS

For cement, Specific gravity test, fineness test, consistency test, soundness test, setting time test, compressive strength test are carried out. For aggregates, sieve analysis of fine and coarse aggregates, Specific gravity and absorption of fine and coarse aggregates, clay lump and Friable Particles of fine and coarse aggregates, Material finer than 75µm Sieve No.(200) of fine and coarse aggregates, flaky and elongated particles of coarse aggregates, Organic Impurities of fine aggregates are tested.

3. TESTING METHOD AND RESULTS OF ORDINARY PORTLAND CEMENT, COARSE AGGREGATE AND FINE AGGREGATE

A. Specific Gravity

Specific gravity test is defined as the density of any substance to the density of other reference substance at a specified temperature. Test results for different cements are shown in Table 1.

Table 1. Specific Gravity of Different Cement

Specification- (ASTM) C-188			
Sample	Specific Gravity of Cement Number of Test I	 II	Average
Apache	3.16	3.19	3.18
Double Rhino	3.14	3.16	3.15
Elephant	3.12	3.14	3.13

B. Fineness of Cement

Fineness of cement affects workability of fresh concrete and long term behavior of structure. The results of fineness test for different cement shown in Table 2.

Table 2. Fineness of Different Cement

Specification- (ASTM) C-204			
Sample	Finess of Cement(cm^2/g) Number of Test I	 II	Average(cm^2/g)
Apache	3357	3357	3357
Double Rhino	4050	4029	4039.5
Elephant	3616	3753	3685

C. Consistency of Cement

Consistency test is used to find amount of water to be mixed with cement. This test helps to determine water content. The standard and normal consistency of ordinary Portland cement varies between 25-35% [1]. The results for the consistency of different cement are shown in Table 3.

Table 3. Consistency of Different Cement

Specification- (ASTM) C-187					
Sample	Plunger Penetration Reading(mm)			Remarks	Water (%)
Test	I	II	III		
Apache=300g Water=72g	6	7	8	Not OK	24%
Apache=300g Water=72g	9	-	-	OK (Allow10±1mm)	24.5 %
Double Rhino=300g Water=72g	7	8	-	Not ok	25%
Double Rhino=300g Water=76.5g	10	-	-	OK (Allow10mm)	25.5 %
Elephant =300g Water=75g	-	8	9.5	OK (Allow10±1mm)	25%

D. Setting Time of Cement

` Initial setting time is important in estimating free time for mixing, transportation, placing, compacting and shaping of cement paste. Final setting time also affects the strength and durability of concrete. Setting time results for different cements are shown in Table 4.

Table 4. Setting Time of Different Cement

Specification- (ASTM) C-191		
Sample	Initial Setting Time(mm)	Final Setting Time(mm)
Apache	1:30	2:45
Double Rhino	1:34	3:15
Elephant	1:25	3:45

E. Soundness of Cement

The ability of cement to retain its volume after it gets hardened is known as soundness of cement. This means that cement should be at minimum volume change after its hardened. Test results of different cement are shown in Table 5.

Table 5. Soundness of Different Cement

Specification-European Standard (EN) 196-3:1987			
Sample	Before boiling (mm)	After boiling (mm)	Difference (mm)
Apache	6.5	7.7	1.2
Double Rhino	5.8	7.1	1.3
Elephant	6.8	8.2	1.4

F. Compressive strength of Cement

Compressive strength of cement is determined by compressive strength test on mortar cubes compacted by means of a standard vibration machine. Standard sand is used for the preparation of cement motor. The test sample and results for compressive strength of cement are shown in Table 6 and 7.

Table 6. Test Sample for Compressive strength of Cement

Materials	Number of Specimens	
	6	9
Cement(g)	500	740
Sand(g)	1375	2035
Water ml for Portland Cement (0.485) (g)	242.5	359
Air-entraining Portland Cement (0.460) other (to flow of 110±5̊ C(g)	230	340

Table 7. Compressive Strength of Different Cement

Specification - (ASTM) C-109						
Mix (g)	500g cement: 1375g sand: 242.5g water					
Sample	Curing Age (days)				Average (MPa)	
	3	3	28	28	3	28
Apache	18.7	19.1	36.5	37.8	18.9	37.1

Double Rhino	32.3	31.7	41.6	43.2	32	42.4
Elephant	33.5	35.6	43.9	44.2	34.5	44.0

G. Test results of Aggregates

Test results of Physical properties of fine and coarse aggregates are shown in Table 8,9,10,11,12,13.

Table 8. Physical properties of Fine Aggregates

Sample	Thaketa (TKT)	Mawlamyaing(MLM)	Mandalay (MDY)
Type	River Sand	River Sand	Crushed Sand
Wtof Sample(g)	500	500	500
Finess Modulus (ASTM C-136-05)	2.14	2.2	3.12
Specific Gravity(ASTM C-128)	2.6	2.58	2.6
Absorption%(ASTM C-128)	1.35	1.25	1.08
Clay Lumps%(ASTM C-142)	2.15	1.78	0.38
Wtof Sample(g)	300	300	300
%Material Finer(ASTM C-117)	3.38	2.10	1.79

Table 9. Physical properties of Coarse Aggregates

Sample	Thaketa (TKT)	Mawlamyaing(MLM)	Mandalay (MDY)
Type	River Shingle	River Shingle	Crushed Stone
Wtof Sample(g)	1000	1000	1000
Grading Size(mm) (ASTM C-136-05)	19	19	19
Specific Gravity(ASTM C-127)	2.62	2.61	2.77
Absorption%(ASTM C-127)	0.66	0.86	0.83
Flaky%(ASTM D-4791)	10.97	5.6	26.23
%Elongated(ASTM D-4791)	4.25	4.11	8.08

Table 10. Clays Lumps and Friable Particles of Coarse Aggregates

Specification-(ASTM) C-142			
Wt of Sample ,g	3000	2000	1000
Sample	Clay Lumps%		
Thaketa (TKT)	0.04	0.11	0.03
Mawlamyaing (MLM)	0.23	0.27	0.41
Mandalay (MDY)	1.51	1.99	1.95

Table 11. Material finer than 75 m of Coarse aggregate

Specification-(ASTM) C-142			
Wt of Sample ,g	5000	2500	1000
Sample	% of Material Finer		
Thaketa (TKT)	0.11	0.17	0.24
Mawlamyaing (MLM)	0.1	0.37	0.32
Mandalay (MDY)	0.88	0.96	1.21

Table 12. Organic Impurities in Fine Aggregates

Sample	Weight of Sample(g)
Distilled Water	97
Tannic Acid	2.5
Sodium Hydroxide	3
Methylated	10
Sand	127

Table 13. Standard Test Colour for Organic Impurities

Gardener Color Standard no	Organic Plate no

5	1
8	2
11	3
14	4
16	5

4. COMPARISON ON TEST RESULTS OF DIFFERENT ORDINARY PORTLAND CEMENT, FINE AND COARSE AGGREGATES

Table 14. Comparison on Results for Specific Gravity of Different Cement

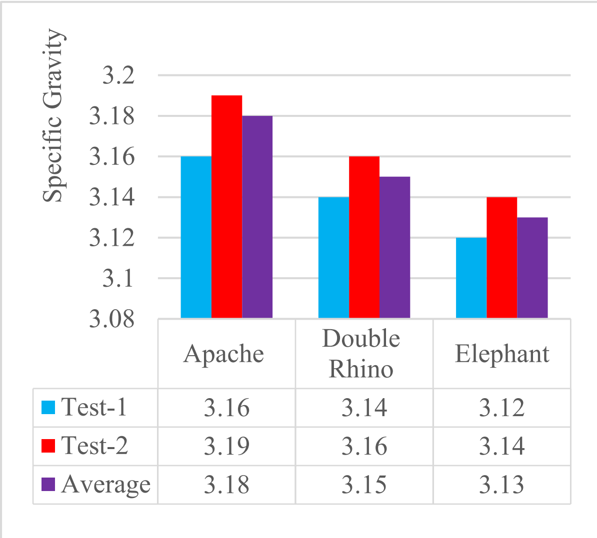

According to ASTM, the specific gravity of Portland cement is 3.15. In this study, the specific gravity of Apache cement is the higher than Double Rhino and Elephant. Comparisons on Results for Specific Gravity of Different Cement are shown in Table 14.

Table15. Comparison on Results for Fineness of Different Cement

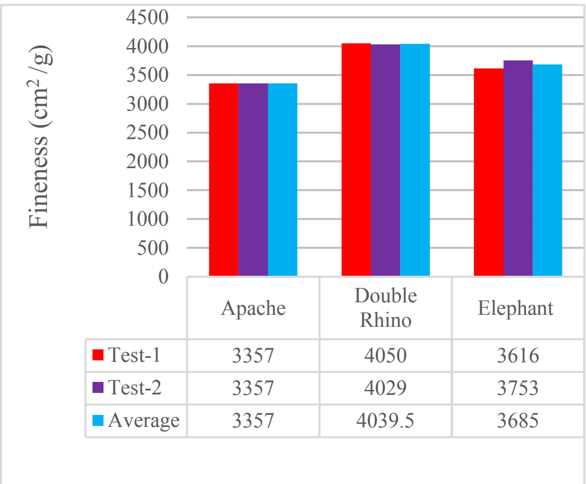

The fineness of Portland cement is generally about 3500-3800cm^2/g. Elephant cement exist in the standard range. Fineness test results are shown in Table 15.

Table16. Comparison on Results for Consistency of Different Cement

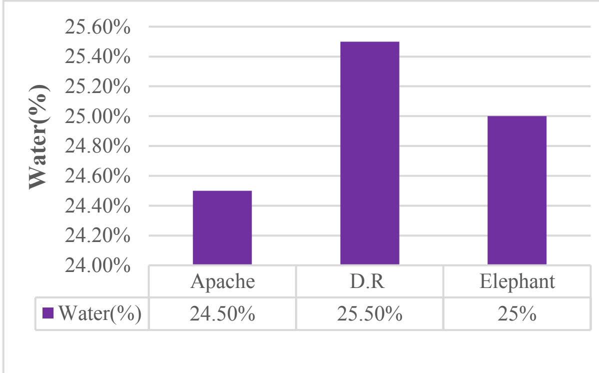

The consistency of Portland cement is generally 25% - 35%. Results for Consistency of Different Cement are shown in Table 16.

Table17. Comparison on Results for Setting Time of Different Cement

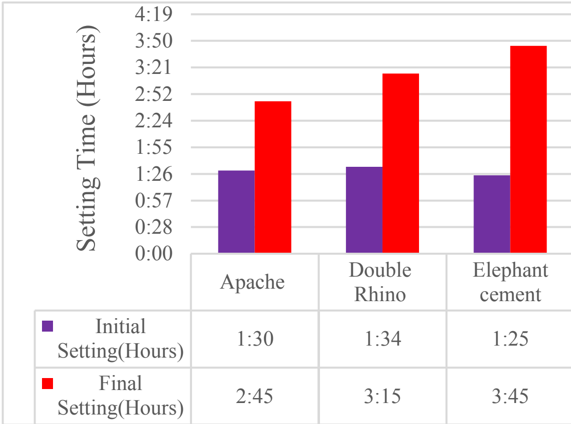

The initial setting time of ordinary portland cement is not less than 45mins, and final setting time is not more than 375mins. From table 17, the initial setting time of Double Rhino cement is the highest and it can be seen that the final setting time of Apache cement is the lowest. All of the cement brands exist in the standard range. Results for setting time of different cement are described in Table 17.

Table18. Comparison on Results for Soundness of Different Cement

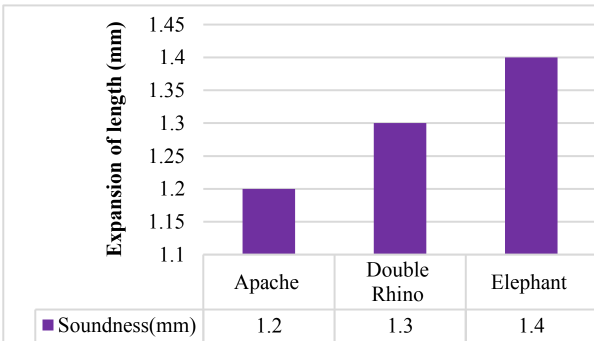

The soundness of ordinary portland cement is not more than 10mm. The soundness of Elephant cement is the highest. Soundness of different Ordinary Portland cement results are presented in Table 18.

Table 19. Comparison on Results for Compression Result of Different Cement

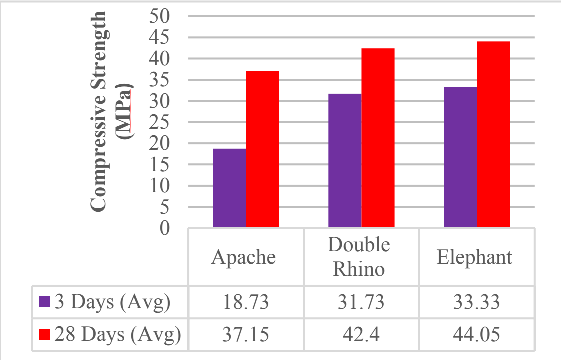

The compressive strength of Ordinary Portland cement is at minimum 12Mpa for 3days, and no limit at maximum. All of the cement brands exist in the standard range. Table 19 shows the compressive strength of Different Ordinary Portland cement.

Table 20. Comparison on Results for Fineness Modulus of Fine Aggregates

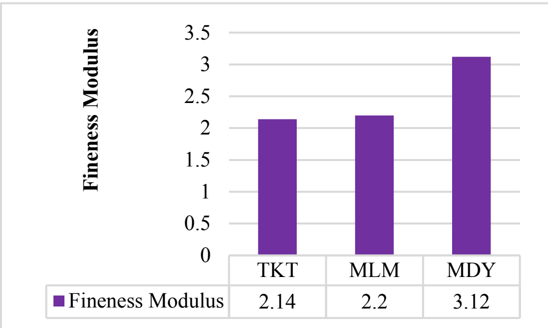

Generally, the fineness modulus of crush sand is more than the river sand. According to the chart, the fineness modulus of crush sand is the highest in TKT is the lowest. Comparison on Results for Fineness Modulus of Fine Aggregates is shown in Table 20.

Table 21. Comparison on Results for Fineness Modulus of Coarse Aggregates

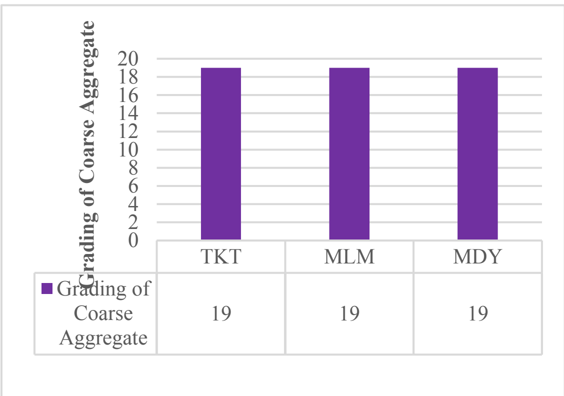

Results for Fineness Modulus of Coarse Aggregates are presented in Table 21. The grading of coarse aggregate well within the limit of 12.5mm to 37.5mm. In this study, all the grading of coarse aggregate exists in the standard limit.

Table 22. Comparison on Results for Specific Gravity and Absorption of Fine Aggregates

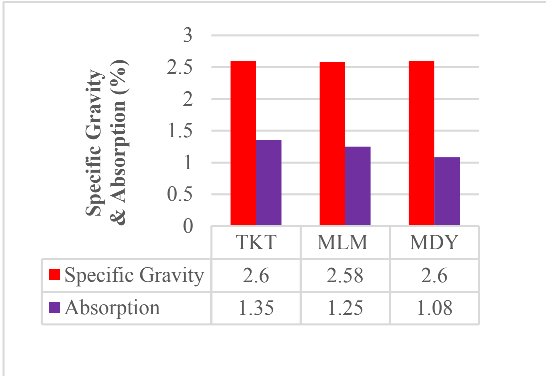

In this study, all of the specific gravity test results are as nearly 2.6. The absorption percent of Thaketa(TKT) river sand is the highest. Test results are shown in Table 22.

Table 23. Comparison on Results for Specific Gravity and absorption of Coarse Aggregate

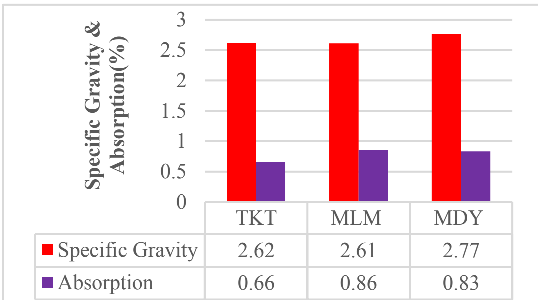

According to Table 23, the specific gravity of Mandalay (MDY) crushed stone is over 2.62. The specific gravity of coarse aggregate is nearly to 2.62. The absorption percentage of Mawlamyaing (MLM) river shingle is the highest and Thaketa (TKT) crushed stone is the lowest.

Table 24. Comparison on Results for Clay Lump of Fine Aggregate

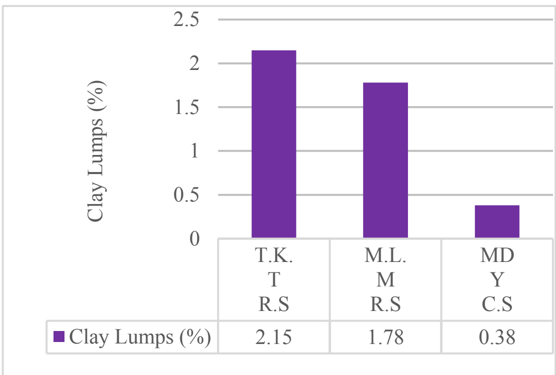

From Table 24, the highest and lowest percentage of the clay lumps are Thaketa (TKT) river sand and MDY crushed sand respectively.

Table 25. Comparison on Results for Clay Lump of Coarse Aggregate

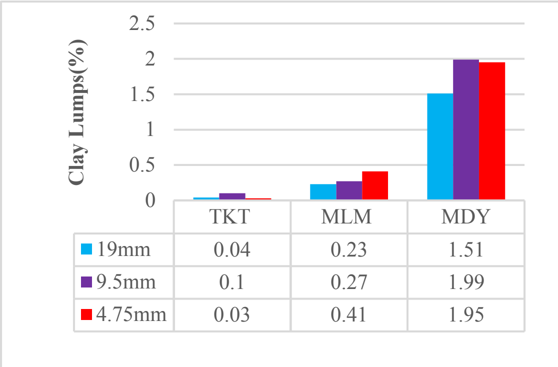

	TKT	MLM	MDY
19mm	0.04	0.23	1.51
9.5mm	0.1	0.27	1.99
4.75mm	0.03	0.41	1.95

From Table 25, The highest and lowest percentage of the clay lumps are Mandalay crushed stone and Thaketa river shingle respectively. According ASTM, the percentage of clay lump allow the aggregates to cool and weigh to nearest 0.1%.

Table 26. Comparison on Results for Material finer than of Fine Aggregate

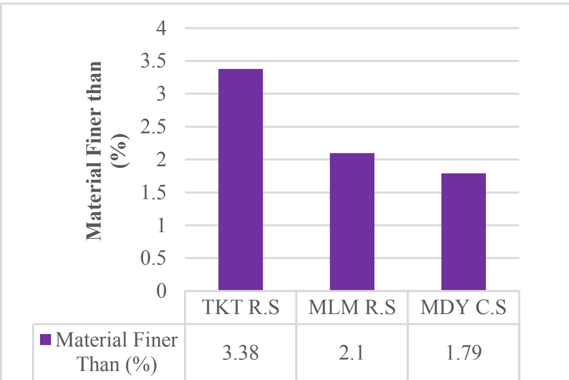

	TKT R.S	MLM R.S	MDY C.S
Material Finer Than (%)	3.38	2.1	1.79

In this study, the highest and lowest percentage of material finer than 75µm sieve (No.200) of fine aggregates are TKT River sand and MDY Crushed sand respectively. Results for Material finer than of Fine Aggregate are shown in Table 26.

Table 27. Comparison on Results for Material finer than of Coarse Aggregate

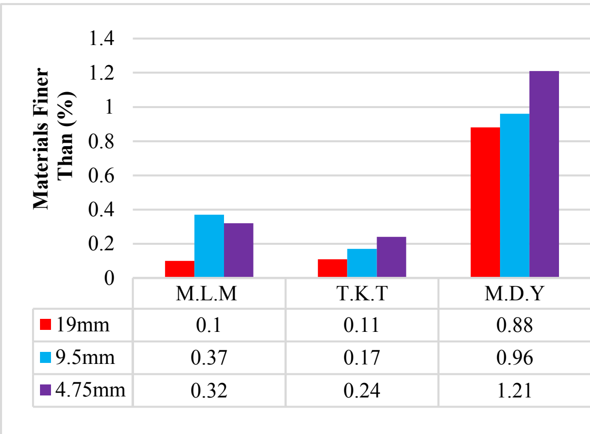

	M.L.M	T.K.T	M.D.Y
19mm	0.1	0.11	0.88
9.5mm	0.37	0.17	0.96
4.75mm	0.32	0.24	1.21

From table 27, the highest and lowest percentage of material finer than 75µm sieve (No.200) of coarse aggregates are Mandalay crushed stone and Tarkata (TKT) river shingle respectively. According to ASTM C-117, the percentage allows the aggregates to cool and weigh to nearest 0.3% for fine and coarse aggregates.

Table 28. Comparison on Results for flaky and elongated % of Coarse Aggregate

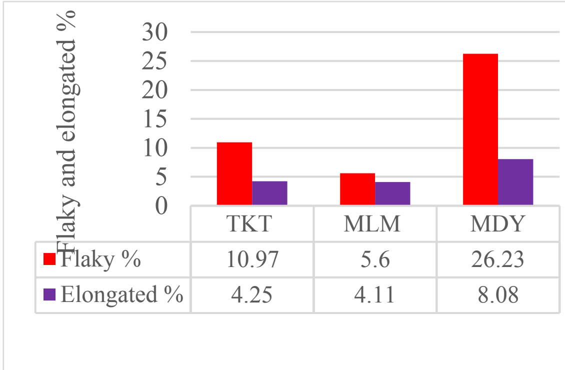

	TKT	MLM	MDY
Flaky %	10.97	5.6	26.23
Elongated %	4.25	4.11	8.08

In Table 28, the highest and lowest percentage of flaky particles of coarse aggregates are Mandalay (MDY) crushed stone and Mawlamyaing(MLM) river shingle respectively. From ASTM D-4791, the percentage of flaky and elongated is not more than 35%.

5. PHYSICAL TEST EQUIPMENTS OF CEMENT AND AGGREGATES

Fig1. Test for Specific Gravity of Cement

Fig 2. Test for Organic Impurities of Fine Aggregates

Fig 3. Test for Compressive Strength of cement

4.

CONCLUSIONS

In this study, different types of cement (Apache, Double Rhino, Elephant) , fine and coarse aggregates which are taken from different regions (Thaketa, Mawlamyaing, Mandalay) are tested. From the physical results of cement, specific gravity of Double Rhino cement is the same as the standard value of cement as 3.15. The fineness of Elephant cement exist in the ASTM standard range (3500-3800) cm^2/g. The consistency of Double Rhino, Elephant cements exist in the standard range. The setting time, the soundness, and the compressive strength of all the cement brands exist in the standard range.

For the results of aggregates, the fineness modulus and grading of all the different fine and coarse aggregates exist in the ASTM standard limit. The specific gravity of all of the fine and coarse aggregates are as nearly 2.62. The absorption (%) of Thaketa (TKT) river sand is the highest and MDY crushed sand is the lowest. The absorption (%) of Mawlamyaing (MLM) river shingle is the highest and TKT River Shingle is the lowest. The highest and lowest percentage of the clay lumps of fine aggregates are Thaketa (TKT) and MDY crushed sand and that of coarse aggregates are Mandalay crushed stone and Thaketa river shingle respectively. The highest and lowest percentage of material finer than 75µm sieve (No.200) of fine aggregates are TKT River sand and MDY crushed sand and that of coarse aggregates are Mandalay crushed stone and TKT river shingle respectively. The highest and lowest percentage of flaky particles of coarse aggregates are Mandalay crushed stone and Mawlamyaing river shingle respectively. The highest and lowest percentage of elongated particles of coarse aggregates are Mandalay crushed stone and MLM River shingle respectively. From this study, the comparative results between different cement brands and different aggregate locations were obtained. These results were beneficial for local quality control engineers to engineers to determine the ready-mixed concrete (RMC) whether or not achieving the required strength. It should be noticed that the strength of concrete was increased with increasing quality of material standards in concrete.

ACKNOWLEDGEMENT

Firstly, the author would like to acknowledge Dr. TheinGi, Rector of Technological University (Thanlyin), for her kind permission to carry out this research work.

The author would like to express her thanks to her member Dr. Kyaw Zeyar Win, professor of the Department of Civil Engineering of Technological University (Thanlyin), for his valuable comments and guidance during this study.

The authors would like to thank many colleagues from Department of Civil Engineering, TU (Thanlyin). The authors would like to express U Ba Nyar Oo, Assistant Lecturer, Department of Civil Engineering, TU (Thanlyin) thanks to all preparation period of this paper.

REFERENCES

[1] Easton, Md., August 1, 2004, "American Society for Testing and Materials",Volume 04.02, Annual Book of ASTM Standard. U.S.A.

[2] Liton Biswas, April 21, 2013, "Building Materials, Concrete Technology".

[3] Rahul Mahajan, Sep-Oct 2015, "IOSR Journal of Mechanical and Civil Engineering(JOSR – JMCE)" Volume 12, Issue 5 Ver.

[4] Suryakanta, October1, 2016, "Aggregate, Concrete Technology, Construction,Materials".

[5] Suryakanta, July 24, 2014, "Concrete, Concrete Technology,Materials".

Seismic Performance Assessment Comparison of Steel Building With Fixed Base and Triple Friction Pendulum Bearing System

Nwe Nwe Win(1), Thazin Thein(2), Thu Thu Win(3)
(1),(2),(3)Technological University (Mandalay), Myanmar

Email: dr.nwenwewin@tum-mandalay.edu.mm

ABSTRACT*:* This study presents the relative understanding of the seismic performance enhancements of eight-storeyed residential steel building through the implementation of base isolation technology. The structures of fixed base building and isolated base building of same member size are used to compare their seismic performance. The nonlinear time history analyses are carried out to investigate the seismic response for eight-storeyed residential steel buildings supported the isolation system that is composed of triple friction pendulum bearings when subjected to earthquake loads at design basic earthquake (DBE) and maximum considered earthquake (MCE) levels. The seismic performance assessment is expressed as probable damage cost, repair time and injuries which are computed by using fragility curves and FEMA P-58 methodology in performance assessment calculation tool (PACT). Damage cost, repair time and injuries are computed for each building at seismic demand levels and the results are compared. This study demonstrated that the base isolation is effective at significantly mitigating and preventing seismic damage to the eight-storeyed residential building.

KEYWORDS: *fragility curves*, *performance assessment calculation tool, seismic demand levels, seismic performance, triple friction pendulum bearings*

1. INTRODUCTION

The protection of civil structures including their material contents and human occupants is without doubt a world-wide priority of the most serious current importance. Such protection may range from reliable operation and comfort to survivability on the other. The common feature of the different proposed approaches is modification of the dynamic interaction between the structure and the dynamic loads. The goal of the modification is to minimize the damage and vibrations throughout the structure.

Seismic isolation and energy dissipation systems are viable design strategies for seismic rehabilitation of buildings. Other special seismic control systems including active control, hybrid combinations of active and passive energy devices, tuned mass and liquid dampers. These systems include devices that enhance building performance primarily by modifying building response characteristics. Conceptually, isolation reduces response of the superstructure by decoupling the building from the ground. Typical isolation systems reduce forces transmitted to the superstructure by lengthening the period of the building and adding some amount of damping. Added damping is an inherent property of most isolators, but may also be provided by supplemental energy dissipation devices installed across the isolation interface. The isolation system reduces drift in the superstructure. Accelerations are also reduced in the structure although the amount of reduction depends on the force deflection characteristics of the isolators and may not be as significant as the reduction of drift. Reduction of drift in the superstructure protects structural components and elements as well as nonstructural components sensitive to drift induced damage and also reduction of acceleration protects nonstructural components that are sensitive to acceleration induced damage.

Myanmar is one of the earthquake prone regions as it is located in the eastern part of Alpide Earthquake Belt, between the eastern end of Himalaya Arc, the collision zone of Indian and Asia Plates, and the northern segments, highly active portions of the Sunda Arc. Therefore, the seismic isolation technique is conducted for the whole of Myanmar and for Mandalay (as pilot area) as well since it is located adjacent to the most active fault in Myanmar, the Sagaing Fault. Many types of isolation system have been developed elsewhere in the world to provide flexibility and damping to a structure in the event of seismic attack.

2. BASE ISOLATION SYSTEM

Base isolation is a passive control system that it does not require any external force or energy for its activation. It is necessary to understand the base isolation is needed to enhance performance levels of the structure subjected to seismic excitations. Base isolator is a more flexible device compared to the flexibility of the structure. Base isolation has specially designed interface at the structural base or within the structure, which can reduce or filter out the forces transmitted from the ground. These systems dissipate part of the energy created on the structure by the earthquake effect and thus increase the seismic performance of the structure and of its contents. A base isolation effectively protects structures against extreme earthquake without sacrificing performance during the move frequent, moderate seismic events. With the conventional methods of building earthquake resistant structures, structure may survive of the earthquake but it is very likely that it may not remain operational after any major seismic event. But base isolation technique not only prevents the earthquake from any serious damages but also maintains functionality that is building remains operational after earthquake.

2.1Sliding bearing

Base isolation using a sliding system is considered an easier strategy to approach and also the earlier method that have been developed. The basic concept of a sliding system is to reduce floor acceleration at the expense of shear displacement between foundation and upper structure. It can be achieved by introducing friction in geometric devices. Sliding bearings are mainly based on friction between stainless steel and Teflon. Depending on their sliding surface geometry, two kinds of sliding bearings are distinguished: flat slider bearings and curved slider bearings. Flat slider bearings take place when horizontal forces are applied and do not have restoring ability so they use with supplementary devices. Curved slider bearings act like flat slider bearings but they are little different in section. They have spherical surface at bottom. To guarantee that a sliding structure can return to its original position, other mechanisms, such as high-tension springs and elastomeric bearings, can be used as an auxiliary system to generate the restoring forces. Sliding isolation systems have successfully used for nuclear power plants, emergency fire water tanks, large chemical storage tanks and other important structures.

2.2 Triple friction pendulum bearing

The triple friction pendulum bearing is a more advanced modification of the single friction pendulum bearing. The triple friction pendulum (TFP) bearing differs from the single friction pendulum (FP) bearing in that there are three friction pendulum mechanisms existing in each bearing instead of just one mechanism. These mechanisms are activated at different stages as the seismic demand gets stronger. The three mechanisms are achieved by using four concave surfaces in a single bearing, with sliding occurring on two of the surfaces at a given time. The triple pendulum isolator's inner pendulum consists of an inner slider that slides along two inner concave spherical surfaces as shown in Fig 1. A cross section of a TFP bearing is shown in Fig 2. The triple friction pendulum isolator offers better seismic performance, lower isolator cost and lower construction cost as compared to other seismic isolation technology. The properties of each isolator's three pendulums are chosen to become sequentially active at different strengths. As the ground motions become stronger, the isolator displacements increase. At greater displacement, the effective pendulum length and the effective damping increase, resulting in lower seismic forces and isolators displacement.

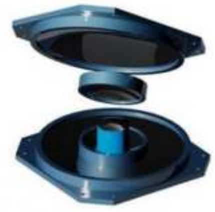

Fig 1. Disassembled triple friction pendulum bearing

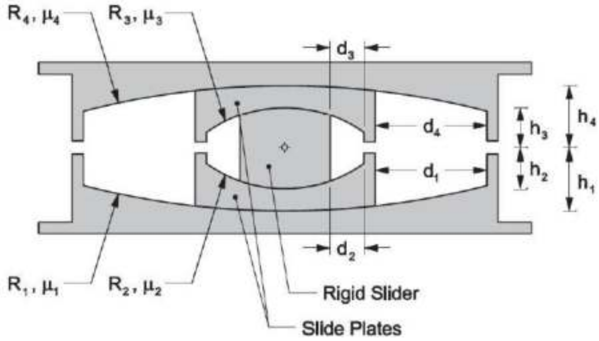

Fig 2. Cross section of triple friction pendulum bearing

3. ANALYSIS AND DESIGN PHASE

The eight-storeyed building has a regular plan 96 ft length and 60 ft width. The storey height is 10 ft high except first storey level. The height of first storey level is 12 ft and the total height of building is 92 ft above existing ground level. The critical damping ratio of superstructure is taken as 5% for isolated cases. The steel superstructure had a lateral system of special moment frames (SMF) in both the transverse and longitudinal directions, and that structural system was used for the fixed base and isolated base buildings designed for this study. The standard material properties in ETABS were used for this study including A 50 steel and 3 ksi concrete. The building is assumed to be located in Mandalay area and to be subjected to a 10% probability of exceedance in 50 years (10% in 50 years) seismic hazard corresponding to design basic earthquake (DBE) and a 2% probability of exceedance in 50 years (2% in 50 years) seismic hazard corresponding to maximum consider earthquake (MCE). According to Myanmar National Building Code the mapped spectral accelerations for 0.2-sec and 1-sec periods are taken as 2.01 g and 0.8 g, long-period transition period is 6 sec respectively. The response modification factors are taken as the value of 8 consistent with special moment frames structure. For all the buildings for nonlinear time history analysis have been performed.

3.1 Design of isolators for the proposed building

In this study, an isolation bearing was placed under every column and calculate gravity load. According to the theory, the period of the isolated base building should have greater than three times the static period of the original fixed base building. Since the same structural members are used for both the fixed base and isolated base structures, this study also encompasses the seismic performance enhancements that would result from retrofitting the fixed base eight-storeyed steel residential building with the same base isolation system.

There are three groups of isolator TPF1, TPF2 and TPF3 according to the range of reaction loads. The design of isolator for each group is done by the critical column load. The outer conclave plates were designed with a radius of curvature R of 88 in. The two inner concave surfaces are the same values for their coefficients of friction (μ_2= μ_3) and radii of curvature R_2 = R_3 = 16 in. For the study, it is assumed that μ_1= μ_4, R_1= R_4 = 88in, h_1= h_4= 4 in, h_2= h_3= 3 in, d_1= 15 in and d_2= 2 in. It had been considered that the isolator is a cylinder with diameter 12 in and total height of the bearing 13 in. The properties of the designed isolators and analysis input properties are shown in the Table 1to Table 3.

Table 1. Design and analysis input properties of TPF1

Property	TFP1	
	Outer	Inner
Effective Damping	0.2793	
U1, Effective Stiffness(kip/in)	126147	
U2,U3: Linear Effective Stiffness (kip/in)	4.49235	
U2,U3: Nonlinear Effective Stiffness (kip/in)	96.2549	98.6028
Friction Coefficient, Slow	0.1166	0.1195
Friction Coefficient, Fast	0.2333	0.2389
Rate Parameter	0.5	0.5
Radius of Sliding Surface (in)	84	13
Stop Distance (in)	0.1143	0.4779

Table 2. Design and analysis input properties of TPF2

Property	TFP2	
	Outer	Inner
Effective Damping	0.3186	
U1, Effective Stiffness(kip/in)	126147	
U2,U3: Linear Effective Stiffness (kip/in)	6.77604	
U2,U3: Nonlinear Effective Stiffness (kip/in)	2070.147	2048.314
Friction Coefficient, Slow	0.1146	0.1103
Friction Coefficient, Fast	0.2229	0.2206
Rate Parameter	0.5	0.5
Radius of Sliding Surface (in)	84	13
Stop Distance (in)	0.0592	0.0306

Table 3. Design and analysis input properties of TPF3

Property	TFP3	
	Outer	Inner
Effective Damping	0. 3058	
U1, Effective Stiffness(kip/in)	126147	
U2,U3: Linear Effective Stiffness (kip/in)	9.0501	
U2,U3: Nonlinear Effective Stiffness (kip/in)	511.4262	481.285
Friction Coefficient, Slow	0.1050	0.0988
Friction Coefficient, Fast	0.2100	0.1976
Rate Parameter	0.5	0.5
Radius of Sliding Surface (in)	84	13
Stop Distance (in)	0.1896	0.1609

3.2 Performance results from nonlinear time history analysis

In order to perform the nonlinear time history analyses, seven ground motions were selected and scaled to both the DBE and MCE response spectrum levels for Mandalay. The scaling of these records is performed by PEER-NGA such that the geometric mean of this record set is a reasonable match to the target spectrum. In order to scale the ground motions, the beta version of the PEER Ground Motion Database tool was used. This online tool linearly scales the acceleration amplitudes of fault-normal and fault-parallel ground motion records to a defined response spectrum over a defined period range, using the geometric mean of the records.

Comparisons of average response values of fixed base building and triple friction pendulum isolated base building from nonlinear time history analysis at DBE and MCE seismic demand levels are presented with storey drift ratio and storey acceleration.

3.2.1 Comparison of storey drift ratio for fixed and isolated base conditions at DBE level

The comparisons of storey drift ratio for fixed and isolatedbase buildings at DBE level in X and Y directions are shown in Fig 3 and Fig 4.

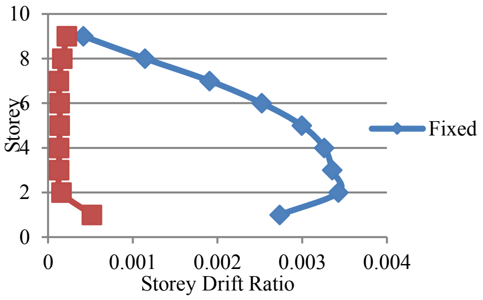

Fig 3. Comparison of storey drift ratio for fixed and isolated base condition at DBE in X direction

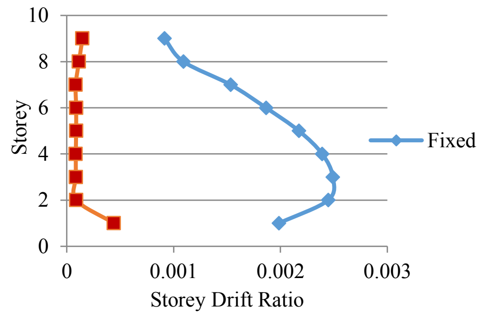

Fig 4. Comparison of storey drift ratio for fixed and isolated base condition at DBE in Ydirection

From the above Fig 3 and Fig4, it can be seen that the average reduction in storey drift ratio is 84.8% in X direction while 67.14% in Y direction for isolated base building in comparison with the fixed base building.

3.2.2 Comparison of storey acceleration for fixed and isolated base conditions at DBE level

The comparisons of storey acceleration for fixed and isolated base buildings at DBE level in X and Y directions are shown in Fig 5 and Fig 6.

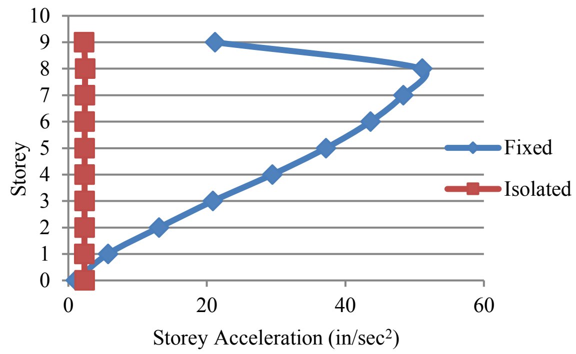

Fig 5. Comparison of storey acceleration for fixed and isolated base condition at DBE in X direction

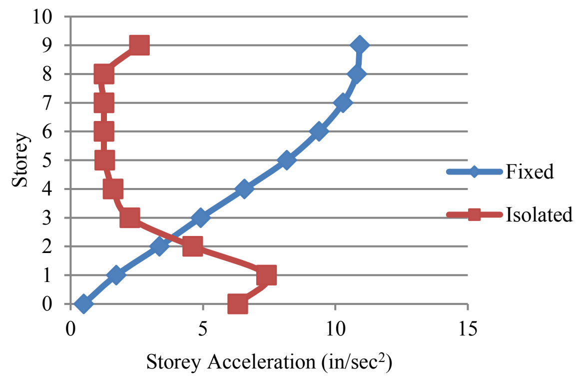

Fig 6. Comparison of storey acceleration for fixed and isolated base condition at DBE in Y direction

From the above Fig 5 and Fig 6, it can be seen that the average reduction in storey acceleration is 91.97% in X direction while 51.98% in Y direction for isolated base building in comparison with the fixed base building.

3.2.3 Comparison of storey drift ratio for fixed and isolated base conditions at MCE level

The comparisons of storey drift ratio for fixed and isolated buildings at MCE level in X and Y directions are shown in Fig 7 and Fig 8.

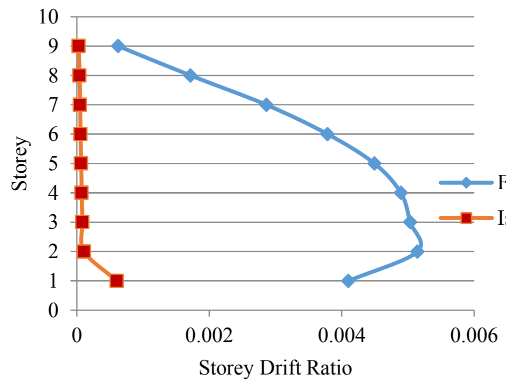

Fig 7. Comparison of storey drift ratio for fixed and isolated base condition at MCE in X direction

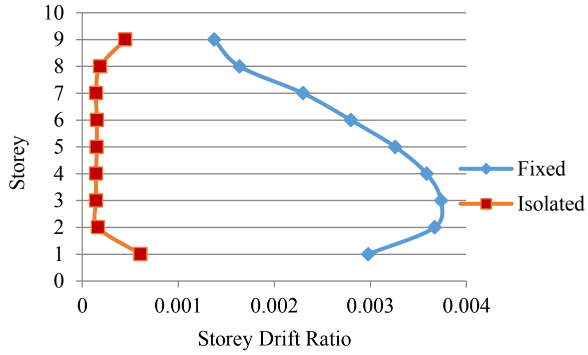

Fig 8. Comparison of storey drift ratio for fixed and isolated base condition at MCE in Y direction

From the above Fig 7 and Fig 8, it can be seen that the average reduction in storey drift ratio is 96.44% in X direction while 90.23% in Y direction for isolated base building in comparison with the fixed base building.

3.2.4 Comparison of storey acceleration for fixed and isolated base conditions at MCE level

The comparisons of storey acceleration for fixed and isolated buildings at MCE level in X and Y directions are shown in Fig 9 and Fig 10.

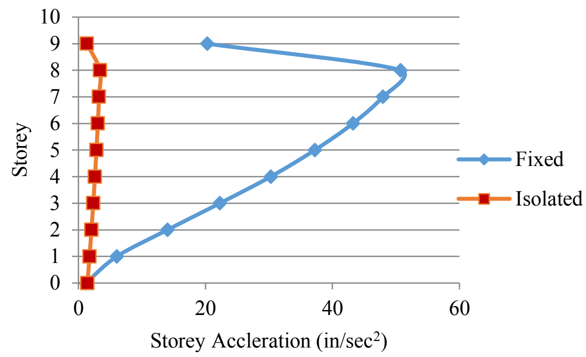

Fig 9. Comparison of storey acceleration for fixed and isolated base condition at MCE in X direction

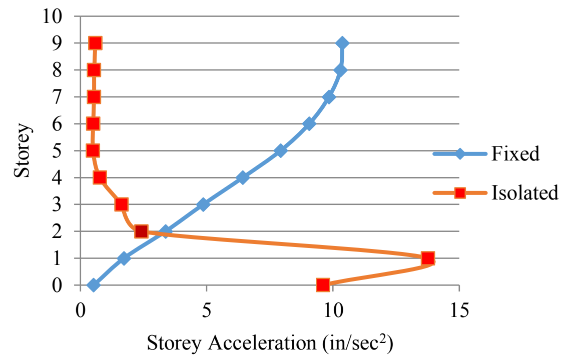

Fig 10. Comparison of storey acceleration for fixed and isolated base condition at MCE in Y direction

From the above Fig 9 and Fig10, it can be seen that the average reduction in storey acceleration is 90.88% in X direction while 52.08% in Y direction for isolated base building in comparison with the fixed base building.

4. PERFORMANCE ASSESSMENT PHASE

The first step in PACT was to enter the basic information of the purposed building into the program. This data included the region cost multiplier and date cost multiplier which linearly scaled the damage cost results based on ratios of how much the results vary from Northern California region and 2011 date values, respectively. Since this was a comparative study and the project's region: Myanmar was expected to yield cost values differ to the Northern California region, therefore assume the region cost multiplier was taken as 1.03. The project was analyzed to be concurrent with the time of this study, so an inflation rate of 6% was calculated based on the inflation rate in Myanmar averaged 6.23 % from 2011 to 2018. Based on this calculation, a date cost multiplier of 1.06 was used for this study.

In the performance assessment phase, the storey acceleration and storey drift ratio obtained from the nonlinear time history analyses in the analysis phase are used to assess the seismic performance of the structures via fragility cures and FEMA P-58 (Federal Emergency Management Agency) are used to compute probable damage costs, repaired time and number of injuries for each base condition at seismic demand levels and the results are compared.

4.1 Comparison of damage cost for DBE fixed and isolated base buildings

The comparison of damage cost for fixed base and isolated base buildings at DBE level seismic events is as shown in Fig 11 and Fig12. The X-axis shows the damage costs in thousands of dollars and the Y-axis gives the probability of repair costs not surpassing the given damage costs. Accordingly, the fixed base and the isolated base buildings have 50% probability of incurring \$3.32million and \$0.23 million in damage costs when subjected to DBE level seismic events. Base isolation therefore reduced DBE level damage costs by \$3.09 million.

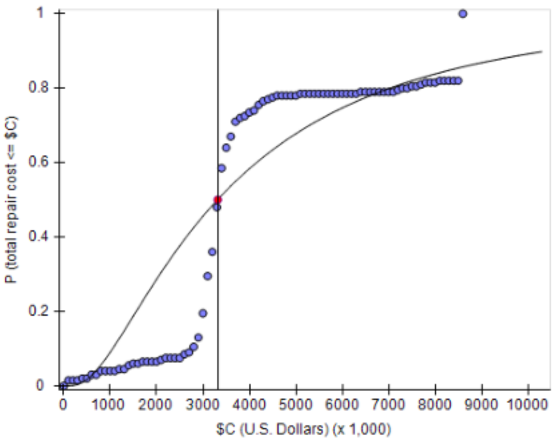

Fig 11. Damage cost for DBE fixed base condition

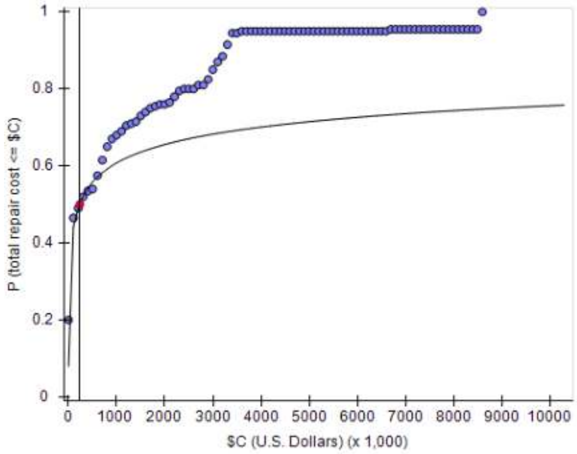

Fig 12. Damage cost for DBE isolated base condition

4.2 Comparison of repair time for DBE fixed and isolated base buildings

The comparison of repair time for fixed base and isolated base buildings at DBE level seismic events is as shown in Fig 13 and Fig14. The probabilities of repair time being incurred for the fixed base and the isolated base buildings subjected to DBE level of seismic demands are88 and 23 days respectively.

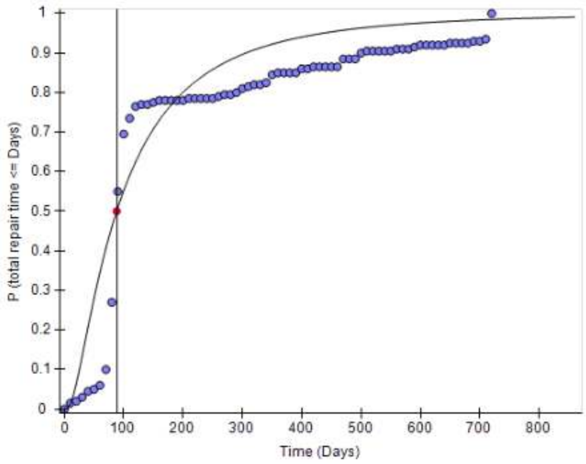

Fig 13. Repair time for DBE fixed base condition

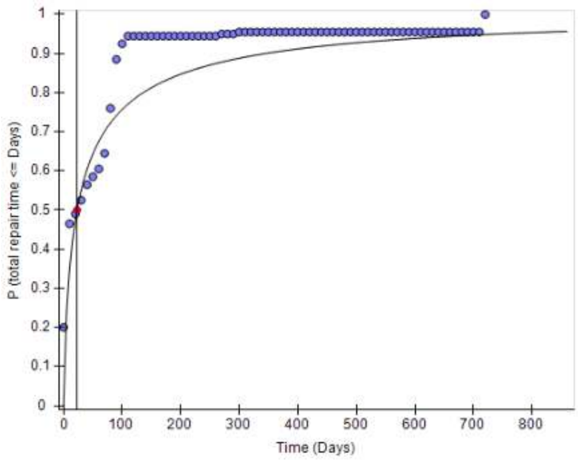

Fig 14. Repair time for DBE isolated base condition

4.3 Comparison of injuries for DBE fixed and isolated base buildings

The comparison of injuries for fixed base and isolated base buildings at DBE level seismic events is as shown in Fig15 and Fig16. When subject to DBE level seismic events, the fixed base and the isolated base apartment buildings have 50% probability of incurring 19 and 0 injuries respectively.

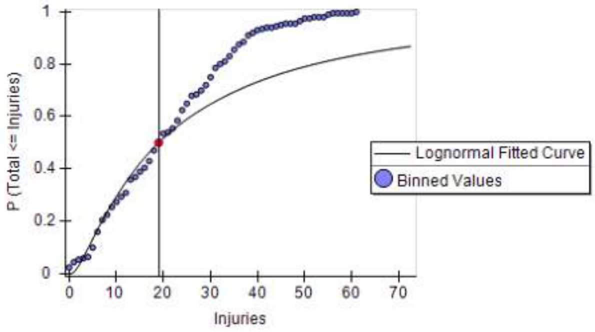

Fig 15. Injuries for DBE fixed base condition

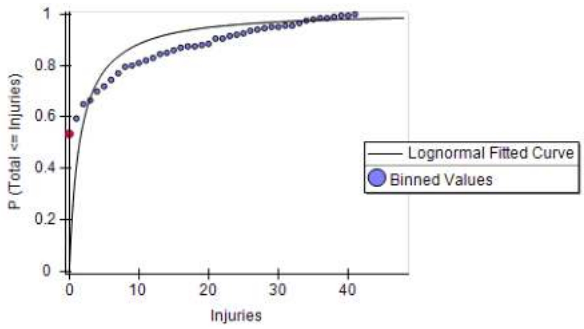

Fig 16. Injuries for DBE isolated base condition

4.4. Comparison of damage cost for MCE fixed and isolated base buildings

The comparison of damage cost for fixed base and isolated base buildings at MCE level seismic events is as shown in Fig17 and Fig18. Accordingly, the fixed base and the isolated base buildings have 50% probability of incurring \$3.775 million and \$0.3 million in damage costs when subjected to MCE level seismic events. Base isolationtherefore reduced MCE level damage costs by \$3.475 million.

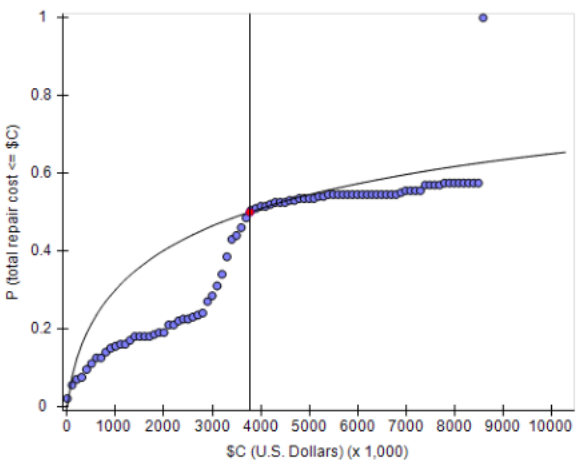

Fig 17. Damage cost for MCE fixed base condition

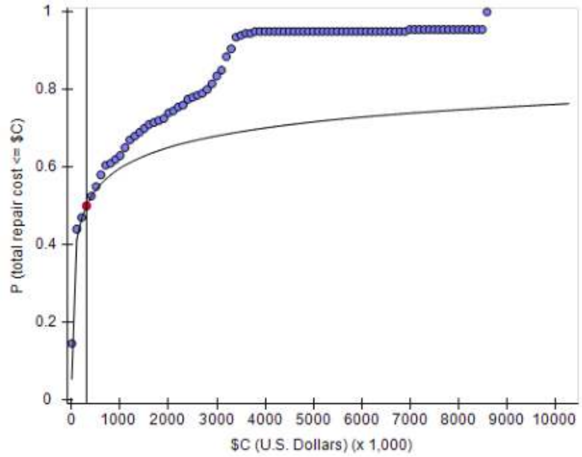

Fig 18. Damage cost for MCE isolated base condition

4.5 Comparison of repair time for MCE fixed and isolated base buildings

The comparison of repair time for fixed base and isolated base buildings at MCE level seismic events is as shown in Fig 19 and Fig20. The probabilities of repair time being incurred for the fixed base and the isolated base buildings subjected to MCE level of seismic demands are 120 and 28 days respectively.

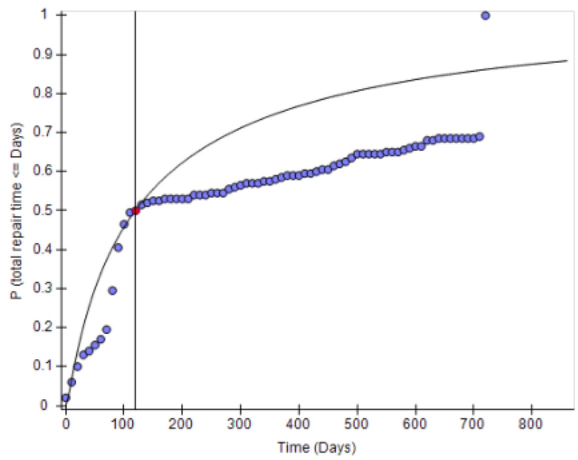

Fig19.Repair time for MCE fixed base condition

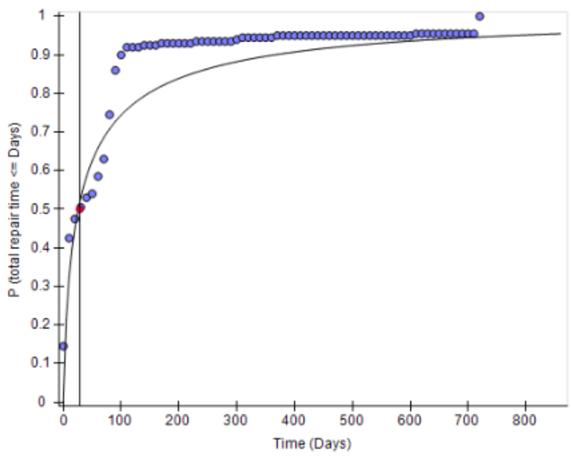

Fig 20. Repair time for MCE isolated base condition

4.6 Comparison of injuries for MCE fixed and isolated base buildings

The comparison of injuries for fixed base and isolated base buildings at MCE level seismic events is as shown in Fig 21 and Fig22. When subject to MCE level seismic events, the fixed base and the isolated base apartment buildings have 50% probability of incurring 9.125 and 0.0667 injuries respectively.

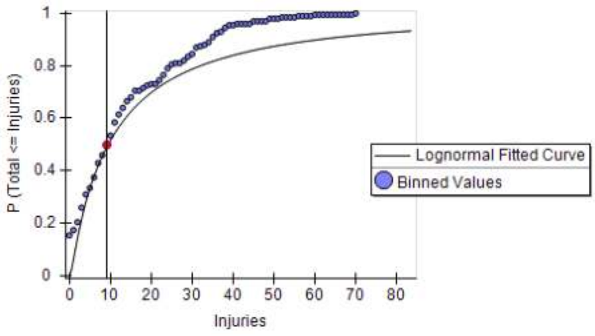

Fig 21. Injuries for MCE fixed base condition

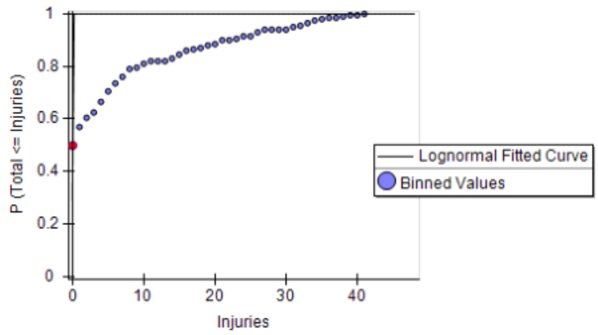

Fig 22. Injuries for MCE isolated base condition

5. CONCLUSIONS

The design of triple friction pendulum bearing for eight-storeyed steel building in risk seismicity region has been carried out and the nonlinear dynamic structural responses are evaluated. Ground motion records for time history analysis are obtained from PEER ground motion database website based on ASCE code spectrum. The performance assessments reported in this study are underestimated due to the number of components and fragility curves available in PACT. From the results of present study, the following conclusions are drawn;

- The storey drift ratio and storey acceleration are both in X &Y directions considerably reduced by using base isolation devices over the conventional structure.
- The savings for damage cost in isolated building are millions of dollars greater than that of fixed base building.
- The conduct of base isolation technology would likely achieve in seismic performance for the residential building are depending on the intensity of the seismic demands levels.
- Base isolation used triple friction pendulum is found significantly effective mitigating and preventing for seismic performance of the proposed building.

ACKNOWLEDGEMENT

The authors would like to express our deepest gratitude and sincere appreciation to the following persons, whose guidance aided towards the competition of this paper. We would like to thank Dr. Yan Aung Oo, Prorector, Technological University (Mandalay), for his kindness, help, permission and suggestion for completion of this paper. Special thanks are extended to Dr. Thiha Zaw, Professor and Head, Department of Civil Engineering, Technological University(Mandalay), for his valuable suggestion and excellent comments to conduct this paper. We would like to thank our parents, teachers and all of friends for their support and encouragement throughout this research.

REFERENCES

[1] Pallavi Wamanrao Taywade, “Sustainability Of Structure Using Base Isolation Techniques for Seismic Protection, International Journal of Innovation Research in Science, Engineering and Technology, vol.4, Issue 3, ISSN 2319-8753, March 2015.
[2] Applied Technology Council (ATC). FEMA P-58: “Seismic Performance Assessment of Buildings”, vol 2 – Implementation Guide. 2012, 26 March 2013.
[3] Applied Technology Council. PACT (Version 2.9.4), Computer Software, Redwood City, California (2012), 26 April 2013.
[4] Santhosh H.P., K.S. Manjunath, and K.S.Kumar: “Seismic Analysis of Low to Medium Rise Building for Base Isolation”, International Journal of Research in Engineering and Technology, 2013.
[5] MNBC: *Myanmar National Building Code,*2016
[6] Pacific Earthquake Engineering Research Center (PEER): *Web-Based PEER Ground Motion Database (Beta Version)* [Interactive Web-site database]. Berkeley, California, 2010.

Tunnel Investigation of Thaukyegat Hydropower Project, East of Taungoo, Bago Region, Myanmar

Aung Kyaw Myat[1], Hlaing Myo Nwe[2], Su Su Kyi [2]
[1] University of Yangon, Myanmar
[2] Bago University, Myanmar
[2] University of Yangon, Myanmar

Email: aungkyawmyat95@gmail.com

ABSTRACT*:* This project provides to use for water supply and hydroelectricity. It lies in Sittaung River Valley.The research are conducted with insitu tests along tunnel by geotechnical behavior of exposed rocks. This area situated within Pupan Shear Zone and Thaukyegat anticline is nearly north-south in direction as east-west compressive stress. The rocks are mainly meta-sedimentary rocks of Mergui Group (Upper Paleozoic) and granitic rock associated with some dykes. Tunnel alignment is nearly east-west which cuts across right angle to the anticlinal axis. Waterway Tunnel with 597.5 long and 8.5 m in diameter is used for hydropower. Purple schist, schist, black schist, meta-sandstone and quartzite are exposed along Tunnel alignment. According to Q-system and Rock Mass Rating (RMR) calculations, the characteristics of the rocks along the Tunnel alignment indicate poor condition. Their rock strength, joint and water inflow and structural condition are quite different where sufficient treatments have been done in accordance with the geotechnical analysis. This project is very applicable for flood control, water supply for irrigation, hydroelectric generation and navigation or for recreation.

KEYWORDS: *Insitu tests, Q-system, RMR, treatment*

1. INTRODUCTION

Thaukyegat Hydropower project lying in Sittaung River Valley as well as in the most eastern unit of 'Sino-Burman Ranges' has a elongated shape in NNW-SSE with 72 km long and 25 km wide, approximately controlled by the geological structures. The area is located approximately 21 km east from Taungoo where a rockfill dam of 92 m high is embanked at the narrow valley at Htonbo.

1.1 Objectives

This research aims to explore geotechnical behavior of rocks along tunnel alignment. The objectives of this research are as follows;

To investigate the rock behaviors along tunnel
To identify the rock mass class by Q-system and RMR
To create the engineering geological map along tunnel

2. THEORETICAL BACKGROUND

2.1 Specification of Insitu Tests

In this research, Q-system for rock mass classification is used by Barton (1974). The quality of the rock mass can be determined by following equation proposed by;

$$Q = \frac{RQD}{J_n} \times \frac{J_r}{J_a} \times \frac{J_w}{SRF}$$

The first term RQD (Rock Quality Designation) divided by Jn (joint set number) is related to the size of the intact rock blocks in the rock mass. The second term Jr (joint roughness number) divided by Ja (joint alteration number) is related to the shear strength along the discontinuity planes and the third term Jw (joint water parameter) divided by SRF (stress reduction factor) is related to the stress environment on the intact rock blocks and discontinuities around the underground excavation.

Bieniawski (1989) proposed that the correlation Q-system and Rock Mass Rating can be calculated by using RMR= 9 log (Q) +44.

2.2 Design of Tunnel Alignment

Well executed site investigation programme is essential for the design of the tunnels and underground excavation works, for adoption of most suitable excavation methods, for cost estimation and contracting basis.

Tunnel excavation is very useful that depends on geological factors, geological structure and their effect, and special problem related to the design of a By-pass Tunnel of Dam. The essential part of the underground excavation are (i) Effect of the spacing of discontinuities, (ii) Fold and Fault in relation to tunneling, (iii) Instability of mountain slope, (iv) geological information obtained from reconnaissance and various investigations, (v) Case histories and (vi)Geophysical exploration. Tunnel layout is shown in Figure (1).

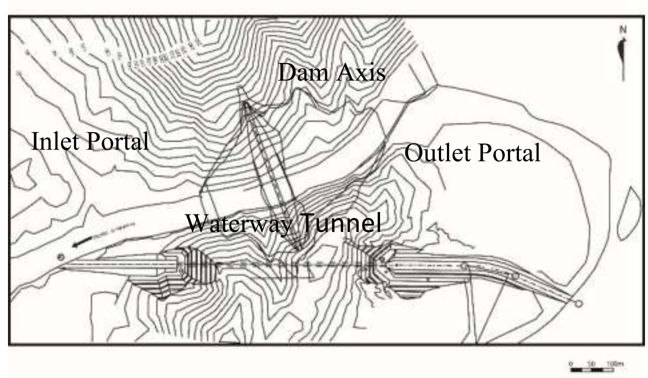

Fig. 1 Tunnel Layout of the Thaukyegat Hydropower Project

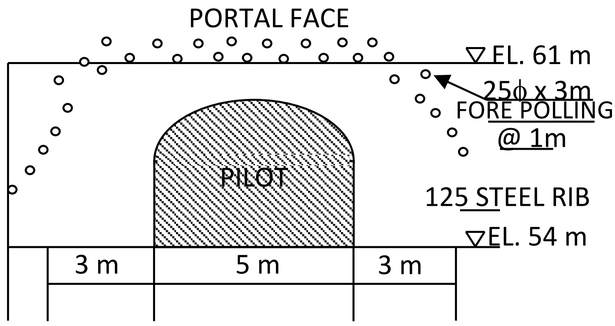

Fig. 3 Cross-sectional view of pilot tunnel (After Kansai Project Report, 2007)

3. EXPERIMENT

3.1 Tunnel Excavation

The following tunnelling sequences are carried out for each round such as (1) surveying, (2) Making for blasting holes, (3) Drilling for blasting holes, (4) Charging in blasting holes, (5) Blasting twin header, (6) Mucking, (7) Scaling, (8) Supporting system, (9)Steel rib installation, (10) Setting of wire mesh, (11) Shotcreting and (12) Rock bolting.

For the tunnel excavation, pre-grouting was carried out as follow: (i) Length of steel pipe: 6.0 m, (ii) Diameter of steel pipe: 40 mm, (iii) Spacing of steel pipes: 40 cm, (iv) Perforation of steel pipes: 4 rows x 20 holes (6-8 mm), (v) Grouting pressure: 0.5 Mpa and (vi)Inclination of steel pipes: +5 to +15 degrees from the horizontal. Typical excavation of tunnel and section of pilot tunnel with dimensions are illustrated in Figure (2) and (3).

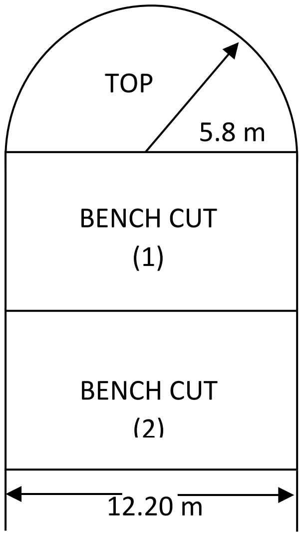

Fig. 2 Typical excavation of tunnel opening (After Kansai Project Report, 2007)

4. ANALYSIS

4.1 Geological Condition of Site Area

The site area is mostly composed of metasedimentary rock and metamorphic rock of Mergui Group (Upper Paleozoic) and granitic rock associated with some dykes. Quartzite, schist intercalated with sandy phyllite and some dolerite dykes are exposed along the site area.

Qaurtzite is rarely exposed along the innermost part of the Thaukyegat Anticline at the adit Tunnel that shows high strength as shown in Figure (4).

Fig. 4 Quartzite with shear plane at the left abutment

Highly jointed phyllite mostly exposed along tunnel alignment. The strength of the rock is 25-35 Mpa and low permeable which is shown in Figure (5).

Fig. 5 Phyllite with highly jointed in the Left bank

The rock distribution along tunnel alignment are described in Figure (6). Most of rocks are moderately hard with highly jointed in nature.

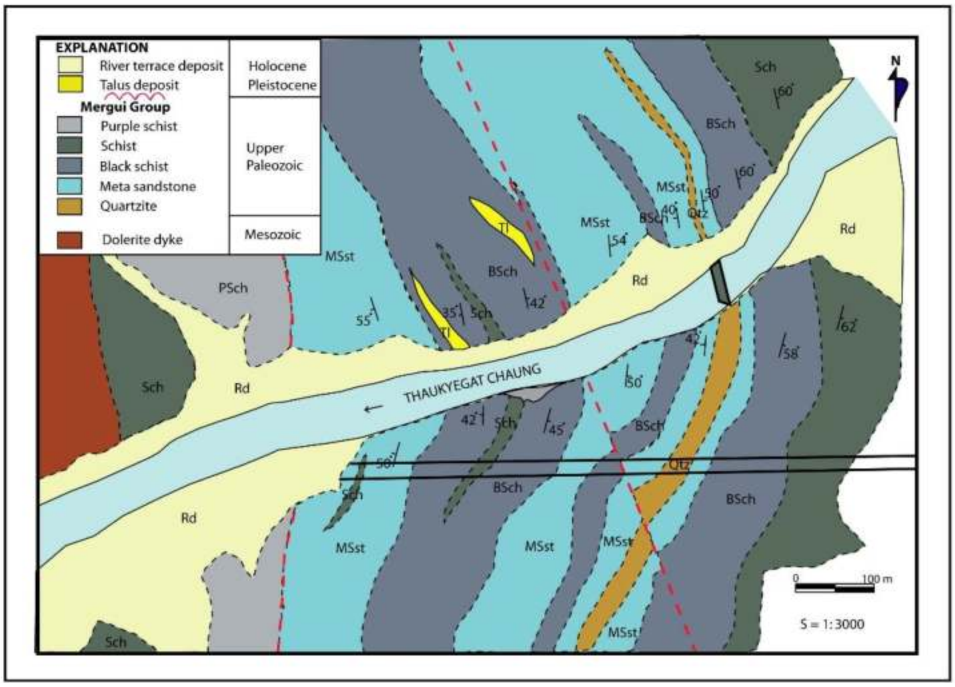

Fig.6 Geological map along the tunnel alignment (Modified after Aung Kyaw Myat and San Oo, 2009)

4.2 Rock Class and Geological Condition of Tunnel

Rocks are classified based on geo-technical factors such as hardness, joint spacing, joint conditions, weathering and alternation along the tunnel as described in Table 1.

Table (1) Geotechnical parameters along Tunnel

Rock class	Description	Location	Shear strength (kgf/m^2)	Internal friction angle (˚)
CH	Rocks almost fresh and hard, bedding/ joint planes wide in spacing, and tight. Slight indication of weathering or alteraltion.	Rare in tunnel section	20	50
CM	Moderately hard and jointed or cracked, stained along geological separations.	Inlet portal, tunnel section	15	45
CL	Rock moderately soft but partly hard. Weathering reaches into inner part of rock and no fresh part is seen, closely cracked.	Inlet portal, tunnel section, outlet portal	7	38
D	Very soft, partly decompoed like soil by weathering and/or aleration.	Outlet portal	3-0	<20

4.2.1 Inlet

Along the road cutting beside the river at the proposed tunnel portal, good rocks mass class of schist crop out well, and the slope inclination is more than 40 degrees. Therefore, the rock conditions are CM class and it thought to be fairly good.

4.2.2 Tunnel Section

The tunnel route is to pass through under four numbers of creeks. The upstream cut deeply the mountains and the tunnel route is selected to keep the rock cover of CM class being more than 20 m in thickness over these creeks. However, consideration of all the drill holes on the right bank show a deep weathering, generally not favourable condition of rock. Some fractured zones and hydro-thermally altered zones might be encountered in the tunnel, though the geological structures such as beds being steep and perpendicular to the tunnel direction might be favourable for tunneling.

4.2.3 Outlet

The slope inclination of outlet portal is rather steep (28 degrees), but it seems to be covered with thick weathered rocks according to the results of drilled core record, indicating that the slope excavation must be very deep and large in order to get the rocks stability for the tunnel portal. According, it might be a big issue to find the ways to minimize the slope excavation.

4.3 Rock Behaviors along Tunnel Alignment

In this area, purple schist, schist, black schist, meta-sandstone and quartzite exposed along the Tunnel alignment. Bieniawaski's Geomechanics Classification system (1989) based on Barton's Q-system provides a general rock mass rating (RMR) increasing with rock quality from 0 to 100. The rocks exposed along tunnel alignment can be classified as Zone I, II and III depending upon their geological condition and geotechnical analysis which are described in Table 2.

Table (2) Geotechnical parameters along Tunnel

Zone	Jv	Jr	Ja	Jw	SRF	RQD	Q -System	RMR
1	28 %	2.7	4	1	1.5	22.6 %	0.678	42.48
2	33 %	2.5	4	1	5.0	6.1 %	0.045	31.87
3	28 %	3	2	1	1.5	22.6 %	1.883	46.47

Zone I is composed of purple schist where the number of joint set of discontinuity is four or more sets (Jn = 15) and joint surface is rough, smooth and wavy (Jr = 2.7). Joint filling is sand or crush rock filling (Ja = 4). Water condition (Jw = 1) is dry. Stress reduction class is low to medium stress (SRF = 1.5). This zone have very poor rock mass class. Zone II is characterized by schist and where the number of joint set of discontinuity is partially crushed rock (Jn = 17) and joint surface is rough, smooth and wavy (Jr = 2.5). Joint filling is sand or crush rock filling (Ja = 4). Water condition (Jw = 1) is dry. Stress reduction class is loose rock with open discontinuties (SRF = 5.0). This zone can be determined extremely poor rock mass class. Zone III is meta sandstone and quartzite that is also class III fair rock mass class by RMR calculation. The number of joint set of discontinuity is three or four set (Jn = 12) and rough, wavy surface (Jr = 3) occurred. Joint filling is slightly to moderately weathered (Ja = 2) where water condition is dry and minor flow (Jw = 1). Stress reduction class is low to medium stress (SRF = 1.5). The structural zoning map are estiblished depending upon their geological condition and geotechnical analysis as shown in Figure (7).

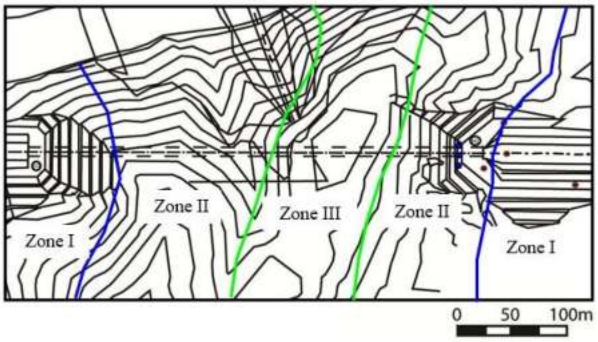

Fig. 7 Different Zones along the Tunnel Alignment

4.4 Tunnel Support System

This system must be designed and placed in tunnelling and underground construction to resist deformation induced by the dead weight of loosened rock as well as those induced by the readjustment of stress field in rock surrounding the tunnel.

4.4.1 Steel Rib Installation

Steel ribs are systematically installed in 0.6 to 1 m interval. The H-beams (125 mm x 125mm x 6 m) are bent by Roller Bending machine to get the fit size for excavated tunnel shape. The two halves of bent H-beams are connected with two bearing plates in crown and bas. Then the steel ribs are connected by 0.75 inches diameter connection bars Steel Rib Installation is shown in Figure (8).

Fig. 8 Steel rip in Edit Tunnel of Thaukyegat site

4.4.2 Setting of Wire Mesh

Wire-meshs are used to support small pieces of loose rocks and as reinforcement for shotcrete. The size of (0.6 cm x 0.6 cm) wire mesh is installed after primary shotcreting as shown in Figure (9).

Fig. 9 Wire mesh at Inlet Portal of Thaukyegat site

4.4.3 Shotcreting

In that power tunnel, shotcreting is performed in rock mass classes IV. The shotcreting is prayer with 500 KVA generators. It can spray in all direction. Two types of shotcrete, dry mix shotcrete and wet mix shotcrete are used to protect inflow leakage water and dewatering outside.

The rapid gaining in strength is done by adding accelerator but ultimate strength is more important. The mixture for shotcrete is the combinatin of cement, quick hardening agent, chippings, sand and water which is shown in Figure (10). Shotcrete ratio are as follows;

Shortcrete Ratio for 1m^3 (Mix-design)
Cement - 423.7kg = 8.5 bag (Say 8 bag)
Fine Sand - 25 cu ft
River Chipping - 33.5 cu ft (Say 33 cu ft)
Q.H.A (7%) - 29.66kg = 1.2 bag
Say = Cement : Q.H.A
8 : 1
Q.H.A = Quick Hardening Accerator

Fig. 10 Shotcrete mix machine in Project Area

Fig. 11 Rock bolt with 3 m spacing at Inlet Portal

4.4.4 Rock Bolting

The rock bolting is accepted as a very effective and relatively cheap support method. In many cases, bolting is done immediately after excavation to stabilize the cavity together with shotcrete.

Lang (1972); Barton et al. (1974); Schach et al. (1979); Farmer and Shelton, (1980); Crawford et al. (1985) described the determination of bolt length and spacing with their discussion for ground support in underground excavations. Choquet and Hadjigeorgiou, 1993 provided a review on the design of ground support. The following presented are the principles for the determination of bolt length and spacing that are used in the practice of rockbolting to date.

According to the support system of Choquet and Hadjigeorgiou, the length of rock bolt is 4 m and 3 mm to 25 mm diameter which is spaced at 1.5 m vertically and 3 m horizontally as shown in Figure (11).

The bolt pattern or the number of bolt is depended on the weight of the block and the nature of joint in the block. Generally the ratio of the length of bolt and the distance between bolts or interval should be at least 2. Then, the bolt length can be determined by

For limited loose blocks

$L = d = 1.0$ m

L = Length of rock bolt

D = Length drilled through block

For tunnel excavated in moderately jointed hard rock masses, the Norwegian Road Authority proposed the following formula to determine the length of un-tensioned bolts in the central section of the tunnel for the purpose of suspending the failure zone on the natural arch described by Staten Vegvesen (2000).

(i) For systematic bolting un-tensioned

$L = 1.4 + 0.184\ B$

B = Tunnel width

(ii) For systematic boltting, Pretensioned

$L = 1.6 + \sqrt{1.0 + 0.012\ B2}$

The equipment used along this tunnel is Drilling Jumbo (2 Boom), Hydraulic Excavation (0.8 m3), Shotcrete machine (8 m3 – 12 m3/hr), Water Bowser (1200 gals), Lining Metal form Roller bending machine, Twin header machine, Dump Truck and Wheel loader.

5. CONCLUSIONS

Thaukyegat area lies in Sittaung river valley and is located approximately 21 km east of Taungoo. This dam is to use for water supply and hydroelectricity.

This region was covered by Mergui Group (Upper Paleozoic) and widely distribution of intrusive bodies of granites associated with dyke. Thaukyegat anticlinal axis runs north-south in direction where Tunnel alignment is perpendicularly acting this axis. Purple schist, schist, black schist, meta-sandstone and quartzite exposed along the Tunnel alignment.

According to Q-system and RMR calculation, it can be classified as three zones that generally composed of poor rock mass class condition. Hence, systematic rock bolting with wire mesh must be installed and additional rock bolts must be applied. Moreover, chemical grouting should be taken in weak zone. Finally, this project is supported to beneficial in terms of power generation (exceed 120 MW and 646.8 GWh) and contribute not only regional development on living and industry but also development of whole country.

ACKNOWLEDGEMENT

I am deeply indebted to Dr. Day Wa Aung, Professor and Head, Department of Geology, University of Yangon, for his advices and permission to carry out this research project.

Sincerely thanks are to Dr. Tun Naing Zaw, Associate Professor, Geology Department, University of Yangon who provided valuable advices throughout the research work.

REFERENCES

[1] Barton N, Grimstad E, “Tunnel and cavern support selection in Norway, based on rock mass classification with the Q system,” Publication No. 23. Norwegian Tunnelling Society. P. 45-77. 2014.

[2] Barton, N.R.; Lien, R.; Lunde, J., "Engineering classification of rock masses for the design of tunnel support". Rock Mechanics and Rock Engineering. Springer. 6 (4): 189–236, 1974.

[3] Bieniawski ZT, “*Engineering rock mass classifications*,” New York: Wiley, 1989.

[4] Chates D. F., Cochrane Ts., “*Development of design specifications for rock bolting from research in Canadian mines*,” Mining Research Centre, Energy,

Mines and Resources Canada, Research Report, R224, Unpublished. 1970.

[5] Choquet P., Hadjigeorgiou J., "*The design of support for underground excavations*," In: Excavation, support and monitoring, Comprehensive rock engineering-principles, practice and projects, Vol. 4, Pergamon Press; P. 189-239. 1993.

[6] Crawford A.M., Ng I., Lau K.C., "The spacing and length of rock bolts for underground openings in jointed rock," In, Einsenstein Z, editor, Proceedings of the 5th international conference on numerical methods in geomechanics, A. A. Balkema, P-1293-1300, 1985.

[7] Farmer I.W., Shelton P.D., "*Factors that affect underground rockbolt reinforcement systems design,"* Transactions of the Institutions of Mining and Metallurgy. P-68-83, 1980.

[8] Kansi, *Basic Design Report on Thaukyegat Hydropower Project, (Unpublished project report)*, Kansai Electirc Power Co., Ltd., 2007.

[9] Lang T., "*Rock reinforcement*," Bulletin of the International Association of Engineering Geology, P. 215-39, 1972.

[10] Schach R, Garschol K., Heltzen A.M., "*Rock bolting: a practical handbook*," Oxford: Pergamon. 1979.

[11] Statens vegvesen, "*Fjellbolting, Handbook 215*," Oslo: Trykkpartner AS, in Norwegian, 2000.

ASSESSMENT OF SEISMIC SOIL LIQUEFACTION POTENTIAL BASED ON SHEAR WAVE VELOCITY DATA USING 2% AND 10% PROBABILITIES OF PGA VALUES WITH EARTHQUAKE MAGNITUDE-7.5M_W FOR AUNGMYAYTHAZAN AND CHANAYETHAZAN TOWNSHIPS OF MANDALAY DISTRICT

Tun Tun Win[1], Myo Thant[2], Pyi Soe Thein[3]
[1] Dr, Associate Professor, Department of Geology, Pang Long University
[2]Dr, Professor, Department of Geology, University of Yangon
[3]Dr, Associate Professor, Department of Geology, University of Mandalay

Email: geolttw73@gmail.com

ABSTRACT: In this study, liquefaction triggering of soils were mainly calculated based on shear wave velocity value (*Vs*) by using 1998 NCEER recommended of Liq.IT v.4.7.7.5 software. The *Vs* values have conducted based on H/V spectral ratio of SMAR 6A3P microtremor test using inversion process. The liquefaction potential maps of the study area were developed by using overall liquefaction potential index (P_L) resulted from 30 shear wave velocity tests at different localities. The P_L map using PGA 2% probability should be considered for the construction of lifeline structures. The P_L map using PGA 10% probability is appropriate for engineering construction of the various sorts of structures especially normal building. According to our resulted data, the very high liquefied zones fall in the western parts of Aungmyaythazan and Chanayethazan townships. The produced liquefaction susceptibility maps will help the structural designers or architect and city planners to check the vulnerability of the area against liquefaction.

KEYWORDS: *Liquefaction potential index (P_L), H/V spectral ratio, shear wave velocity (V_s), SMAR 6A3P microtremor test, 1998 NCEER recommended*

1. INTRODUCTION

Liquefaction events during numerous devastating earthquakes all over the world were mostly observed near water bodies such as river, lake, bays and oceans. According to previous data, all liquefaction events in Myanmar were caused at nearly water body. The study area, Aungmyaythazan and Chanayethazan townships lies on the eastern bank of Irrawaddy River. This area is located about 8 km east of seismically active Sagaing fault. By historical records, Mandalay region had been impacted several times by strong to major earthquakes in the past due to this active fault. According to Chibber, 1934 & Win Swe, 2013, liquefaction effects were caused as a serious problem nearly saturated soils in this region during 23rd March, 1839 Innwa earthquake [1][2]. By above factors, the study area suffers threatening the seismic related hazard especially, liquefaction near future. Thus, liquefaction risk assessment should be carried out for these townships.

In this study, liquefaction triggering of soils were mainly calculated based on shear wave velocity (*Vs*) value resulted from SMAR 6A3P microtremor test. The simplified procedure of the Liq.IT software provided the NCEER1998 recommendation method. This method was used for evaluating liquefaction potential index of soils (P_L) in the present area. The liquefaction potential analysis of the study area had been developed by using 2% and 10% probabilities of PGA values exceedance in 50 years with a scenario earthquake magnitude; 7.5 Mw.

2. SEISMICITY OF THE STUDY AREA AND ITS REGION

Mandalay region has experienced many destructive earthquakes since it lies very close to the Sagaing fault. The seismicity of this region is analyzed by using historical and instrumentally record. Figure (1) shows the distribution of seismicity around Mandalay region with different colors representing different earthquake depths [3]. Most of the earthquake source in this region mainly come from the subduction zone of Indian plate and Burma (Myanmar) plate, and active Sagaing fault [4]. The shallow focus events have mostly observed along Sagaing fault than subduction zone.

By seismological record, the last event with large magnitude is M 7, 16 June, 1956 earthquake. This segment therefore seems to be locked. The most significant earthquakes of the area, March 23, 1839 Innwa earthquake and July 16, 1956 Sagaing earthquake caused severe damage and the great number of casualties in Mandalay and its surrounding cities. Due to those earthquakes, on the banks of both Ayeyarwady and Myitnge rivers between Amarapura and Innwa, several chasms of from five to twenty feet in width were resulted and from which large quantities of water and sand were ejected, representing the liquefaction characteristics [1].The other earthquake rather than 1839 Innwa earthquake, caused the severe damage and some casualties to Mandalay city was the magnitude 7, July 16, 1956 ***Sagaing earthquake***. This earthquake caused 40 to 50 death tolls and several buildings including pagodas were destroyed [1]. The Sagiang bridge was displaced[3] for a few feet. The damage properties in Sagaing was higher than in Mandalay.

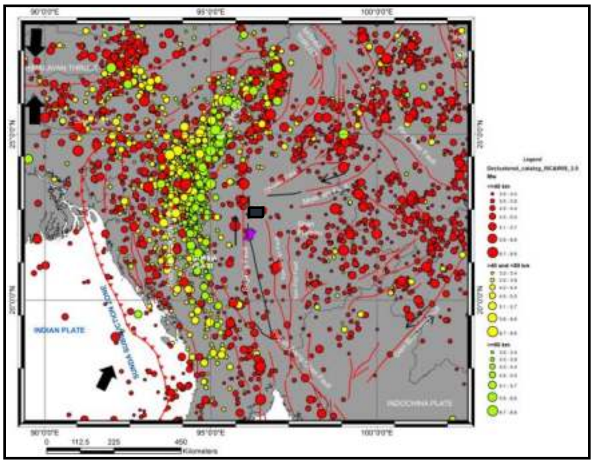

Fig 1. Regional seismicity map including the study area

3. THEORETICAL BACKGROUND

3.1 Microtremor

Microtremor is used to measure human activities and natural phenomena. There are two methods of microtremor measurement such as single station method and array method. The present researchers for determining local site effects of soil has been used single-station measurement. Microtremor is a low amplitude ambient vibration of the ground caused by man-made (artificial) or atmospheric (natural) disturbances, which have amplitude varying between 0.01-0.001 mm and period of 0.01-20 seconds. The frequency >1Hz of microtremor are associated with man-made features such as road traffic, trains, industrial noises, etc., and <1 Hz are associated with natural phenomena such as wind and ocean wave action and variation in atmospheric pressure [5]. Period of microtremor has relationship with the nature of local soil deposits and dynamic characteristic of subsoil.

The SMAR-6A3P instrument with data logger number Ls8800 that produced by Akashi Corporation (Figure 2). was made up of a short-period, three components sensors (NS, EW and UD) with natural period of one second, and external GPS is used to determine the locations. The seismometer consists of a small easy-to-use-damping acceleration sensor, with two horizontal (NS, EW) and one vertical (UD) components to record the velocity of microtremor, built-in amplifier, data logger and batteries. The sensor is vibration proof and high sensitivity electrical output proportional to acceleration is resulted from it and recorded in data logger. The built-in amplifier two stages; amplification with a factor of one, twenty, fifty, or one hundred and one with a factor of 01,1,10, or 100. The factor is low pass filter with three components: 2 Hz, 5 Hz, and 50 Hz.

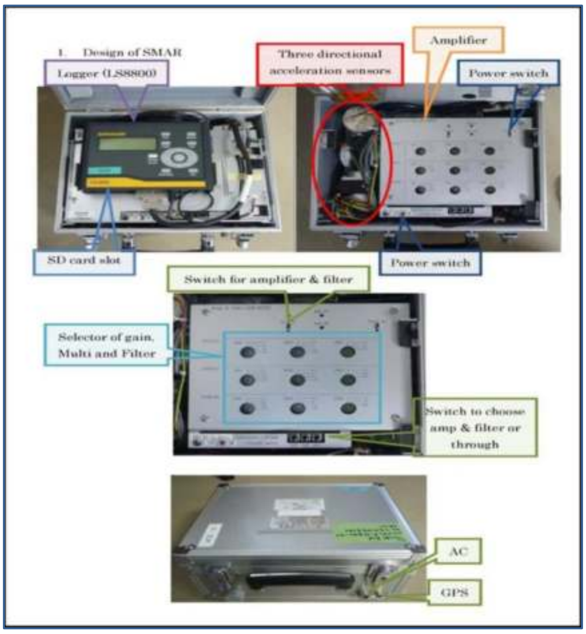

Fig 2. SMAR 6A3P microtremor survey instrument

4. RESEARCH METHODOLOGY

The main objective of this research is to estimate liquefaction potential index of various soils (P_L) in the study area using shear wave velocity to a depth of 30m (V_s^{30}) based on microtremor horizontal vertical spectral ratio (*HVSR*) data compare with SPT-N value. A total of 30 shallow boreholes and 55 microtremor points were collected from various soil deposits at different locations of the research area. Among them, *HVSR* data obtained from only the best 30 microtremor points nearly selected from the present borehole points (Figure 3) were conducted for evaluating soil liquefaction resistance of the study area. In this study, the calculation procedures for liquefaction potential analysis of soils have been used Liq.IT v. 4.7.7.5 software.

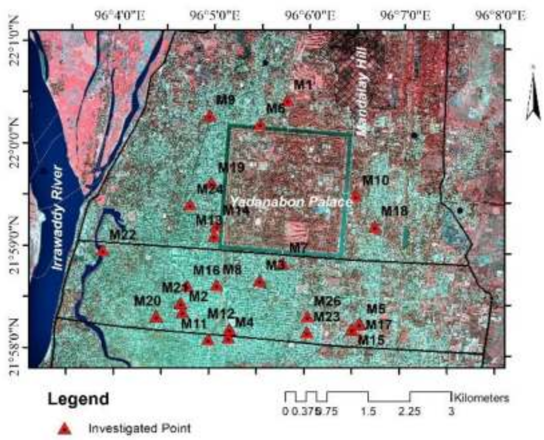

Fig 3. Location map of the sites where liquefaction potential index assessment is carried out.

4.1 Evaluation of Vs30 by Using HVSR ratio

The horizontal vertical spectral ratio (HVSR) obtained from microtremor data. Every data resulted from microtremor has 3 data types such as EW (East-West), NS (North-South) and UD (vertical) component data. The horizontal vertical spectral ratio (HVSR) of microtremor measurement data was confirmed that the fundamental frequency and the amplification factor are able to be estimated [6]. Nakamura pointed out that the H/V spectral ratio of microtremors and earthquake motions are similar to each other and mostly similar to the amplification spectrum.

The average HVSR noise components at each frequency can be defined as

$$\frac{H}{V}(f) = \sqrt{\frac{H_{NS}(f)+H_{EW}(f)}{V(f)}} \qquad (1)$$

Where, H and V are the spectra of the two horizontal (North-South and East-West direction) and vertical components, respectively [7].

According to Kawase et al., 2011, shear wave velocity (Vs) values have resulted from microtremor H/V ratios by using inversion process. In the present study, empirical equation have been used for the estimation of shear wave velocity $V_{s,d}$ is computed for different depths [8]:

$$V_{S,d} = \frac{d}{\sum_{i=1}^{N}\frac{h_i}{V_i}} \qquad (2)$$

where d is the depth in meters, and h_i and V_i denote the thickness and shear wave velocity of the i-th layer based on microtremor measurements, for a total of N layers [9].

The average shear wave velocity of the top 30m (V_s^{30}) model is shown in Figure (3.6) which is calculated as the following equation;

$$V_{S\,30} = \frac{30}{\sum_{i=1}^{N}\frac{h_i}{V_i}} \qquad (3)$$

where, Vs^{30} is the shear wave velocity of upper 30m, h_i and v_i denote the thickness (m) and shear wave velocity of the i^{th} layer, in a total of N, existing in the top 30m, V_s^{30} [10][11].

4.2 Procedure of Liquefaction Potential Index (P_L)

For present research, liquefaction potential index was calculated by using Liq.IT v.4.7.7.5 software based on NCEER recommended (1998). Liq.IT is soil liquefaction analysis software for the assessment of liquefaction potential based on commonly used field data as SPT, CPT and Vs methods. In this study, shear wave velocity to a depth of 30m (V_s30) value is essential parameter for determining P_L by using Liq.IT v.4.7.7.5 soil liquefaction assessment software. The liquefaction assessment of various soils in the study area was performed using shear wave velocity tests at 30 different positions of the study area. Each point is subdivided into four layers for liquefaction potential analysis (Figure 4). Figure 5 shows the summary of calculation procedures for the P_L index of the study area.

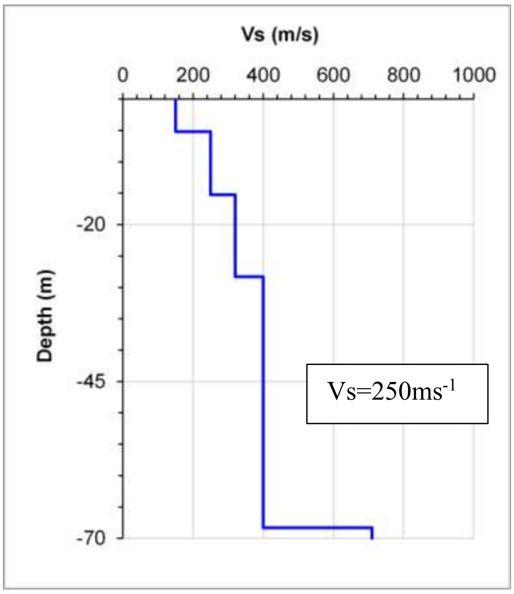

Layer. No	Thickness(m)	Vs(ms^{-1})	P_L
1	5.19	150	34.49
2	9.05	146	18.01
3	11.06	320	0.00
4	4.7	400	0.00

Fig 4. Comparison of Vs30 model and liquefaction potential index of each layer in site no. MDY-22 (27x28 St-Thinkazar canal)

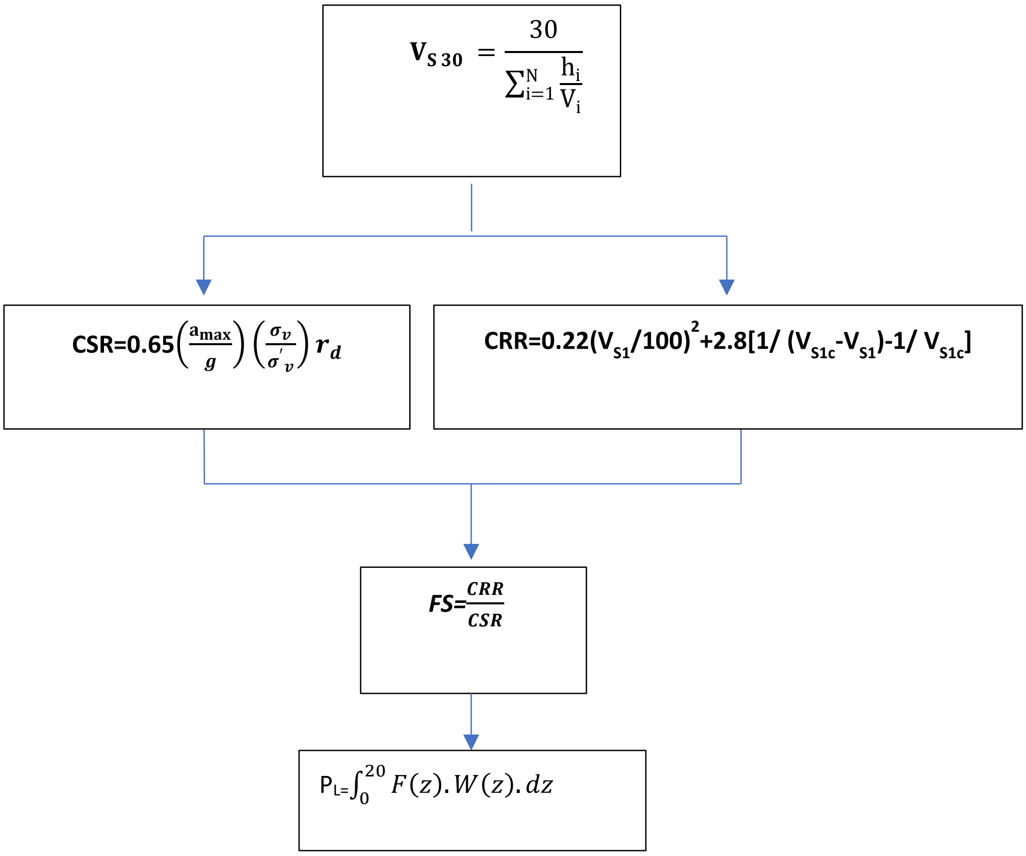

Fig 5. Flow chart of calculation procedure of P_L index

5. RESULTS AND DISCUSSION

Shear wave velocity (Vs), depth to water table (z), peak ground acceleration (a_{max}) and earthquake magnitude (Mw) are mainly four input parameters for calculation procedure of the Liq.IT software. The above factors are considered to be very important for causing liquefaction at a certain place. The smaller total stress value of soil that may be more liquefiable. It should be noted that liquefaction predictions are performed for various peak ground acceleration values as 0.7 – 1.4 g for 2% and 0.5 – 0.9 g for 10% with a scenario earthquake magnitude; 7.5Mw. In the present research, PGA values for liquefaction potential analysis were considered based on probabilistic seismic hazard assessment (PSHA) map of Myo Thant [3].

Table (1) shows some resulted data of very high liquefied layers of the study area. According to present resulted data, low velocity, shallow depth to water table (z) and high peak ground acceleration (a_{max}) in soils lead to a higher liquefaction potential. Normally liquefaction susceptibility of the study area is not probable where water table is > 15 m from surface. Liquefaction potential (P_L) values for present results were designated based on Iwasaki (1984) namely as very low or not probable for $P_L=0$, low for $0< P_L < 5$, moderate for $5< P_L <15$ and high for $15< P_L <25$ and very high $P_L >25$.According to P_L resulted values, we should need to obey the following recommendations [12];

- For very low liquefaction susceptibility ($P_L=0$), detail investigations on soil liquefaction aren't needed in general
- For low liquefaction susceptibility ($0<P_L<5$), detail investigations on soil liquefaction are needed only for especially important structures.
- For moderate liquefaction susceptibility ($5<P_L<15$), detail investigations for soil liquefaction are needed for important structures and countermeasures of soil liquefaction are needed in general.
- For high liquefaction susceptibility ($15<P_L<25$), detail soil investigations are mandatory
- For very high liquefaction susceptibility ($P_L>25$), area should be avoided for developing structures

Table (1) Some resulted data of very high liquefied layers in the study area by using Mw 7.5 & PGA 2% probability

Site No	Location	Depth(m)/ Layer	GWT (m)	PGA (g)	Vs (ms^{-1})	CSR	CRR	Overall P_L Value
MDY-03	22x90 St	5.53/1	6	1.2	173	0.68	0.12	33.18
MDY-28	Kannar St x 35 St	5.24 /1	4	1.35	120	0.81	0.04	52.43
		8.05 /2			150	0.84	0.07	
MDY-27	25x88 St	6.10 /1	6	1.2	120	0.68	0.05	39.46
MDY-22	27x28 St-Thinkazar canal	5.19/1	3	1.3	150	0.81	0.08	52.50
		9.05 /2			146	0.91	0.13	

5.1 Development of Liquefaction Potential Maps of the Study Area

For the study area, liquefaction potential maps are created by means of QGIS software using overall potential (P_L) values of each point. These maps show five liquefaction susceptibility zones such as very low, low, moderate, high and very high (Figures 6 and 7). Each map represents different intensity (P_L) values because of using different PGA values. Most of the area falling P_L index > 25 are more suffered the liquefaction susceptibility than other one. The Figure 6 depicts liquefaction potential map of the study area using PGA value of 10% probability in Mw-7.5. The maximum P_L index value of this map is 49.63. Figure 7 shows liquefaction potential map of the study area using PGA 2% probability of Mw-7.5. The highest P_L index value of the Figure 7 is 52.50. By the resulted P_L value, increasing PGA value may be increasing liquefaction susceptibility index.

The P_L map using PGA 10% probability is appropriate for engineering construction of the various sorts of structures especially normal building. The liquefaction potential (P_L) map by using PGA 2% probability should be considered for the construction of lifeline structures such as water pipe line, gas pipe line, transportation ways and telecommunication lines. According to our resulted data, the very high liquefied zones represent at the western portions of Aungmyaythazan and Chanayethazan townships. Thus, these portions should not construct large building.

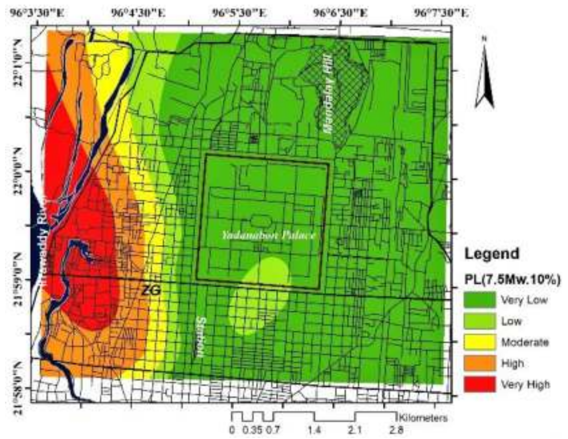

Fig 6. Liquefaction potential map of Mandalay City using PGA 10% probability and Mw-7.5

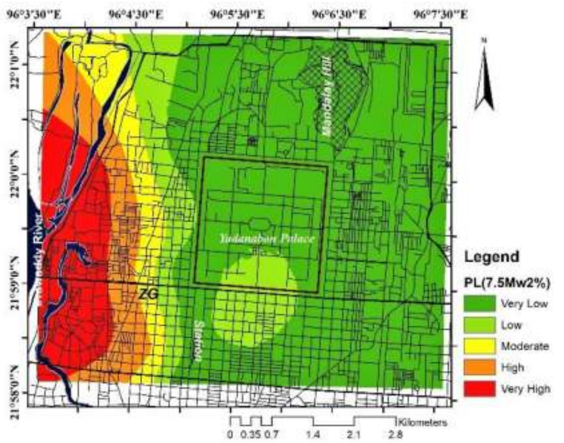

Fig 6. Liquefaction potential map of Mandalay City using PGA 2% probability and Mw-7.5

5. CONCLUSIONS

The main objective of the present research was to prepare the various liquefaction susceptibility maps of the study area by using shear wave velocity method. In the study area, liquefaction susceptibility soils have been observed in low frequency <0.7 Hz, low V_s^{30} <220ms^{-1}; shallow ground water depth <7m; high PGA and FS<1. According to observed data compare with other liquefied data, this area may be appeared liquefied effects for near future if it could be very vulnerable earthquakes. Exactly the western portions of the study area fall under the very high liquefied zone due to representing maximum P_L index and low Vs30 value. Thus, liquefaction susceptibility analysis is urgently needed for the study area in order to provide an effective mitigation plan for coming future earthquakes related hazards. The produced P_L maps can be effectively used for development plans and risk management practices in the study area.

ACKNOWLEDGEMENT

We would like to express the heartfelt gratitude to Professor Hiroshi Kawase and Professor Junji Kiyono in Tokyo University, Japan for their constructive suggestion and supporting the machine to measure microtremor for various assessments in this research.

REFERENCES

[1] Chibber, H.L., 1934. The Geology of Burma, Macmilland. Com. & Limited, London, P538.

[2] Win Swe (2013) "The Sagaing Fault of Myanmar: a brief overview, Geology of Sagaing Fault, in Commemoration of 9th Anniversary of MGS", Myanmar Geosciences Society, Yangon, Myanmar, pp.1–20.

[3] Myo Thant. (2013) Development of Seismic Microzonation Maps of Mandalay City, Mandalay Region, MES and MGS, Myanmar.

[4] Soe Thura Tun & Ian M Watkinson (2017) The Sagaing Fault, Myanmar, Geological society London, Memoirs, Vol.48, Myanmar Geology Resources and Tectonics, Ch-19, pp. 413-441, https://doi.org/10.1144/M48.19.

[5] Del Gaudio V, Wasowski J. (2013). Advances and Problems in Understanding the Seismic Response of Potentially Unstable Slopes, Eng Geol 122: 73-83.

[6] Nakamura, Y. (1989) "A Method for Dynamic Characteristics Estimation of Subsurface using Microtremor on the Ground Surface," *Quarterly Report of RTRI*, 30:1, 25-33.

[7] Kawase, H., Francisco J. Sánchez-Sesma & Matsushima, S. (2011) "The Optimal Use of Horizontal-to-Vertical Spectral Ratios of Earthquake Motions for Velocity Inversions Based on Diffuse-Field Theory for Plane Waves", *Bulletin of the Seismological Society of America*, Vol. 101, No. 5, pp. 2001–2014, doi: 10.1785/0120100263.

[8] CEN. (2004) EN 1998-1:2004, "Eurocode 8: Design of Structures for Earthquake Resistance – Part 1: General Rules, Seismic Actions and Rules for Buildings", European Committee for Standardization.

[9] Bessason, B., and Erlingsson, S. (2011) Shear Wave Velocity in Surface Sediments, *JÖKULL No. 61, 2011,https://www. Research gate. Net/ publication/268384698*

[10] Dobery, R. et al. (2000) "New Site Coefficients and Site Classification System Used in Recent Building seismic Code Provisions, Earthquake Spectra, 16, pp. 41-67.

[11] Seco e Pinto, P. S. (2002) "Eurocode 8 –Design Provisions for Geotechnical Structures". Special Lecture, *3rd Croatian Soil Mechanics and Geotechnical Engineering Conference,*

[12] Iwasaki, T., Tokida, K., and Arakawa, T. (1984) Simplified Procedures for Assessing Soil Liquefaction during Earthquakes. *Soil Dynamics and Earthquake Engineering, v. 3(1)*, pp. 49–58.